SINTERING OF REFRACTORY COMPOUND ENRICHED HIGH SPEED STEELS AND THEIR PROPERTIES

By

PRADIPTA KUMAR KAR

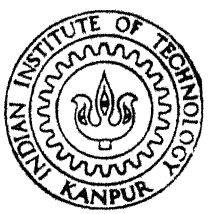

DEPARTMENT OF METALLURGICAL ENGINEERING

INDIAN INSTITUTE OF TECHNOLOGY KANPUR

MAY, 1991

SINTERING OF REFRACTORY COMPOUND ENRICHED HIGH SPEED STEELS AND THEIR PROPERTIES

A Thesis Submitted
in Partial Fulfilment of the Requirements
for the Degree of
DOCTOR OF PHILOSOPHY

By
PRADIPTA KUMAR KAR

to the
DEPARTMENT OF METALLURGICAL ENGINEERING
INDIAN INSTITUTE OF TECHNOLOGY KANPUR
MAY, 1991

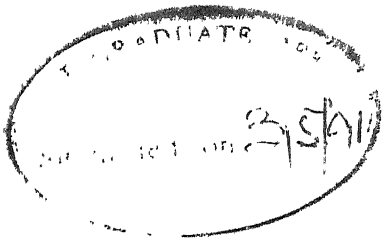

CERTIFICATE

It is certified that the work contained in the thesis entitled "SINTERING OF REFRACTORY COMPOUND ENRICHED HIGH SPEED STEELS AND THEIR PROPERTIES", by Mr. Pradipta Kumar Kar, has been carried out under my supervision and that this work has not been submitted elsewhere for a degree.

3/5/91

G. S. UPADHYAYA
Professor
Department of Metallurgical Engineering
Indian Institute of Technology
Kanpur, India

May, 1991

To

my father,

Late Dr. Binayak Kar

ACKNOWLEDGEMENTS

I am very pleased to acknowledge with gratitude the generous help, invaluable guidance and constant inspiration at every stage tendered to me by Prof. G.S. Upadhyaya throughout the course of this work.

I specially thank M/S S.C. Soni, M.N. Mungole, K.P. Mukherjee and B.K. Jain for their help and cooperation in the experimental work.

I express my appreciation to all my research colleagues namely Subir, Hamid and Bhaskar who were ever-ready to help and made the working in the Powder Metallurgy Lab. a pleasure.

I am grateful to the management of the Tata Iron and Steel Company for granting me study leave and giving me permission to utilize some of their R&D facilities. The help and cooperation of all my colleagues in TISCO in connection with the present study is highly appreciated and remembered.

I am thankful to the management of M/S British India Steels, Ahmedabad, India for allowing me to utilize some of their facilities and to their staff for extending all the help and cooperation.

I am also thankful to the Head, ACMS for allowing me to utilize some of their laboratory facilities in ACMS.

I am indebted to Shyambabu and Babynani, but for whose help and care for my family this work would have remained incomplete.

I congratulate M/S R.N. Srivastava and B.K. Jain for excellent typing and tracing work respectively.

Finally, but not the least, I want to thank my wife, Mani and our two children Anjela and Anurag for their immence patience, moral support and constant love, without which this venture would never have materialised.

- P.K. Kar

PUBLICATIONS

Based on the work presented in this thesis, the following papers have been published.

1. "Liquid Phase Sintering of P/M High Speed Steels", Powder Metallurgy International, Vol. 22, No. 1, Feb. 1990, pp. 23-26.

2. "Liquid Phase Sintering and Heat Treatment of T15 Grade PM High Speed Steel", Metal Powder Report, Vol. 45, No. 12, 1990, pp. 841-843 and Trans. PMAI, Vol. 17, 1990, pp. 25-32.

3. "Novel Liquid Phase Sintered High Speed Steels", In "Proceedings of First International High Speed Steel Conference", Ed. H. Hackl and B. Hribernick, Montan-universitat, Leoben, Austria, 1990, pp. 477-485.

4. "Liquid Phase Sintering of TiN Enriched T15 Grade High Speed Steels and Their Mechanical Properties", Steel Research (In Press).

5. "Liquid Phase Sintering and Heat Treatment of T42 High Speed Steel" (submitted for publication in "Scandinavian Journal of Metallurgy").

TABLE OF CONTENTS

LIST OF TABLES

LIST OF FIGURES

SYNOPSIS

The hardness and wear resistance of any grade of high speed steel (HSS) depend on the volume fraction of the hard phases in the matrix and the matrix hardness. This has led to the development of high vanadium and high cobalt grades of HSS which contains high volume fraction of primary carbides in a temper resistant matrix. The difficulties associated with hot working and low material yield when processing these grades through ingot metallurgy route, have led to the development of powder metallurgy routes for manufacture of HSS products. It is well known that P/M route provides a means of making new alloys and composites which cannot be made by conventional methods. The HSS tools produced through P/M route have the distinctive advantages of the absence of carbide segregation and minimal carbide and matrix grain coarsening, which are the well known problems associated with the conventionally produced tools. By enrichment of the HSS compositions using hard, stable refractory compounds, it is possible to get a still higher volume fraction of hard phases in the matrix, thus further improving wear resistance and cutting ability. Through the use of liquid phase sintering route, a near-net shaped part is obtainable requiring grinding as the only finishing operation.

Although work has been reported on the enrichment of HSS compositions by various refractory compounds, not much has been reported on the use of monocarbide or nitride of

titanium for enrichment of high alloy tungsten grades of HSS, such as T15 and T42.

The present technological investigation singularly focusses on the liquid phase sintering route for the development of HSS composite cutting tool materials. The process is less capital intensive and could be easily adopted in a plant processing conventional sintered products.

In the present investigation, T15 and T42 HSS based particulate composites with different mass fractions of refractory TiC and TiN (0-8%) were prepared by blending their respective proportions with the water atomised HSS powder, cold compacting in a pressure range of 800-850 MPa to a constant green density of 74-76% and vacuum sintering to full density. The sintering temperature selected were from 1220^{o}C to 1320^{o}C in steps of 10^{o}C. Using the full dense product (>98% Th. density) of the respective straight composition, the heat treatment conditions were optimised. In addition to the microstructural study and analysis using both optical and SEM, various mechanical properties like hardness, TRS and elevated temperature compressive yield strength and magnetic coercivity measurements were carried out for the sintered as well as heat treated HSS.

Cutting tool life as per ISO 3685 was determined using a standard single point turning test for the potential fully dense HSS compositions in the heat treated condition . The work material was forged, normalized CK-45 grade steel.

The results showed that the optimum sintering temperature (for achieving full density) for T15 HSS was rather higher (1270^{o}C) in comparison to that of T42 grade (1230^{o}C). The densification behaviour of the T42 HSS based composites were better in comparison to the similar composites based on T15 HSS. Similarly, for either of the HSS, the densification of the TiC containing composites was better as compared

to the corresponding composites containing TiN. The optimum sintering temperature required for achieving full density, increased with the increase in the refractory compound content in the composite. It was noticed that the use of relatively high sintering temperatures for refractory compound enriched compositions had adverse coarsening effect on the microstructure. In case of TiC containing composites, full density could be obtained for all the composites, except 8 mass % TiC containing composite, which did not achieve full density even after sintering at 1320^{o}C. All the TiN containing composites could be sintered to full density.

Coming to the heat treated mechanical properties, the triple tempered hardness of all the composites were higher as compared to the as sintered hardness. In case of T15 HSS based composites, the triple tempered TRS was higher than the corresponding sintered TRS, whereas the reverse was true for the TiC containing composites based on T42 HSS. There existed a peak hardness and TRS value for the 4% TiC containing composite of either HSS. In case of TiN containing composites based on T15 HSS, the hardness and TRS values decreased beyond an addition of 2% TiN, whereas in the case of T42 HSS based composites a peak hardness and TRS value could be observed for 4 mass % TiN, either in sintered or triple tempered conditions.

In case of the elevated temperature compressive yield strength, 4 mass % TiC containing composite based on either HSS showed a peak compressive yield strength. In case of TiN containing composites based on T15 HSS, the compressive yield strength decreased in case of relatively enriched composites, whereas in the case of T42 HSS based composites, it practically remained unchanged up to 4 mass % TiN beyond which it decreased.

As far as the tool lives of fully dense composites are concerned, it increased with the increase in TiC/TiN

content in the composites. It was noticed that the maximum tool life was obtained for 4 mass % TiC containing T42 HSS. However, the percentage increment in the tool life above the straight HSS base was higher for composites based on T15 HSS as compared to those based on T42 grade.

Coming to the discussion part of the thesis, the lower optimum sintering temperature for T42 HSS (1230^{o}C) as compared to that of T15 HSS (1270^{o}C) can be related to the lower solidus temperature for the former. The high sintered hardness of T15 HSS as compared to T42 grade can be attributed to the greater solution hardening effect associated with the greater dissolution of alloy carbides in T15 HSS matrix which required a rather higher sintering temperature than T42 HSS. The high triple tempered hardness, compressive yield strength but lower TRS of T42 HSS may be attributed to relatively higher cobalt content, which strengthens matrix, induces greater secondary hardening and temper resistance by resisting the coarsening of the alloy carbides and maintaining the dislocation substructure.

The relatively poor densification behaviour of the composites is attributed to the presence of hard refractory particles which act as diffusion barriers during sintering and hinder the particle rearrangement during the super-solidus sintering. The relatively better densification behaviour of T42 HSS based composites as compared to the corresponding based on T15 is attributed to the better wetting behaviour of the concerned refractory compounds i.e. TiC/TiN with the T42 HSS melt, which contains higher amount of Mo. The better densification behaviour of TiC containing composites based on either HSS as compared to TiN may be attributed to the better wetting behaviour of the former. The enhancement in the mechanical properties for the 4 mass % TiC containing composites based on either HSS is attributed to better bonding of refractory compound i.e. TiC particles with the matrix and their high intri sic hardness.

Better tool life of any cutting tool material is related to a greater combination of hardness, wear resistance and toughness along with elevated temperature compressive yield strength. The higher tool life of T42 HSS containing 4% TiC can be very well related to the presence of higher contents of TiC particles in a strong, temper resistant matrix.

The discussion also covers the relative differences in the bonds of TiC and TiN from the framework of stable electronic configuration model and their relative role on densification and mechanical properties of such particulate composites.

CHAPTER I

LITERATURE REVIEW

I.1. INTRODUCTION:

High speed steels (HSS) are amongst the most important engineering materials in todays life. It takes its name from its capacity to retain a high level of hardness while cutting metals at high speed. It is also appropriately named in view of more recent applications such as bearings for aircraft jet engines and for space-vehicle components. In either event the important factor is that the steel can be hardened to a level up to 1000 HV and that no appreciable softening takes place until about a temperature range of 500-600^{o}C is reached [1].

HSS tools have continued to be of importance in industry for about a century despite the inroads made by competitive cutting tool materials such as cast cobalt alloys, cemented carbides, ceramics and cermets. The superior toughness combined with high hardness of HSS guarantees its place as a cutting tool material [2, 3].

High speed steels are a range of highly alloyed steels which have been developed to possess a desirable blend of the following properties [4]: (a) High hot-hardness, (b) Wear resistance and (c) Toughness. These properties are best achieved by an alloy consisting of uniform dispersion of fine, hard, stable particles, such as carbides in a tough

matrix. In HSS, this has been achieved by alloying high carbon steels with several of the elements W, Mo, Cr, V, Co to give a dispersion of hard alloy carbides in a relatively tough tempered alloy martensitic matrix [5, 6].

The evolution of various grades of HSS has occurred to meet the growing demand of cutting ability for machining high strength alloys. The earliest composition of HSS, T_1 (18% W, 4% Cr, 1% V) is still in use since 1900. Vanadium content in HSS was increased for improving wear resistance but it was limited to 5% owing to the difficulty in hot-working [1]. To get the full benefit of the vanadium addition, the carbon content was correspondingly increased. For improving the hot hardness and secondary hardening characteristics cobalt was added to the basic T_1 grade during the First World War (1914-18) period. But the increased addition of cobalt to HSS results in the strengthening of the matrix which impairs the hot workability in Ingot metallurgy products [1, 78]. Due to the scarcity of tungsten, it was found that Mo could be used in addition to or in place of tungsten in HSS. During the Second World War period, molybdenum and tungsten-molybdenum grades were developed. Since then there has been very little change in the composition of standard HSS grades [3, 7].

In addition to the selection of the best chemical composition, optimum heat treatment is important to achieve the required end properties. The heat treatment of HSS starts with an annealing treatment during which the internal

stresses developed during the previous manufacturing step is relieved and the steel is softened for imparting machinability required for the manufacture of tools. Further, an annealing treatment before a hardening operation provides optimum grain size in the hardened sample which improves the mechanical properties of the tool. During the process of austenitization, the carbides get progressively [1, 8] dissolved into austenite. Therefore, the hardened HSS contains highly alloyed tetragonal martensite (58-80%), highly alloyed retained austenite (15-30%) and undissolved M_6C and MC carbides (5-15%). The steel in this condition is hard, highly stressed, brittle and dimensionally unstable [1, 5, 9, 10]. During multiple tempering, the room temperature as well as hot-hardness is further enhanced due to the transformation of the retained austenite to martensite and secondary hardening due to the precipitation of very fine, stable alloy carbides in the martensite. Techniques for hardening and tempering have been refined considerably over the years to counteract the problems of decarburisation during austenitizing, distortion during quenching and the uniformity of hardening response throughout the cross section. Vacuum heat treatment is the recent advancement in the HSS tool manufacture [73, 74].

In conventional HSS, a problem that has existed for many years is that of carbide segregation and grain growth. The segregation of hard, brittle carbide regions in final large tool steel sections results in undesirable characteristics

which affect the performance of tools both directly and indirectly. Therefore the Powder Metallurgy (P/M) processing of HSS was developed commercially since seventies. P/M route provides a means of making new alloys and composites of tool-steels which cannot be made by conventional melting, casting and hot extrusion methods. In addition to providing a method for making new alloys, the P/M process provides a means of significantly improving the properties of existing tool steels. The other advantages of P/M processed products over their conventionally produced counterparts are [3, 10-12, 21, 22]:

- Superior grindability in the hardened condition.
- Improved toughness of tools in service.
- Isotropic mechanical properties.
- Faster response to hardening treatment.
- More uniform size change as a result of hardening heat-treatment.
- Greater cross-sectional uniformity of hardness.
- Near net-shape processing requiring minimal finishing operations for making finished tools.
- Greater metal yield from the melt.

I.2. VARIOUS P/M ROUTES OF HSS PRODUCTION:

The initial attempts to use P/M technique for the manufacture of HSS was through premix route where use of iron powder, tungsten powder and highly dispersed ferro-vanadium and ferro-chromium was made. The report of first

successful sintering of a standard T1 grade HSS appeared in 1958 [89]. But the process could not be commercialised owing to compaction and homogenisation difficulties. The use of prealloyed HSS powder was reported in 1965 [90] which could be successfully sintered and commercially exploited. All the manufacturing methods used today use a prealloyed HSS powder as the starting material [12].

Various commercial methods for manufacture of P/M HSS have been developed. They differ in terms of their methods of powder production and consolidation techniques. All the P/M processes in general produce a fully dense material with a fine and uniform microstructure giving performance equal or superior to conventional HSS. P/M steels are much better than conventional steels on large sections in higher alloys. The sintered product tend to have coarse microstructure and a certain amount of residual porosity which renders performance inferior to normal steels but still adequate for a wide range of applications [13, 14].

I.2.1. Hot Isostatic Pressing (HIP) of Gas Atomised Powders:

This process consists of producing fully prealloyed powder by inert gas atomisation (Ar, He or N_2) following which the powder is sealed in an evacuated steel capsule, heated and subjected to gas pressure in a hot isostatic press (HIP). The resulting compact is 100% dense, low in oxygen content and segregation free.

This process has been independently developed to the production stage by Asea-Stora (now Uddeholm) in Sweden [18,

19] and crucible steel in U.S.A. [7, 22]. Early technical problems of 100% reliable welds in the steel capsules and that of Argon dissolution during processing which tends to bubble, nucleating at the grain boundaries within the steel during hardening and the consequent embrittlement, have now been overcome. Now, more highly alloyed grades of HSS such as Uddeholm ASP 60 and crucible steel CPM Rex 76 have been introduced. These have better performance than conventional alloys in certain high performance applications. Production of very large pieces weighing several tonnes is now being made by this process.

The HIP process has succeeded in taking a relatively small share of the HSS market because of its high process cost. These costs arise from the fact that in effect an ingot is produced by the HIP of canned gas atomised powder, which still requires extensive hot working to the finished bar. The easier hot working and higher yields offered by the HIP ingot in processing to bar sizes do not appear to offset the lower cost of the conventional cast ingot. This apparantly precludes its use in the bulk bar and rod market on a larger scale. The HIP route is best suited to the production of large sections, where conventional production costs are highest and where major increases in performance have been demonstrated on Hipped P/M HSS [15, 16, 20].

I.2.2. <u>The P/M Extrusion Process</u>:

This process was first developed by Davy-Loewy in the U.K. [23]. Water atomised prealloyed powder of irregular

shape is annealed and cold isostatically pressed into large billets which can be optionally sintered in vacuum before hot extrusion to bar. The principal advantage of this process is its economy. The extrusion press performs for hot compaction also and the separate costs of hot compaction are thus avoided. The hot extrusion press is also a well developed productive machine capable of cycling at rates exceeding 60 cycles per hour with a large consequent throughput. As projected, the operating costs for a medium sized plant show processing costs of M2 HSS (which is claimed to be 85% of HSS market) to be roughly half that of conventional production for sizes capable of direct extrusion. Thus it is also economical to further roll or redraw into smaller sizes.

Unlike gas atomisation, water atomisation produces a powder containing 1500 to 2000 ppm of oxygen almost entirely in the form of surface oxides. This may be reduced to 50-300 ppm by vacuum annealing prior to extrusion; a level comparable to many gas atomised powders. Other than the oxygen content, P/M HSS extruded from water atomised powder is a typical P/M product having an uniformly fine microstructure and cutting performance equivalent to or superior to the conventional product. One interesting variation on the development of improved HSS possible with this process is the introduction of high levels of up to 1% nitrogen into the steel which results in high hardness (an increase of 60-70 HV) without any apparent loss of toughness. A recent

modification to the above process is the use of gas atomised powders in evacuated sealed cans for hot extrusion. By this process the advantages of low oxygen content of the gas atomised powders combined with the reduction in the cold isostatic pressing step helps to further minimise the operating costs and the quality of the products matches with that of the HIPped route [15, 19, 20, 76].

I.2.3. Powder Forging/Sinter-Hot Work:

This technique uses water atomised annealed powder which is cold isostatically (CIP) or die pressed to green preforms. These preforms are sintered in vacuum to a density level of 90% theoretical and then hot forged/rolled to the required sections. The products are fully dense and segregation free. Its oxygen content depends upon the degree of reduction during powder annealing or reduction during sintering. A major problem appears to be the cost of tooling for both cold compaction and hot-working which restricts the process to components needed in long production runs. The microstructure is coarsened by sintering but is still finer and more uniform than conventional products of equivalent size [15, 24, 25, 83].

I.2.4. P/M Near-net Shape Processing:

In this technique annealed water atomised powder having good compressibility is pressed into parts. These are vacuum sintered near the solidus (super solidus sintering)

to densities approaching 100% of theoretical density. The parts are semi precision blanks needing only finish grinding. Suitable products are threading dies, trimming dies, thread chasers, turning tools, automotive engine valve inserts etc. This process has been developed to a production stage in the U.S.A. by C.M.I. [13, 26, 27] (Fullden process) and in the U.K. by Powdrex [28, 29, 30] and Edgar Allen tools. The sintered product has a low oxide content but some retained porosity. The higher sintering temperatures used lead to the formation of coarse carbides as compared to a HIPped product. There is thus doubt as to the suitability of this form of product for severe shock or fatigue loaded applications. However it has already proved commercially acceptable for both cutting and non-cutting applications. This process is generally limited to parts which may be die pressed and are hence required in large numbers [15, 19, 31, 32].

I.2.5. Sinter HIP:

Vacuum sintered HSS, originally developed for metal cutting applications are currently under development for automotive and aerospace applications. Whilst as-sintered materials will probably be adequate for automotive applications, the much more demanding requirements of the aerospace industry have necessitated the development of a near-net shape production route involving the production of very clean powders and post-sinter HIPping (containerless HIP). Such a product will combine the benefits of near-net shape with

that of a HIPped product i.e. finer and more uniform carbide distribution with no residual porosity. Components produced through this process should call for more reliability in service than its cost effectiveness for example the main shaft bearings for aero-gas turbine engines[33, 34, 59].

I.2.6. CAP (Consolidation by Atmospheric Pressure) Process:

This is an expanded P/M technique to manufacture HSS developed by the Cyclops Corporation of U.S.A. This process uses pre-alloyed, gas atomised powders. After a chemical treatment the powders are dried. This chemical treatment removes the surface impurities and activates the powder surface by the uniform coating of the chemical all over the surface. As claimed, the chemical forms an integral part of the steel composition and the quantity is so little that it is not detectable by normal chemical analysis. The dried powders are then loaded into glass moulds (inexpensive boro-silicate glass) and sealed after evacuation. The sealed mould is then placed into a refractory container for handling and charged into a standard air atmosphere furnace for consolidation.

As the temperature of the assembly increases, the glass softens and the vacuum-to-atmospheric pressure differential results in an atmospheric isostatic pressure on the outside wall of the glass mould. The previously applied chemical treatment enhances the diffusion operation, and in combination with the isostatic atmospheric pressure

differential, results in compaction. Upon removal of the refractory container from the furnace, the molten glass surrounding the consolidated preform spalts off as cooling occurs leaving a 95 to 99% dense preform. This preform can then be directly fabricated by hot working operation (rolling/forging) and the product is 100% dense. The material utilisation in this case is 98%. Grades like M2, M3/2, T15 etc. are already being produced.

The primary advantage of this process is its economy. This process has all the advantages of HIP and can be extended to higher volume, intermediate and lower priced grades [35].

I.3. Liquid Phase Sintered HSS and Their Properties:

The most critical step in the P/M production of near-net shape HSS parts is the liquid-phase sintering. Achievement of full density (>98% Th.) during the sintering process is very important from the technological as well as economic point of view [11].

I.3.1. Super Solidus Sintering of HSS:

The liquid phase sintering of HSS pertains to super-solidus category where solid and liquid phases have similar composition. The concept of such sintering was first introduced by Lund [36] who tried to sinter a loose powder mass of Fe containing 0.95% carbon. The sintering temperature chosen was in between the equilibrium solidus and liquidus temperatures.

The liquid phase is formed originally on the free surfaces of the powder particles. Because the particles themselves are the sources of liquid, wetting tends to be immediate, uniform and perfect. Thus the force provided by the surface tension of the liquid acts to rearrange the solid particles and eliminate interparticle voids. The effective viscosity of the liquid is drastically reduced when the temperature is increased and rapid densification occurs. If the amount of liquid present is restricted by temperature, the porosity remaining between powder clusters would be continuous. Under these conditions, an increase in sintering time will cause some decrease in the size of voids, but they will tend to remain continuous for long times. In contrast, if the sintering temperature is increased to produce enough liquid phase, the clustering of particles and the subsequent closing of pores proceeds very rapidly. The original powder particle surfaces totally lose their identity which is evident from the granular fractured surface consistent with grain boundaries but not spherical surface boundaries. Increasing the sintering time at a given temperature results in the growth of the larger pores at the expense of the smaller ones [36-39].

On the basis of sintering studies on M2 HSS, Takajo [40] claims the mechanism of the liquid phase sintering of HSS to be similar to that of heavy alloys, Fe-Cu alloys and other typical metallic systems which are

sintered in the presence of liquid phase [38, 39]. There seems to be disagreement with the supersolidus sintering mechanism that was initially proposed by Lund [36]. In this case a difference in the composition of the liquid phase from that of the solid is being claimed which was not experimentally verified. Takajo's [40] findings that before the liquid phase appears, powder particles are sintered in solid phase to form a skeleton which gets disintegrated by the penetrating liquid to the individual solid grains corroborates the findings of Lund. The grains rearrange their configuration and a rapid densification follows. The solid grains grow by a solution reprecipitation process in which the material transport occurs through the liquid phase. The austenite grain size after cooling is almost determined by the solid grain size at the end of liquid phase sintering. During cooling the liquid phase decomposes into austenite and carbide phases, which are mainly present along grain boundaries. Additional carbide precipitation from the austenite phase is characterised by finer carbides inside the grain.

On the basis of another set of experiments, using water atomised, annealed M2 and T15 HSS powder, Kulkarni [41, 42] has reported different set of findings regarding the densification during supersolidus sintering of HSS. According to his findings a very limited amount of densification occurs through solid state diffusion till the temperature is within a few degrees of the optimum sintering temperature range. In the optimum sintering temperature

range, fine particles melt preferentially to form a small quantity of liquid phase. Melting also occurs over the surfaces of the larger particles and to some extent at grain boundaries within particles. Due to the high viscosity of the liquid phase it does not move over large distances. The densification very likely occurs through rearrangement with substantial contribution by particle deformation as the matrix is very low in strength at this temperature. According to Kulkarni [42], the solution-reprecipitation stage does not play any significant role in the densification of HSS by supersolidus sintering owing to the high viscosity of the liquid phase.

I.3.2. Sintering Variables:

Optimal vacuum sintering occurs on heating within a narrow temperature range located within the austenite, carbide, and liquid phase field i.e. 'sinter gate' [34, 87]. This sinter gate depends on the composition of the particular steel. A relatively wide freezing range [36] and steep liquidus and solidus lines are desirable [39]. In this case the volume fraction of liquid does not change rapidly with temperature fluctuations and the temperature control is less critical. As an example, the sinter gate for M2 is $<5^{\circ}C$ whereas for T1 (and other T grades) it is of the order of $20^{\circ}C$. For this reason the sintering of M2 is more difficult than T1 or any other T grades of HSS. Once the composition is selected, there are other

controllable sintering variables which determine the properties of the sintered product. Figure 1.1 indicates the sintering temperature range for T1 grade HSS.

Powder Production Method: For liquid phase sintering of HSS, a powder compact having high green density, high green strength and low oxygen content produces excellent sintered properties. Gas atomised powders have less oxygen content but result in very poor green strength owing to their round shape. Attempts have been made to consolidate gas-atomised powders by cold compaction and sintering but the high temperature required for effective densification destroys the fine carbide distribution. Finely milled powders could be densified to 99% of theoretical density at relatively low temperature [14] without carbide coarsening or by double pressing and double sintering. Water atomised powders after reduction anneal either in H_2 or in vacuum give green strength, green density and low oxygen content required for achieving the optimum sintered properties [11].

Powder Characteristics and Compaction Pressure: Green and sintered densities for M2 and T15 grades are studied by Kulkarni [42]. The study shows that the green density for the finest fraction is somewhat higher than the coarse fractions and at temperatures less than the optimum, the finest fraction achieves higher sintered density than the coarser fractions (Figure 1.2). The difference in density persists for the samples compacted at lower compaction pressure and sintered at higher temperature, with the

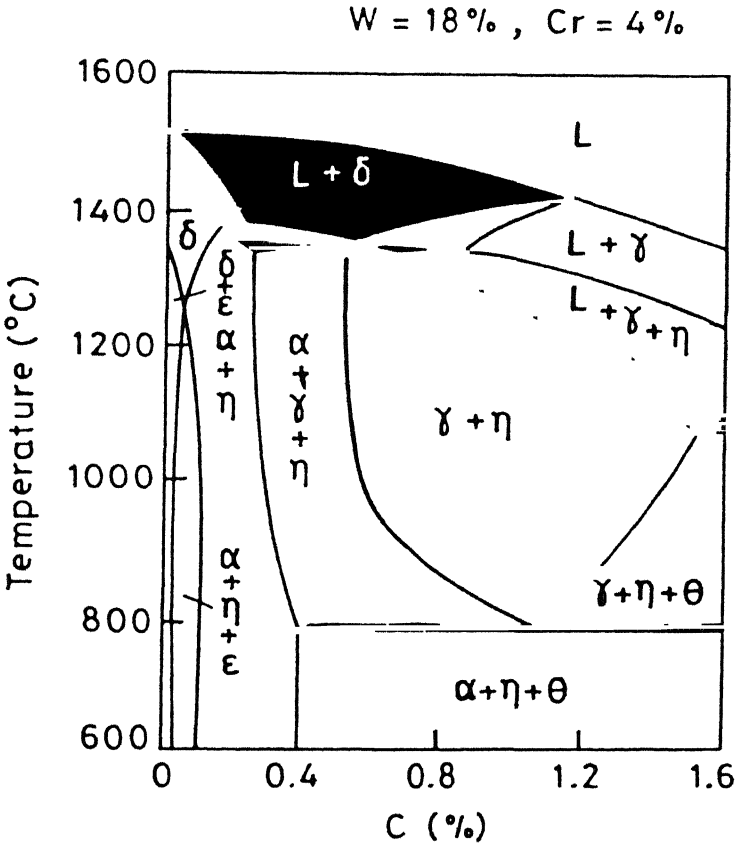

Figure 1.1. Phase diagram of Fe-W-Cr-C system at W = 18%, Cr = 4%, showing the region with liquid phase and the supersolidus sintering temperature range [40].

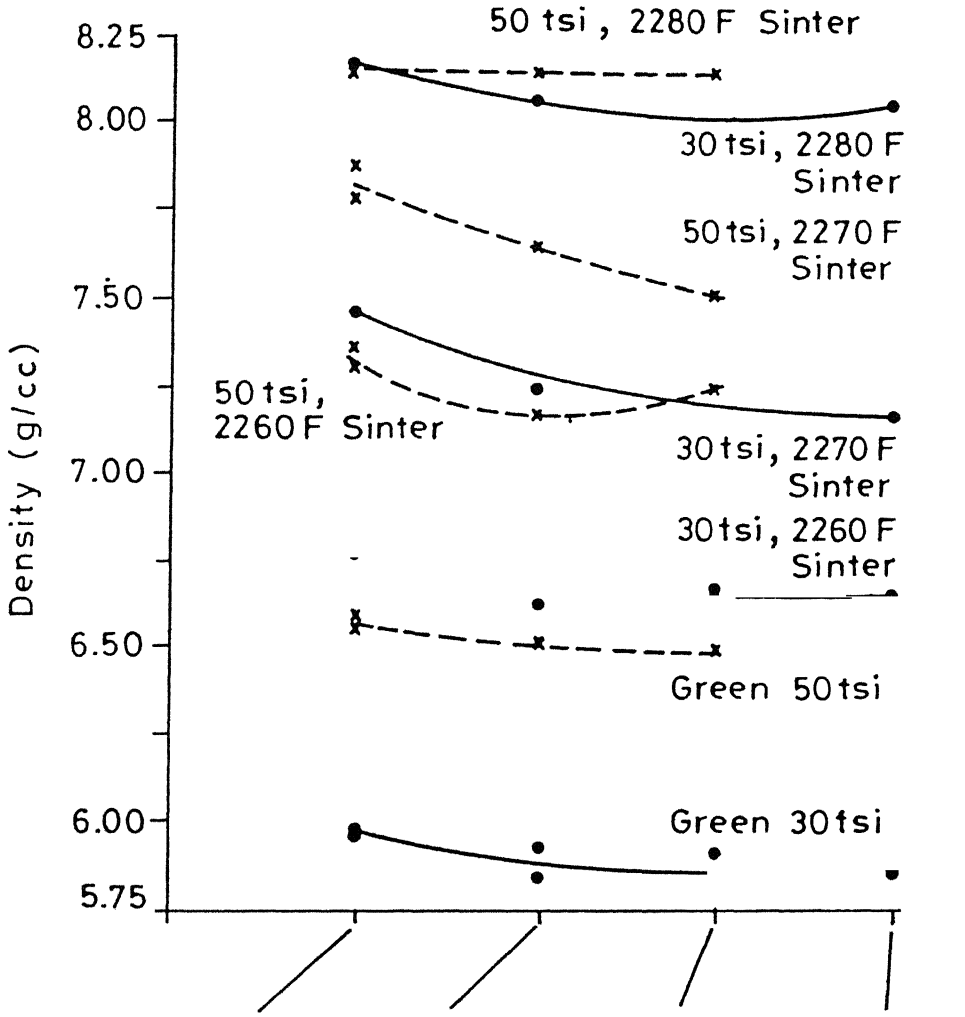

mesh	-400	325/400	270/325	200/270
microns	-37	44/37	53/44	74/53
	Green Strength of 30 tsi (414 MPa) Compacts			
ksi	2.33	3.95	3.89	3.79
MPa	16.1	27.2	26.8	26.1
	Green Strength of 50 tsi (690 MPa) Compacts			
ksi	4.54	7.42	7.66	
MPa	31.3	51.2	52.8	

Figure 1.2. Density and green strength of different sized fractions of water atomised and annealed M2 HSS [42].

coarser fractions showing some large residual pores. At lower sintering temperature, the coarser fractions show many large pores. The large residual pores seen in the coarser fractions sintered at higher temperature would be difficult to eliminate by longer sintering time or with higher temperatures without adversely affecting the microstructure. Thus, to get full density and satisfactory microstructure, it is important to have a reasonable amount of particles of fine size say, less than 45 μm. There is no upper limit on such fine powder fraction provided that the fine fraction does not have excessive oxygen content and the powder lot as a whole has adequate green strength. The oxygen content should not be a problem for vacuum deoxidised powder and for water atomised HSS, low green strength is rarely a problem. Gas atomised powders have coarser carbides than water atomised powders and due to their round shapes, have very poor green strengths [14, 30, 39].

Particle Shape: The sintering temperatures and conditions mentioned for very fine milled powder which are equiaxed [43] and for water atomised powders which are irregular in shape [42] are remarkably similar. Any differences in sintering of the fine milled or pulverised powders seem more because of their higher oxygen content and effect of carbon content. Given the same green density and surface properties, the particle shape per se does not have a bearing on sinterability of HSS powders.

Green Density: As the compaction pressure increases, the green density increases. This higher green density of compacts helps in achieving greater sintered density at the given sintering conditions [42]. Green densities in excess of approximately 85% will trap gas in the pores. Also, higher green densities have an adverse effect on capillary flow of the liquid and hinder final densification. In practice, a green density of about 70% results in effective densification. Density gradients in the green compact is a source of distortion during sintering [39].

Heating Rate: The heating rate is dictated by the furnace capabilities and a need to reduce surface oxides prior to significant densification. Faster heating gives faster densification in the supersolidus liquid phase sintering of HSS since less homogenisation occurs. With slow heating, the compositional gradients in the powder are reduced, giving less densification at temperatures below the optimal sintering temperature. When the powder is heated slowly or annealed prior to supersolidus sintering the volume of liquid becomes invariant with sintering time. Typical heating rates in practice are between 0.5^{o}C and 10^{o}C/min [39].

Sintering Atmosphere: Vacuum sintering is usually the best choice for supersolidus sintering. The use of vacuum avoids the trapping of gas in the pores during the

final densification stage. The pores become closed at approximately 90 to 92% density. An inert gas gives a limiting density of approximately 94 to 96% of theoretical density. Hydrogen is soluble in most metals so the limiting density is higher [39]. Investigations carried out by Grinder et al. [43] indicates that samples sintered in argon or hydrogen contained as a rule relatively large amounts of pores. The pore size decreased with increase in the compaction pressure, but the pore volume seemed to be virtually unaffected. The pores were rounded and fairly evenly distributed in the specimen which led to the assumptions that they were gas pores. Palma et al. [44] have reported on the densification characteristics while sintering T42 HSS added with carbon in gas atmosphere (mixture of N_2-H_2-CH_4). While sintering in the gas atmosphere, over sintering by up to 40°C did not significantly modify the microstructure and did not produce a continuous film of eutectic phase but 10°C over sintering was enough to produce such a film in vacuum. The sintering in the gas atmosphere gave rise to nitrogenation of the steel and allowed a reduction of 20-30°C in the optimum sintering temperature. This increase in the nitrogen content of steel during gas atmosphere sintering did not affect the size, morphology or chemical composition of the type M_6C carbides as compared to those found in the vacuum sintering.

Sintering Temperature: Liquid formation is the first dictate in the supersolidus sintering. The process

temperature must exceed the solidus temperature to induce densification. When surficient liquid forms, there is rapid densification [36, 39, 40]. For each alloy, there is an optimal maximum sintering temperature that relates to the volume fraction of liquid. At temperatures lower than the optimum, pores are not eliminated even with prolonged durations at these temperatures [45]. Temperatures in excess of the optimal range result in grain growth, swelling, slumping or sweating of the liquid out of the compact. Thus, temperature control is essential for good densification, minimum microstructural coarsening and compact distortion.

The temperature range required for sintering to full density is extremely narrow, necessitating uniform temperature distribution in the furnace [39, 40]. Figure 1.3 schematically represents the effect of sintering temperature on carbide size and sintered density, from which, the optimum working range is established [46].

Sintering temperature is undoubtedly the most important process variable in supersolidus sintering of HSS. The optimum temperature of sintering a specific lot of powder depends on its actual chemistry and some process variables. For example, finer powder, carbon addition and higher green density may allow the use of somewhat lower sintering temperature. Therefore, it is prudent to select sintering temperature based on a few sintering tests. The solidus of HSS is extremely difficult to measure experimentally and attempts aimed at that goal have been unfruitful

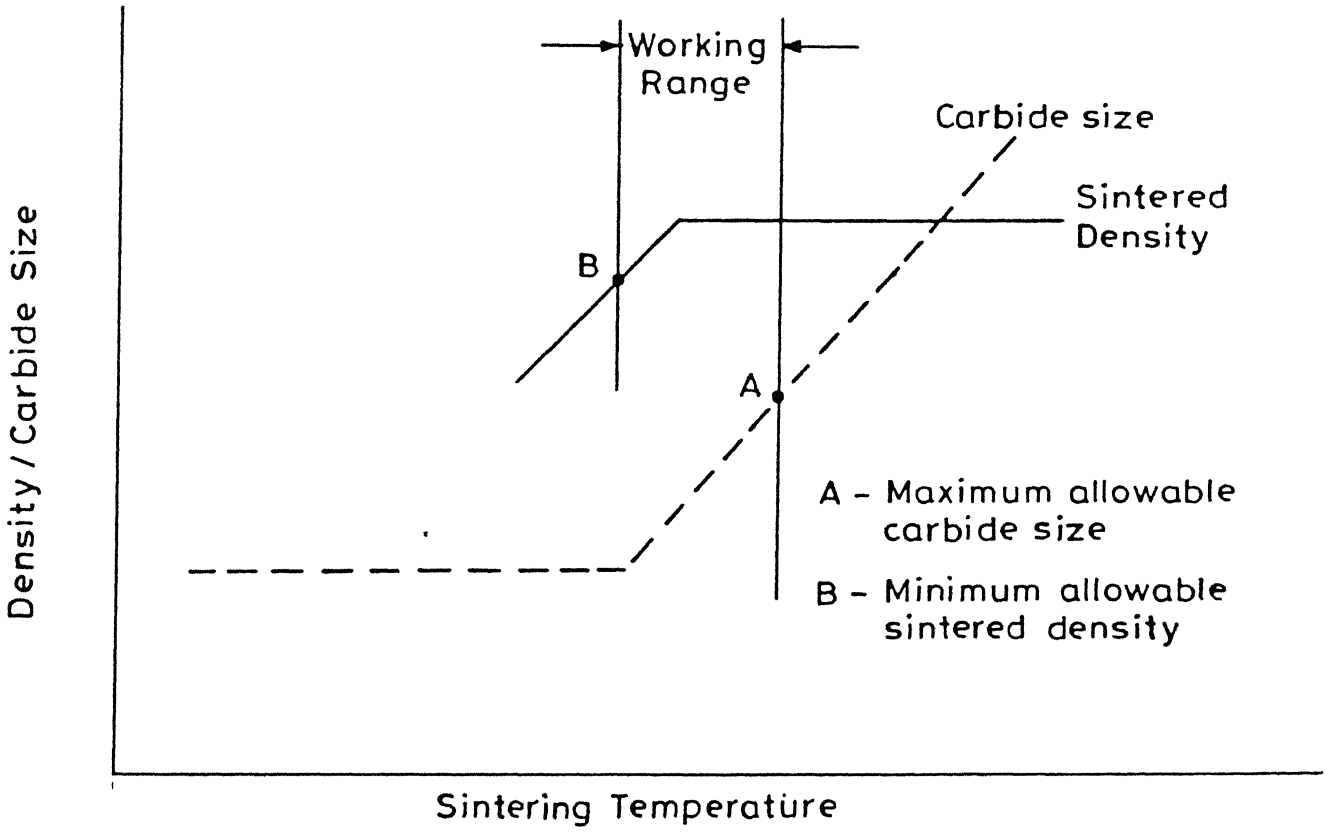

Figure 1.3. Sintering response of high speed steels (schematic) [46].

[47]. Moreover the solidus can be expected to depend on the local composition which may be different from the average bulk chemistry [41].

Sintering Time: At the optimum sintering temperature, full density is obtained within reasonable sintering period [36, 37, 39, 40, 48]. Prolonged holds give relatively minor benefits and often cause property or density decrements. One consideration would be the increased homogeneity achieved with prolonged holds, but this may come at the expense of microstructural coarsening.

Cooling Rate: The microstructure and properties observed after sintering depend on the cooling rate [30, 39, 40, 51]. Additionally phase transformations can take place during cooling which affect the properties. There is danger in very rapid cooling because solidification pores may form. Holds at temperatures just above the solidus during cooling increases the final density by minimising solidification porosity. During slow cooling, the grain boundary films that were liquid at the sintering temperature will decompose. This can be beneficial to the mechanical properties but adds expense to the sintering cycle.

Effect of Oxygen Content: Oxygen affects the sintering of HSS by reducing carbon content during sintering. Oxygen from the annealed powder reacts with carbon during sintering to form carbon monoxide. About 0.01% C is lost in the atmosphere for every 0.01% of oxygen present

in the annealed powder. This reaction reduces the oxygen to less than 200 ppm during vacuum sintering [30, 54, 75]. Figure 1.4 shows the effect of oxygen content in the HSS powder during sintering.

Role of Carbon Addition: Given the total carbon content, Kulkarni et al. [52] have studied the effect of graphite addition on the sinterability between powder that is fully prealloyed and powder which has a small quantity of graphite added to it. It was felt that the free graphite may enhance sinterability by forming low melting eutectic phase at the interfaces with the powder particles. The study has indicated that given the total carbon content and sintering conditions, there was little difference in terms of density achieved or the quality of the microstructure. This study suggested that graphite addition up to 0.3% for a close control of the carbon in tool steels is sound. This is due to the high rate of diffusion of carbon in steel at the full density sintering temperature. The addition of carbon was found to promote [44, 45, 53] sintering in several ways as well as bringing the final composition up to the specified value. The residual porosity with carbon addition was eliminated, the temperature range extended over which maximum density was achieved and the microstructure at the optimum sintering temperature improved. Kulkarni et al. [52] have proposed an empirical formula for the quantity of carbon to be added to get the optimum carbon content, which is:

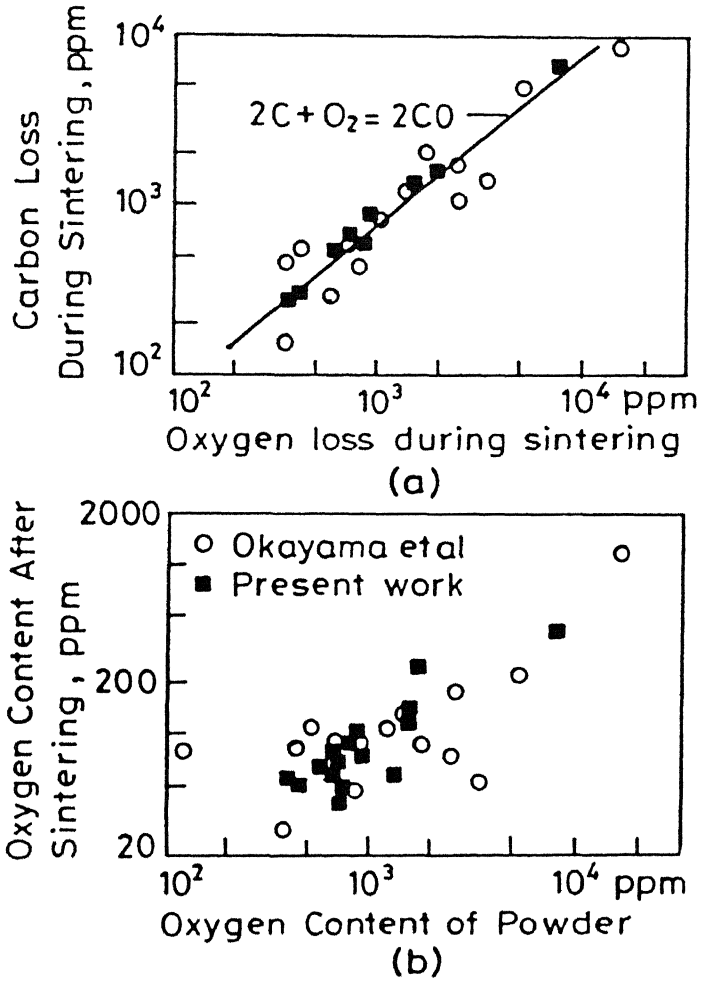

Figure 1.4. Relationship between oxygen content of powder and carbon loss during sintering and between oxygen contents before and after sintering [30].

$$\text{Carbon to be added} = 0.0326(W' - W) + 0.0625(Mo' - Mo) + 0.2353(V' - V) + 7.5 \times 10^{-5}(O' - O)$$

Here, W', Mo', V' indicate the wt. % of elements in powder and O' in ppm of O_2 in powder. W, Mo, V are the wt. % and O in ppm in the compact desired.

Role of Sintering Aids: Similar to the beneficial effects of carbon addition in improving the sinterability of HSS, other additives in smaller quantities have been tried which lower the sintering temperature, increase the liquid volume % resulting in rapid and uniform densification and microstructure. Carbon is an integral part of the HSS composition and does not result in unwanted phases, but the use of any other additive such as boron [12, 54], Cu-P [55-58] result in newer phases. The effect of these additives has negligible effect in the carbide morphology and mechanical properties of the sintered products.

I.3.3. Mechanical Properties of Liquid Phase Sintered HSS:

The mechanical properties are dependent on the residual porosity and sintered microstructure. Figure 1.5 schematically shows the as sintered microstructure in P/M tool steels. Sintered HSS can suffer from three major strength reducing microstructural defects viz. (i) metallic/non-metallic inclusions caused by contamination during powder processing, (ii) porosity, if the sintering time or temperature are chosen too low, (iii) carbide/grain coarsening if the sintering temperature or time are too high

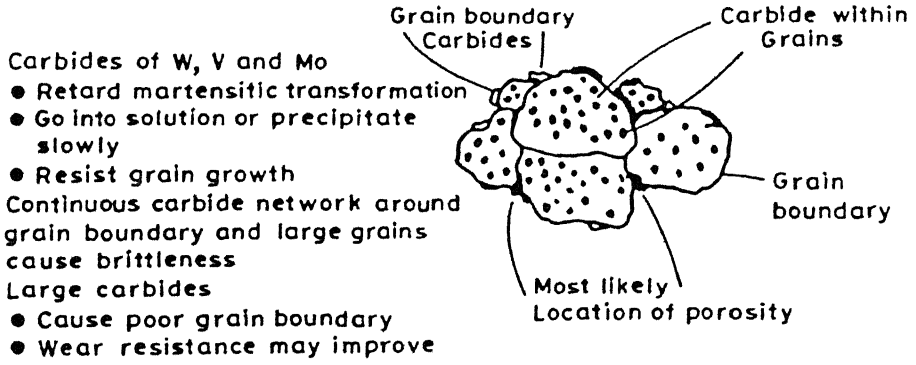

Figure 1.5. Microstructure of as-sintered P/M HSS (schematic) [illegible]. [52]

[59, 60]. Porosity of 1% reduces the toughness in terms of TRS (Transverse Rupture Strength) more than 10% for M35 and 25% for 3% porosity. Over sintering due to excessive temperature or time yields a coarse carbide structure again causing unfavourable TRS. The decrease in TRS is of the order of 10-25% for slight to excessively overheated case. P/M HSS is always used after a suitable hardening treatment and the starting point in achieving optimum end properties is an optimum sintering in terms of full density with a sound and uniform microstructure. Table I.1 gives a survey of mechanical properties as reported by various workers while processing various grades of P/M HSS through direct sintering route.

I.4. P/M HSS BASED PARTICULATE COMPOSITES:

The hardness and wear resistance of any grade of HSS depend on the volume fraction of the hard phases in the matrix and the matrix hardness itself. The superiority of any grade of cutting tool material depends on the high temperature stability of the different phases, for which the hot compressive yield strength can be an indicator [1-4].

The wear resistance of HSS is directly related [2, 10, 16] to the volume fraction of primary carbides (MC + M_6C types) in the matrix. It has been reported [61, 62] that the wear resistance can be linearly related to the volume fraction of MC type of carbides. Through alloy addition, it is possible to reach a very high primary carbide content

Table I.1: Mechanical properties of high speed steels processed through direct sintering route.

Grade	Processing conditions	Mechanical properties	Author/s	Reference No.
M2	Vacuum sintered at 1245°C, Oil quenched from 1200°C, Triple tempered at 550°C, 45 min	Triple tempered, Hardness = 820 HV Impact strength = 10 J/cm^2	I. Kvasnicka	85
M3/2	Vacuum sintered at 1150°C, Cu-P alloy used as sinter aid	Sintered hardness = 730 HV_{10} Sintered TRS = 1595 MPa	I.M. Martins, M.M. Oliveira, and H. Carvalhinhos	57
M3	Vacuum sintered at 1220°C, 1 hr Hardened and triple tempered (conditions not mentioned)	Triple tempered, Hardness = 53 HRc TRS = 2100 MPa	R.A. Queeney, J.L. Miller, R.J. Beltz, and J.D. Dankoff	63
M35	Vacuum sintered to full density, Hardened and triple tempered (temperatures not mentioned)	Triple tempered, Hardness = 65 HRc TRS = 2400 MPa	P. Beiss, R. Wahling, and D. Duda	59
T15	Vacuum sintered to full density, hardened and triple tempered	Triple tempered Hardness = 67.7 HRc TRS = 1550 MPa	P. Beiss, R. Wahling, and D. Duda	59
T15	Vacuum sintered at: (i) 1260°C, 1 hr (ii) 1270°C, 15 min (iii) 1270°C, 1 hr All samples austenitized in salt bath at 1220°C and oil quenched, Triple tempered at 520°C, 1 hr	(i) Sintered hardness -HV_{30} = 589; Triple tempered hardness = 885; Triple tempered TRS, MPa = 2027 (ii) 602; 877; 2001 (iii) 599; 883; 1850	M. Santos, I.M. Martins, M.M. Oliveira, and H. Carenlhinhos	33

contd...

Table I.1 (continued)

Grade	Processing conditions	Mechanical properties	Author/s	Reference No.
T42	Vacuum sintered at 1245°C, Salt bath heat treated. Austenitized at 1175°C, Triple tempered at 525°C	Hardness: HV_{50}-1000	C.S. Wright, A.S. Wronski, and M.M. Rebbeck	84
Steel 12-8-10, W = 12%, Mo = 8%, V = 10%, Co = 10%	Vacuum sintered at 1180°C, Quenched from 1200°C, Triple tempered at 550°C, 1 hr	Triple tempered, Hardness = 70.3 HRc BRS = 1800 MPa	N. Uchida, and H. Nakamura	66
Steel 13-11-8, W = 13%, Mo = 11%, V = 8%, Co = 8%	- do -	Triple tempered, Hardness = 71.6 HRc BRS = 2100 MPa	- do -	66
Steel 19-14-6, W = 19%, Mo = 14%, V = 6.5%, Co = 8%	Vacuum sintered at 1180°C Quenched from 1220°C, Triple tempered at 550°C, 1 hr	Triple tempered, Hardness = 72.1 HRc BRS = 1700 MPa	- do -	66

in HSS. The high vanadium, high carbon grade of M2 HSS is an example. But, indefinite increase in vanadium and carbon is not practicable in wrought processing due to difficulties in hot working [1, 62]. Through P/M route it is possible to get a HSS with higher volume fractions of hard phase by enriching the HSS composition with hard, refractory oxides/nitrides/carbonitrides/carbides. The hardness and melting temperature of the various candidate additives is given in Table I.2. This process of enrichment of HSS with hard particles to form a composite for greater wear resistance is still in research stage and there has been no report of its commercial adoption.

I.4.1. Oxide Enriched HSS Composites:

Queeney et al. [63] and Martins et al. [57] reported the work on enrichment of M3 and M3/2 grades of HSS respectively by Al_2O_3. Al_2O_3 is hard (HV 24 GPa) and stable at high temperatures. It was therefore considered to be a potential candidate [64] for reinforcing HSS for enhancing the wear resistance properties. Composites with 5 wt. % Al_2O_3 could be vacuum sintered to full density. Even though there was enhancement of wear resistance properties, the toughness decreased. Queeney et al. [63] reported a drop in the modulus of rupture value in 4-point bend test to 1500 MPa from 2000 MPa when the Al_2O_3 increased to 5% from 2.5%. It further dropped to 1000 MPa for 10% addition. Martins et al. [57] reported a low TRS of 1240 MPa for fully dense samples containing 5% Al_2O_3 addition. The increase in the

Table 1.2: Hardness and melting points of various refractory compounds as candidate additives to HSS.

Refractory compound	Melting point, ^{o}C	Room temperature hardness, HV Kg/mm^2
Al_2O_3	2015	2600
AlN	2235	1225 (Knoop 100 gm)
BN	3000	10600
TiN	2900	1770 (Knoop 100 gm)
TiC	3180	2900
VC	2810	2800
NbC	3500	2400
TaC	3877	1800
HfC	3887	2913
WC	2867	2400
Mo_2C	2687	2000
SiC	2500	3000
ZrC	3532	2600
Cr_3C_2	1890	1300
$Cr_{23}C_6$	3532	2600

wear resistance was directly proportional to the Al_2O_3 content. It is explained that due to lack of interaction between the Al_2O_3 particles and the matrix, porosity is frequently observed which leads to poor toughness of the composite.

I.4.2. Nitride Enriched HSS Composites:

Work on the enrichment of HSS by refractory nitrides such as AlN, TiN, BN has been reported by various workers. Arai and Komatsu [65] have reported the effect of AlN, TiN and BN addition to M2 HSS. Composites were prepared by canning and extrusion of the mixture of water atomised HSS and the nitride powders (up to 20%). An addition up to 5% of the various nitrides resulted in the improvement of wear resistance of M2 HSS. Further addition resulted in a decrease in wear resistance which the authors attribute to the lack of densification. They reported an increase in hardness up to 63 HRc for 5% AlN, and 65 HRc for 5% TiN addition. Beyond 5% addition, the hardness as well as wear resistance deteriorated. Similar results were reported by Uchida and Nakamura [66] and Martins et al. [57]. As through normal vacuum sintering, TiN enriched samples did not achieve full density, Uchida and Nakamura [66] resorted to post sinter HIPping. Martins et al. [57] while using M3/2 grade HSS had to use a sinter aid (Cu-P alloy) along with free carbon for enhancing the densification during liquid phase sintering. 98.5% relative density was achieved for the composites

containing 5% TiN, but the TRS values obtained was only 1632 MPa which was considered to be low. Uchida and Nakamura [66] while working on very high alloy steels, reported the Bend Rupture Strength to be ranging from 1000-3000 MPa on samples HIPped after sintering.

I.4.3. Refractory Carbide and Carbonitride Enriched HSS Composites:

The potential carbides which have been investigated as additives were VC, TiC, TaC, NbC, SiC, WC, Mo_2C, HfC, ZrC and Cr_3C_2. The steels which provided the matrix were M2, M3/2 and T1 grades of HSS. The earliest report on the sintering of a mixture of VC/TiC with highly alloyed steel powder was by Heiss and Kieffer [67]. Wilson and Jackson [68] studied the effect of VC/TiC addition to M2 HSS and reported that the sintering temperature for achieving full density increases with the addition of monocarbides more so for TiC than VC. They had to resort to hot-working after sintering to achieve full density. The addition of either TiC or VC to M2 resulted in marked improvement in wear resistance.

Kieffer et al. [12] studied the effect of VC, TiC, NbC, TaC, HfC and ZrC addition to M2 HSS and reported the substantial increase in the cutting tool life or cutting speed of M2 HSS. Full density could be achieved after hot forging of the liquid phase sintered composites. Addition of these monocarbides extends the sintering temperature and

time possibly because of poor wetting of the carbides by the matrix metal at the sintering temperature. As reported, the hardness increased from 63 HRc to 69 HRc at the cost of TRS which went as low as 130 Kg/mm^2 for samples containing 10% TiC. On the basis of their study, they suggested the addition of $TiC.Mo_2C$ or $TiC.VC.Mo_2C$ for improvement of mechanical properties.

The effect of VC (up to 30 mass %) addition on the mechanical properties of sintered high speed steel of PX 16 grade (nearest AISI equivalent grade T15) made from water atomised powder has been reported by K. Yamada, H. Kohzuki and Y. Okuno [86]. They reported that though there was increase in the Vickers hardness with the increased addition of VC, the TRS decreased. Also, with increased addition of VC, higher sintering temperature was required and this resulted in increased carbide grain size.

Bolton [55] while studying the effect of various carbide addition to M3/2 HSS, classified the carbides into 3 groups. The first group consists of carbides formed from elements which are not strong carbide formers e.g. chromium and silicon, and which dissolve completely within the HSS matrix at the required sintering temperature. They are unlikely to give improvements in wear performance. The second group consists of carbides formed from elements intrinsic to the normal HSS composition e.g. molybdenum and tungsten. They partially dissolve during sintering and become altered in composition and structure. The effect of

adding such carbides was to increase the volume fraction of primary carbide phase, but the carbides formed were of the same type that occur naturally in high speed steel. The third group, consisting of carbides from strong carbide forming elements e.g. the cubic monocarbides of vanadium and titanium have some but limited solubility in HSS. The wetting and interfacial bonding during sintering associated with limited solubility lead to the essential carbide additive being retained as a dispersed phase which improves the wear resistance. An addition of up to 5% of these carbides could be blended into the HSS without significant loss of sinterability. The author reported an increase in the as sintered hardness up to 800 HV for Mo_2C addition. Arai and Komatsu [65], while working on SiC, WC and TiC addition to M2 HSS, and other workers [69, 70, 71], while studying the effect of TiC/NbC addition to T1 HSS, reported similar findings.

Addition of Ti(C,N) (up to 10%) to T1 HSS were studied by Kiparisov et al. [72]. Their finding indicates that the Ti(C N) particles increase the sintering temperature and addition up to 10% can be made without hampering sinterability. As found with TiC addition, Ti(C,N) remained unaffected at the sintering temperature and their presence enhanced the tempered hardness as well as wear resistance.

I.5. SCOPE OF THE PRESENT INVESTIGATION:

The cutting ability and wear resistance property of HSS depends on a desirable blend of properties such as:

(a) Room temperature hardness, (b) Toughness, (c) wear resistance and (d) Hot compressive yield strength. These properties are best achieved by an alloy consisting of uniform dispersion of fine, hard and stable particles in a tough matrix. In HSS, this has been achieved by alloying high carbon steels with several of the elements W, Mo, Cr, V and Co to give a dispersion of hard alloy carbides in a relatively tough tempered alloy martensitic matrix.

The wear resistance in HSS is directly related to the volume fraction of MC type of carbide. Through alloy addition such as increasing V and carbon content, it is possible to reach a very high volume fraction of primary carbides in HSS, but indefinite increase in vanadium and carbon is not practicable in wrought processing owing to difficulties in hot working. Through P/M route it is possible to get a HSS with high volume fractions of hard phase by enriching the HSS composition with hard, refractory, oxides/nitrides/carbonitrides/carbides. Such a composite will have greater wear resistance and improved cutting ability. Through near-net shape processing route, a semi-precision part is obtainable which needs only finish grinding.

In the present investigation two refractory titanium based compounds viz. TiC and TiN have been selected. This was done taking into view the subtle distinction in their properties because of their different bond strengths [88]. Among various P/M processing routes, the present investigation

singularly focusses on liquid phase sintering route, as the process is less capital intensive and could be easily adopted in a plant processing conventional sintered products.

The sintering study of HSS enriched with refractory TiC/TiN compounds necessitated the selection of the composition of the high speed steels which offer wider 'sinter gate' as in this case the precise temperature control is less critical. The tungsten grades of HSS have relatively wider 'sinter gates' (20^{o}C) as compared to molybdenum grades (<5^{o}C). T15 and T42 grades are well known as wear and cutting tool materials owing to their high contents of carbide forming elements like W and V. In addition, T42 has a higher cobalt content (10%) as compared to T15 (5%). The matrix strengthening effect of cobalt combined with enhanced resistance to tempering enables T42 tools to be used for larger cuts at faster speeds. Any further improvement in the cutting ability and wear resistance using hard phase enrichment would result in further techno-economic advantage associated with these grades. These grades therefore provide ideal matrix for further studies using hard refractory compound enrichments.

The starting point in achieving the optimum heat treated properties in P/M HSS is an optimum sintered product in terms of full density with a sound and uniform microstructure. These attributes can be achieved through judicious control of the sintering parameters during liquid phase sintering of which temperature is most critical. The

optimum sintering temperature depends on its actual chemistry and some process variables like powder characteristics, compaction pressure etc. With the addition of refractory carbides to the HSS powder, the sinterability becomes unpredictable. It is therefore prudent to select sintering temperature based on careful sintering trials.

P/M HSS is always used after a suitable hardening and tempering treatment. The type of heat-treatment dictates the end properties of sintered HSS. For making a comparative study, between the two grades of HSS, it becomes necessary that they be given similar hardening treatments and tempered at the temperature which results in peak secondary hardness. This requires the optimisation of tempering temperature and the number of temperings through tempering experiments.

Evaluation of the mechanical properties like hardness, TRS and the study of the microstructure and magnetic properties are the process control requirements after every manufacturing stage for ensuring the best of processing of a HSS product. Compressive yield strength at room as well as elevated temperature of the fully heat treated tool sample is an important criteria in the selection of a cutting tool. The various properties determined on the tool samples in the laboratory only help to select the potential tool materials as no conclusive prediction of the actual tool performance can be made from these results. It is therefore necessary

to conduct a standard cutting tool life test for any potential cutting tool material . With this it becomes possible to make a direct comparison of the actual cutting performance of various tools and select the best composition.

CHAPTER II

EXPERIMENTAL PROCEDURE

The detailed experimental procedures carried out in the present investigation are presented in this chapter.

II.1. POWDERS AND THEIR CHARACTERISTICS:

High Speed Steel Powders: The HSS powders used in this investigation were prealloyed, water atomised and annealed. T15 HSS powder (obtained from two sources) and T42 HSS powder had the following composition and physical characteristics as furnished by the suppliers.

i) T15 HSS Powder:

Source-I: Sinter-Metallwerk Krebsoge, Germany

This powder was used for the optimisation of heat treatment conditions and for T15-TiC particulate composites.

Chemical Composition, mass %		
carbon	-	1.59
Chromium	-	4.23
Cobalt	-	4.99
Copper	-	0.08
Manganese	-	0.26
Molybdenum	-	0.55
Nickel	-	0.15
Tungsten	-	12.50
Vanadium	-	4.75
Oxygen	-	1000 ppm

Physical Characteristics

AD = 2.1 gm/cc

Flow rate = 42.7 sec/50 gms

Compressibility = 5.52 gm/cc (at 30 Tsi)

Sieve Analysis

mesh	% cumulative mass fractions
+100	0.08
+150	7.53
+200	29.10
+350	64.30
-350	35.70

Source-II: M/s British India Steels, Ahmedabad, India

This powder was used for the enrichment study using TiN.

Chemical Composition, mass %		
Carbon	-	1.60
Chromium	-	4.12
Cobalt	-	4.95
Manganese	-	0.40
Molybdenum	-	1.31
Tungsten	-	12.30
Vanadium	-	5.26
Sulphur	-	0.04 max
Phosphorous	-	0.04
Oxygen	-	1400 ppm

Physical Characteristics

A.D. = 2.49 gm/cc

Flow rate = 41 sec/50 gms

Compressibility = 5.54 gm/cc (at 30 Tsi)

Sieve Analysis

mesh	% cumulative mass fraction
+100	0.09
+150	9.15
+200	27.95
+350	68.15
-350	31.85

ii) T42 HSS Powder:

Source: M/s British India Steels, Ahmedabad, India

This powder was used for the optimisation of the heat treatment parameters of T42 HSS as well as for the enrichment studies using both TiC and TiN.

Chemical Composition, mass %		
Carbon	-	1.38
Chromium	-	3.96
Cobalt	-	10.60
Manganese	-	0.22
Molybdenum	-	4.01

Physical Characteristics

A.D. = 2.42 gm/cc

Flow rate = 43.3 sec/50 gms

Compressibility = 5.58 gm/cc (at 30 Tsi)

Tungsten	-	9.70
Vanadium	-	2.39
Sulphur	-	0.044
Phosphorous	-	0.044
Oxygen	-	700 ppm

Sieve Analysis

Mesh	% cumulative mass fraction
+100	4.49
+150	15.32
+200	35.85
+350	81.62
-350	18.38

Refractory Compounds:

i) TiC Powder

Source: Treibacher, Austria

Chemical Composition, mass %			Physical Characteristics
Carbon (total)	-	19.40	Particle size (FSSS) = 3.45 μm
Carbon (free)	-	0.08	
Fe	-	0.05	
O	-	0.06	

ii) TiN Powder

Source: Hermann C. Starck, Berlin, Goslav, Germany

Chemical Analysis, mass %			Physical Characteristics
Titanium	-	77.8	A.D. = 1.48 gm/cc
Nitrogen	-	21.9	Particle size (FSSS) = 7.2 μm
Oxygen	-	0.3 (max)	

Powder Characterisation: The as received powders were characterised to check the validity of the supplier specifications.

Chemical Analysis: The carbon and oxygen analysis

of the as received T15 and T42 HSS powders was done to find out the concentration of these elements prior to sintering. Their determinations were carried out on 'Leco' carbon and oxygen determinator.

Particle Shape: The microphotographs of as received T15 HSS, T42 HSS, TiN and TiC powders were taken under 'JEOL' JSM-840A Scanning Electron Microscope (SEM) at a magnification of 500X.

Powder Size: Sieve analysis of the HSS powders were carried out in an automatic sieve shaker machine as per MPIF Standard No. 05. For sieving, 100 gms of powder was taken and the Tyler Series sieves corresponding to numbers 100, 150, 200 and 350 were used.

The size distribution of TiC and TiN powder was checked using Coulter Counter analysis using Coulter Counter (Model Z_B and B). In the present investigation, NaCl was used as the electrolyte.

II.2. POWDER MIX PREPARATION AND ROOM TEMPERATURE COMPACTION:

0.7 mass % magnesium-stearate as solid lubricant powder was blended with the as received T15 and T42 powders respectively for 30 minutes using a laboratory double cone blender of Netzsch-Feinmahltechnik, Gmbh make.

For the composite composition, 2, 4, 6 and 8 mass % refractory compounds (TiC or TiN) respectively and 0.7 mass % Mg-stearate were added to T15 or T42 HSS powder and blended

for one hour. The uniformity of mixing was checked under an illuminated magnifying lens.

The blended powder was pressed into green compacts in the shape of tool-bits of dimensions 7.00 X 11.00 X 76.70 mm^3 on an automatic mechanical press of 200 Tons capacity of 'Dorst', Germany make. These green dimensions were derived in to achieve the specified sintered dimension of 6.5 X 9.5 X 75.0 m^3.

Compaction pressure used was fixed at 850 MPa for straight compositions and in the range of 850-900 MPa for the composite compositions to ensure a constant green porosity of 24-26%. Green porosity was calculated on the basis of dimensional measurements.

From each of these green tool-bits, smaller samples of approximately 10 mm length were cut using a fine HSS hackshaw blade for sintering study. For the sintering of the TRS samples, three samples of approximately 25 mm length each were cut.

II.3. SINTERING:

Sintering experiments were carried out in a SiC resistance heated tubular furnace. The furnace of 4.4 cm internal diameter had a constant temperature zone of 7 cms length. The sintering was carried out under a dynamic vacuum of the order of 5 X 10^{-2} m bar and the components were cooled down to 300°C before opening the vacuum system to air. Green samples were placed on a fused alumina tile, which in

turn was kept on a graphite boat within the constant temperature zone. The furnace temperature was controlled within $\pm 2.5^{\circ}C$ using a proportional temperature controller.

The sintering temperature was varied from $1250^{\circ}C$ to $1320^{\circ}C$ for T15 HSS based composites and from $1220^{\circ}C$ to $1320^{\circ}C$ for T42 HSS based composites in steps of $10^{\circ}C$. Presintering soak [75], at $90^{\circ}C$ less than the selected sintering temperature was given for 2 hours to all the samples after which faster heating to the sintering temperature was done. The holding period at the sintering temperature was maintained uniformly for 90 minutes for all the samples. Then natural cooling under vacuum to room temperature followed.

II.3.1. Sintered Density Measurement:

The sintered densities of the samples were measured using water displacement method described by Arthur [77]. The sintered samples were impregnated with xylene in vacuum and the following formula was used to calculate the sintered density:

$$\text{Density} = \frac{\text{Weight of compact in air}}{\text{Wt. of xylene impregnated compact in air} - \text{Wt. of xylene impregnated compact in water}}$$

The samples which achieved densities in excess of 98% theoretical density were considered to be fully dense. The theoretical density for the composites were calculated using the rule of mixture. The lowest sintering temperature at which full density obtained, was taken as the optimum

sintering temperature for that composition. All subsequent sinterings were carried out at the optimum sintering temperature.

II.4. HEAT TREATMENT:

Samples sintered to full density were chosen for heat treatment studies. The critical temperature for transformation annealing was initially determined. All the heat treatment operations such as transformation-annealing, austenitizing and oil quenching and triple tempering were done in air. To prevent the samples from decarburization, they were wrapped in a special graphite coated foil (Sintercast Protectool wrap of stainless steel) before introducing into the heat treatment furnace.

II.4.1. Determination of Critical Temperature for Heat Treatment:

Due to scant informations on the critical transformation temperatures of P/M grade of T15 and T42 HSS, the AC_1 and AC_m temperatures were determined. For this purpose a DTA of Linseis, Germany make was used. Heating rate during the test was $5^{\circ}C$/min to $1100^{\circ}C$ after which cooling was done at the same rate to the room temperature. The temperature at which an endothermic reaction peak appeared indicated the AC_m temperature during heating and the temperature at which the exothermic reaction peak ends during cooling indicated the AC_1 temperature. On the basis of this information, the transformation annealing temperatures were determined.

II.4.2. Transformation Annealing:

The purpose of the transformation annealing was to relieve the internal stresses developed in the sintered compacts during cooling from the sintering temperature and to provide a refined grain structure prior to further hardening and tempering treatments. Samples were held at 900°C, for 1 hour and at 760°C for 4 hours. From 760°C, the samples were air cooled to room temperature.

II.4.3. Hardening:

An uniform austenitization temperature of 1200°C was selected for both the grades of HSS i.e. T15 and T42 and their based composites. Each batch of annealed samples was heated in the same furnace as was used for sintering. During austenitization, samples were slowly heated to 850°C and soaked for 60 minutes after which faster heating was done to 1200°C. Holding time at the austenitization temperature was kept fixed for 10 minutes in each case. After this, the samples were quenched in mineral oil to room temperature.

II.4.4. Tempering:

Oil quenched samples were subsequently triple tempered isothermally in still air. The tempering time was kept uniform for 1 hour during each tempering. Tempering temperature was determined in tempering trials where the temperature was varied from 520°C to 600°C in steps of 20°C. After every tempering the samples were air cooled to room temperature

and Vickers hardness was measured. On the basis of the tempering temperature vs. hardness plot, the optimum tempering temperature was selected. Samples for mechanical property evaluation such as TRS and elevated temperature compressive yield strength were triple tempered at this optimum temperature prior to the tests.

II.5. MECHANICAL TESTS:

Hardness, Transverse Rupture Strength (TRS), and compressive yield strength measurements at room and elevated temperature were carried out.

II.5.1. Hardness:

Hardness of the sintered as well as heat-treated samples after every stage of heat-treatment were measured on Vickers hardness testing machine Model HPO 250 of "Fritz Heckert", Leipzig make, using a load of 10 Kg (98 N). At least 5 indentations were taken on each specimen and the average value reported.

II.5.2. TRS (Transverse Rupture Strength):

For the measurement of TRS, samples sintered at the optimum sintering temperature and heat treated as per schedule described earlier were used. Samples having approximate dimensions of 6.5 X 10.0 X 22.0 mm^3 were positioned in the standard TRS test fixture (ASTM B406-81). The tests were carried out at room temperature on the MTS-810 material

testing system machine at a cross head speed of 0.5 mm/min. The transverse rupture strength (TRS) was calculated according to ASTM Standard B528-76, as follows:

$$\text{TRS in MPa} = \frac{3PL}{2t^2w}$$

where P is the force in Newtons required to rupture the specimen, L is the distance between the bottom supports in meters, w and t are the width and thickness of the specimen in meters respectively.

The average result of 4-specimens from each condition were taken as the TRS value.

II.5.3. Compressive Yield Strength:

Room temperature as well as elevated temperature compression tests were performed to find out the 0.2% offset compressive yield strength of the materials in triple tempered condition. MTS-810 materials test system machine was used for this purpose and the test temperatures chosen were, room temperature (18°C), 200°C, 400°C and 600°C respectively. Cylindrical samples of approximate dimensions 6 mm diameter and 9 mm length were machined out of the transformation annealed bars and were hardened and tempered prior to the test. Samples were compressed at a cross-head speed of 0.1 mm/min to well beyond the yield point after which the test was stopped. From the plot of the variation in load and height, the yield point load at 0.2% offset was found out.

II.6. X-RAY DIFFRACTION STUDIES:

X-ray diffraction patterns were taken after every stage of heat treatment for T15 and T42 HSS samples in sintered, oil quenched, single tempered, double tempered and triple tempered conditions on a continuously recording diffractometer of Rich-Seifert, Germany make. For this purpose Cr-K_α monochromated radiation was used with a fixed scanning rate of 3°/min. Qyalitative information as regards the transformation of retained austenite during heat treatment was obtained using direct comparison of peak intensities.

II.7. MICROSTRUCTURAL STUDIES:

Microstructural studies included optical metallography (qualitative and quantitative), SEM and EDX studies and SEM fractography.

II.7.1. Optical Qualitative and Quantitative Metallography:

Samples for metallographic studies were selected after every stage of processing such as sintering, transformation annealing, oil quenching and after every tempering. Microstructure was prepared using the conventional process starting from the belt grinding followed by wet polishing on 'Lunn Major' unit over 120, 400, 600 and 1000 grit size SiC coated paper successively. This was followed by disc polishing (Struers DAP-2 unit) using diamond paste of 6 μm and 1 μm grit size successively. Polished samples were then etched according to the features required to be examined.

The etchants used for the metallographic study had the compositions as given in Table II.1.

Quantitative metallographic studies were performed on "Bausch and Lomb" Omnicon Image Analyser. Quantitative information as regards grain size and volume % of various types of primary carbides (M_6C and MC), their size distribution were obtained.

II.7.2. SEM and EDX Studies:

For SEM and EDX studies, samples were prepared using the same procedure as was followed for optical metallography. Both etched and unetched samples were observed under 'JEOL' JSM-840 A scanning electron microscope fitted with 'Kevex' EDX analyser for the chemical analysis of the observed phases.

The fracture surfaces of the TRS broken pieces in sintered as well as triple-tempered condition were observed under 'JEOL', JSM-840 A scanning electron microscope.

II.8. MAGNETIC PROPERTY:

For the measurement of coercive force in the sintered as well as triple tempered conditions, the broken TRS test pieces were used. The coercive force measuring equipment of "Electromagnets and Tool Room", Thane, India, make consisted of three units i.e. magnetiser, solenoid and the coercimeter. The function of the magnetiser is to magnetise the sample to saturation. When this magnetised sample is placed inside

Table II.1: Composition of various etching reagents used for microstructural examination

	Etchant composition	Features under study	Reference
i)	HNO_3: 5 ml Methanol: 95 ml	For general microstructure	79
ii)	HCl: 10 ml HNO_3: 5 ml Methanol: 85 ml	Grain boundary in tempered HSS	79
iii)	4% aqueous Naoh saturated with $KMnO_4$	For selective etching of M_6C carbide in HSS	80
iv)	1% chromic acid, electrochemical etching	For selective etching of MC type carbide in HSS	80
v)	8% aqueous NaOH - 80 ml Phosphoric acid - 80 ml Sulphuric acid - 10 ml Copper sulphate - 10 gm	For TiC Electrolytic etch, 3.5 VDC, Cu-cathode, 30 sec approx., 0.9 A/cm^2	81
vi)	Dist. water - 10 ml Glacial acetic acid - 10 ml Nitric acid - 10 ml	For TiN	81

the solenoid, the solenoid gets energised. The coercimeter unit applies a callibrated demagnetising force to the solenoid so as to demagnetise the sample. This demagnetising force from the coercimeter is displayed in a digital display unit as the coercive force for the particular sample in oersteds.

II.9. TOOL LIFE EVALUATION:

The compositions for which full density was achieved during sintering were only selected for tool life evaluation as per ISO-3685 standard [82]. As the sintered and heat treated samples did not have the true cross-section as specified in the standard, a modification to the tool tip geometry was done purely to get a comparative evaluation. T15-TiC composite tools had square cross-section (9.5 mm^2) whereas all other tools had rectangular section (6.5 X 9.5 mm^2). Figure 2.1 indicate the actual tool-tip geometry used. For the tool-life tests, tool-bit compacts were sintered to full density and heat treated before the tip was ground to the required geometry. While grinding the tips on the universal tool grinder, care was taken to ensure that the tip temperature during grinding did not go up. The lathe machine (HMT make, Type LB-20) on which the cutting tests were performed was replaced with a compound wound D.C. motor where infinite speed variation was possible by changing the input voltage to the motor through a variac.

Top rake = 0°
Side clearence = 2-3°

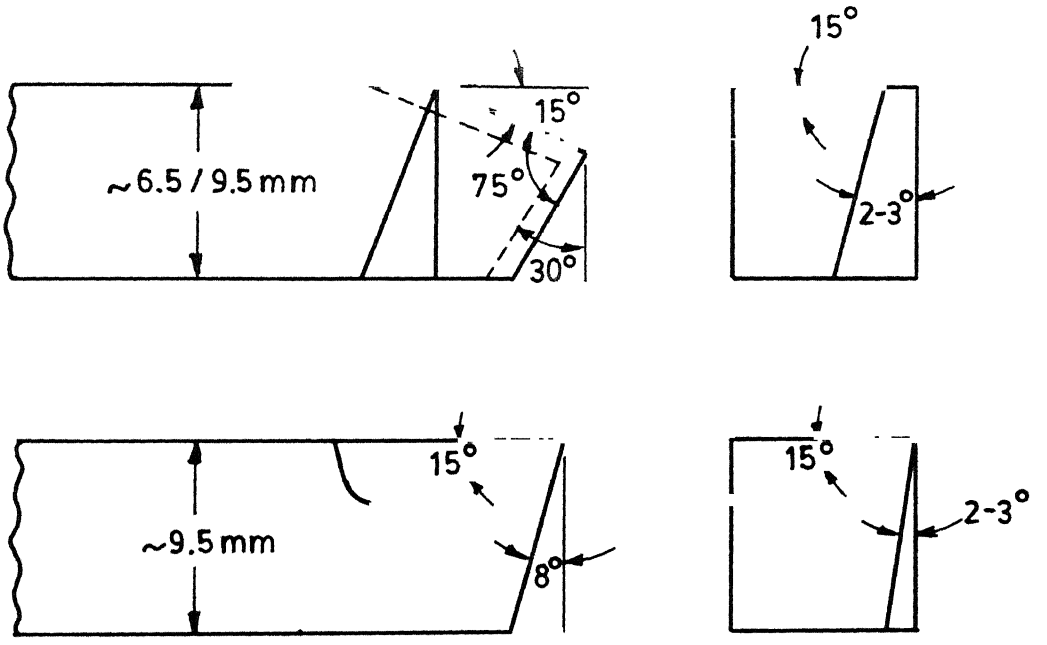

Fig 2.1 Tool - Tip geometry used for the tool life evaluation (Not to scale).

The work material was forged, normalized round of CK-45 grade of steel (composition: C = .43%, Si = .25%, Mn = .75%, S & P = .035% max.) having uniform hardness of 175 HV_{30} across the diameter. A tool holder with mechanical clamping arrangement was developed to hold the 25-35 mm long bits. Before the initial run, the scaly, oxidized surface on the work material was removed using a dummy tool. Knowing the diameter of the work piece, lathe r.p.m. was set on load for constant surface speeds using the non contact type digital Tachometer. The cutting condition throughout the test was kept constant i.e., feed = 0.1 mm/rev., depth of cut = 1.0 mm. No lubricant/coolant was used at the selected cutting speed . The actual tool life in minutes for the selected cutting speed was recorded using a stop-watch till the catastrophic failure took place.

CHAPTER III

EXPERIMENTAL RESULTS

III.1. POWDER CHARACTERISATION:

III.1.1. Particle Shape:

The SEM micrographs of various powders used in the present investigation are shown in Figure 3.1. The T15 and T42 HSS powders had the typical irregular shape, characteristic of the water atomisation process (Figure 3.1a and b). The shapes of the TiC and TiN powders (Figure 3.1c and d) were more towards rounded than irregular.

III.1.2. Size Distribution of TiC and TiN Powder:

The results of the Coulter counter analysis of the particle size distribution of TiC and TiN powder is given in Table III.1. TiN powders are relatively coarser as compared to the TiC powder. This is also evident from the SEM micrographs (Figure 3.1c and d respectively).

III.2. T15 and T42 Grade HSS:

III.2.1. Densification:

The densification behaviour of straight T15 and T42 HSS is shown in Figure 3.2a and Figure 3.3a respectively. Sintered density increased with the increase in sintering temperature from about 87% of theoretical density at 1250^{o}C

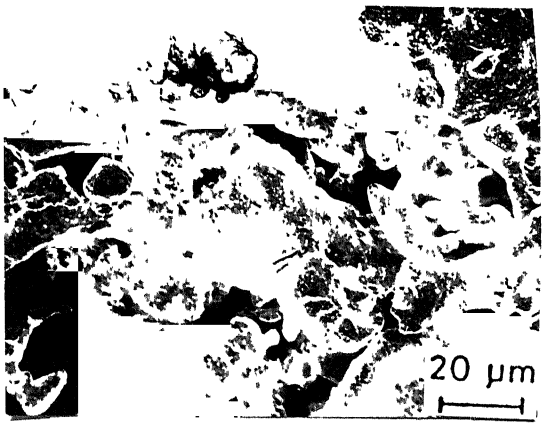

(a) T15 HSS

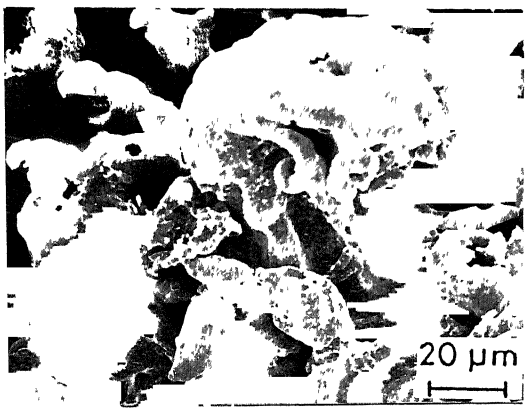

(b) T42 HSS

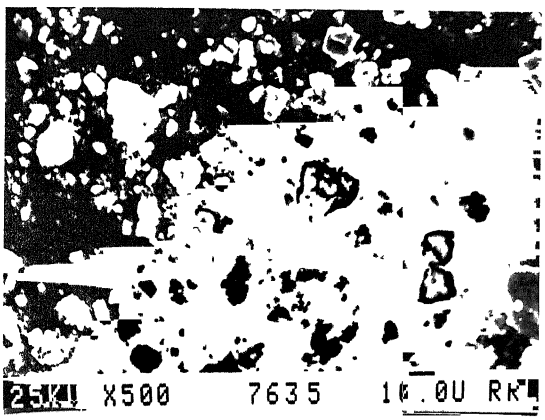

(c) TiC

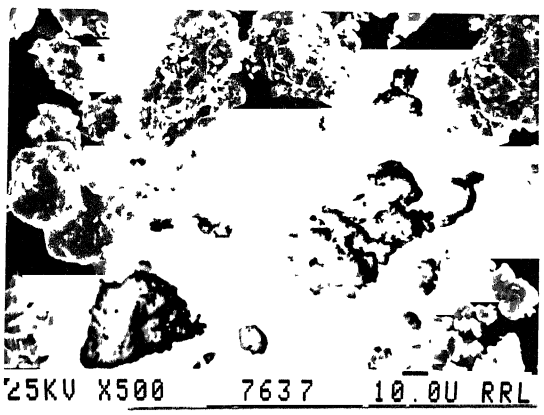

(d) TiN

Figure 3.1. SEM photomicrographs of as received powders.

Table III.1: Coulter counter analysis of particle size distribution of TiC and TiN powder.

$d_L \geq \mu m$	TiC powder		TiN powder	
	Wt. %	Cum. Wt. %	Wt. %	Cum. Wt. %
17.26	1.09	1.09	1.70	1.70
13.70	1.90	2.99	3.19	4.89
10.87	3.26	6.25	5.22	10.11
8.63	5.10	11.35	8.46	18.57
6.85	9.04	20.39	11.07	29.64
5.43	12.78	33.17	13.25	42.89
4.31	7.32	40.49	12.19	55.09
3.42	12.56	53.05	12.13	67.22
2.72	11.34	64.39	8.52	75.73
2.16	16.10	80.49	10.01	85.74
1.71	9.54	90.03	6.23	91.97
1.36	9.97	100.00	8.03	100.00

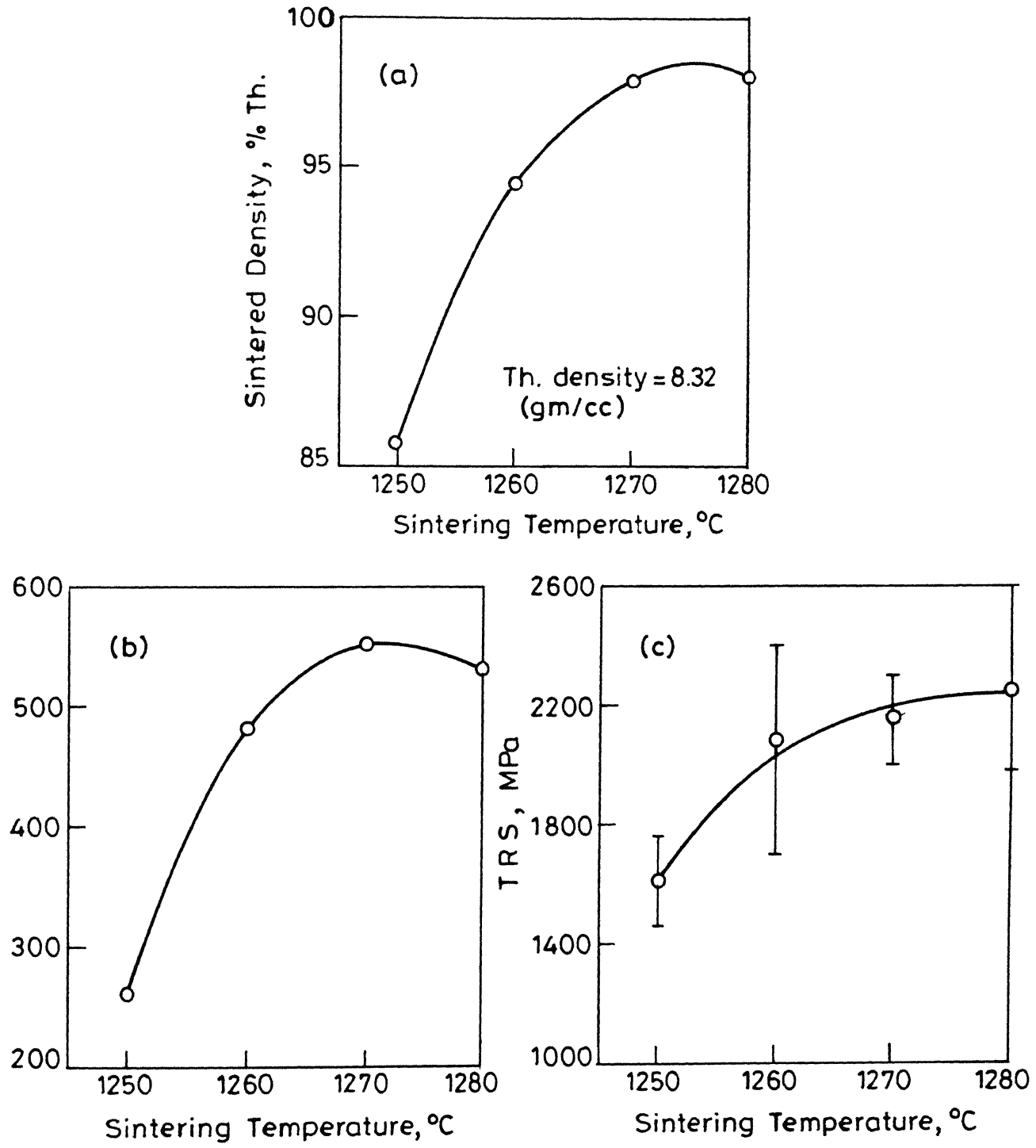

Fig. 3.2 Effect of sintering temperature on properties of T15HSS (a) Sintered density (b) Vickers hardness (c) Transverse Rupture Strength (TRS)

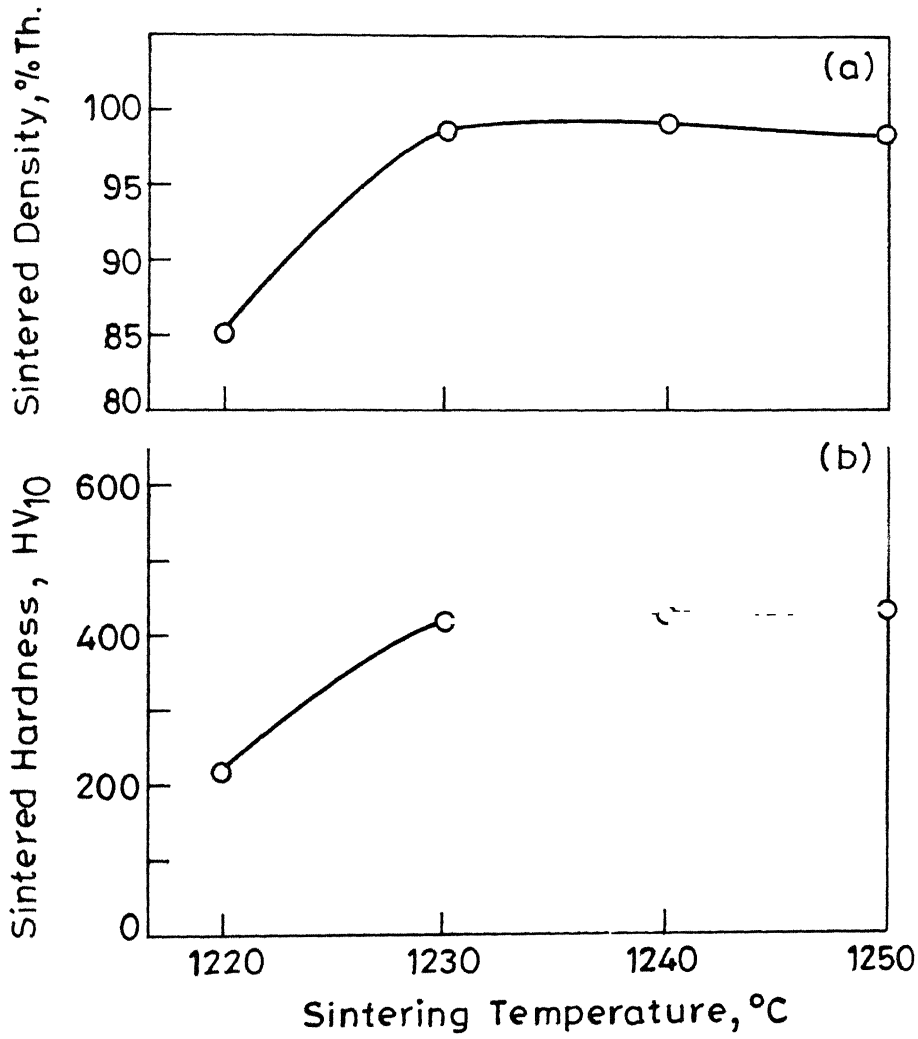

Fig. 3.3 Effect of sintering temperature on:
(a) Sintered density and (b) Sintered hardness of T42 HSS.

to 98% at 1270°C, which was the optimum sintering temperature for this grade. Similarly, the sintered density of T42 HSS increased from 85% at 1220°C to 98.5% at 1230°C, which was the optimum sintering temperature for this grade. When the sintering temperature was increased beyond optimum temperature, the sintered density either remained constant or decreased a little for either of the HSS.

III.2.2. Critical Temperatures for Transformation Annealing:

Figure 3.4 shows the result of DTA study on the sintered, stress relieved T15 and T42 HSS samples for the determination of the upper and lower critical temperatures. The start of the $\alpha \rightarrow \gamma$ transformation during heating is noticed from the appearance of the endothermic peak. For T15 HSS, this peak (indicating AC_m temperature) appeared at a temperature of 850°C whereas for T42 HSS, it is at 860°C. During cooling, the completion of the $\gamma \rightarrow \alpha$ transformation is seen from the end of the exothermic peak (indicating AC_1 temperature) at 780°C for T15, 770°C for T42 HSS. Above the AC_m temperature, the structure containing γ plus carbides and below the A_1 temperature, the structure contains ferrite plus carbides. On the basis of these two temperatures, the isothermal heating conditions required for transformation annealing was determined. In the present investigation, the first and second hold temperatures for transformation annealing were fixed as 900°C and 760°C respectively for either grade of HSS.

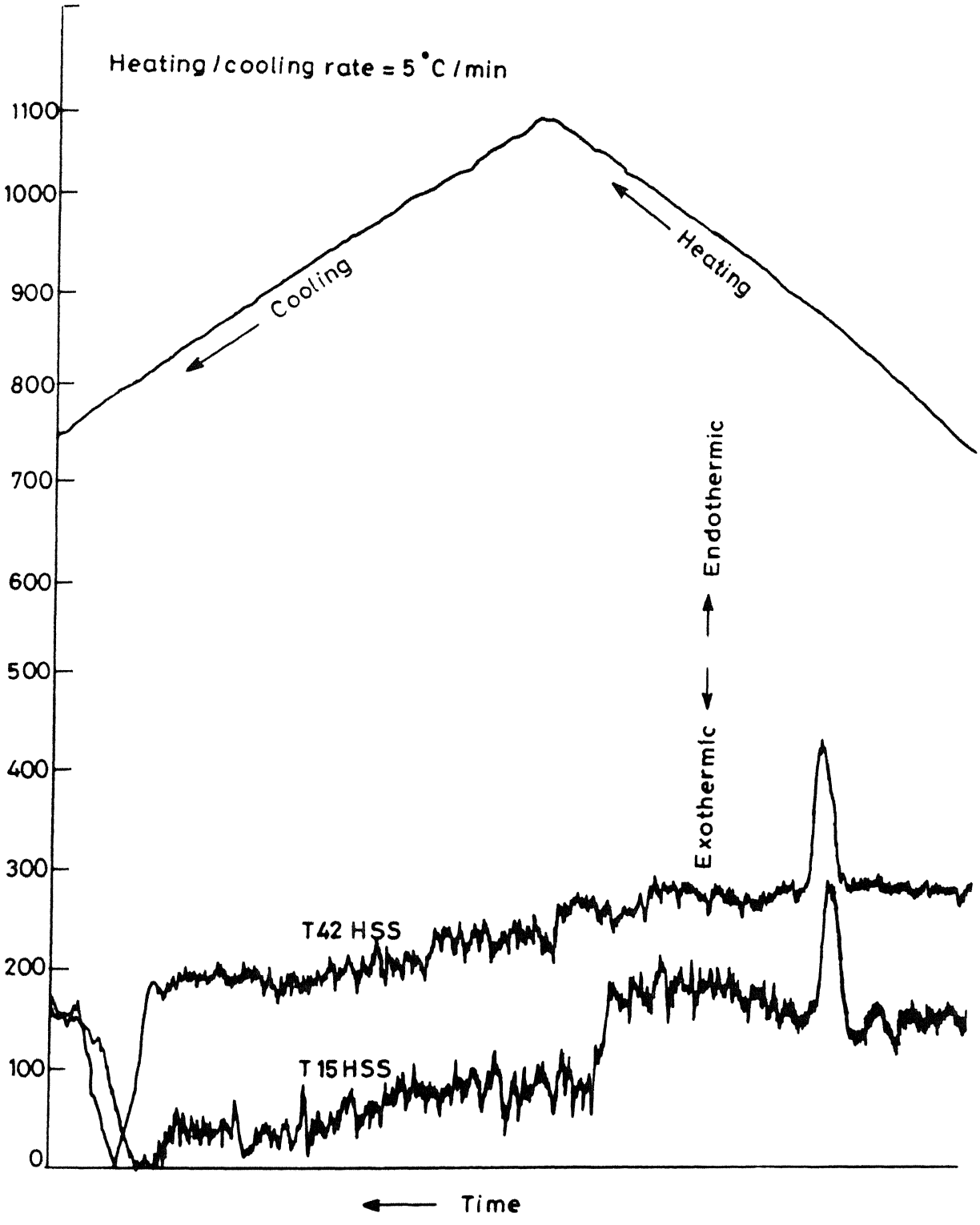

Fig 3.4 Critical temperatures for transformation annealing as determined from DTA.

III.2.3. Hardness:

The sintered hardness variation of T15 and T42 HSS with respect to sintering temperature is shown in Figure 3.2b and Figure 3.3b respectively. The plot follows a similar trend to that observed for densification with respect to the sintering temperature. The as sintered hardness of T15 HSS sintered at the optimum sintering temperature (1270°C) was 550 HV_{10}, which was higher than the corresponding hardness of T42 HSS sintered at 1230°C.

The as quenched hardness also followed a similar trend to that of densification with respect to sintering temperature (Figure 3.5a and Figure 3.6a) for either grades of HSS. The hardness variations with respect to the tempering temperatures for T15 and T42 HSS are shown in Figure 3.7 and Figure 3.8 respectively. Every tempering temperature was associated with a hardness peak, but the highest hardness was observed after triple tempering at 560°C for T15 HSS and at 540°C for T42 HSS. The highest triple tempered hardness obtained for T15 grade was 900 HV_{10} corresponding to a sintering temperature of 1270°C and tempering temperature of 560°C. In case of T42 HSS, the highest hardness of 960 HV_{10} corresponded to 1230°C sintering and triple tempering at 540°C. On the basis of tempering results for T15 and T42 grade HSS, a mean tempering temperature of 550°C was selected for all the subsequent temperings of either of HSS grade in order to make a comparison between them.

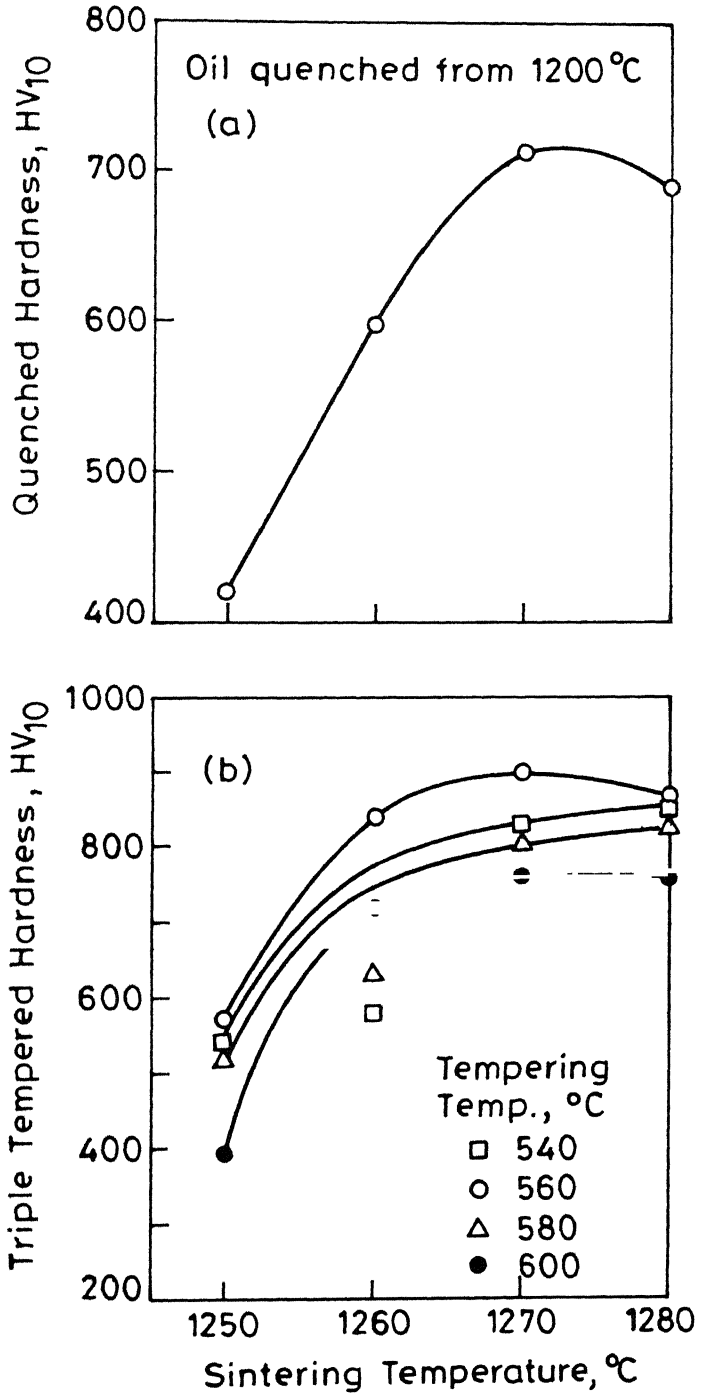

Fig. 3.5 Effect of sintering temperature on
(a) As quenched hardness of T15 HSS
(b) Triple tempered hardness of T15 HSS tempered at various temperatures.

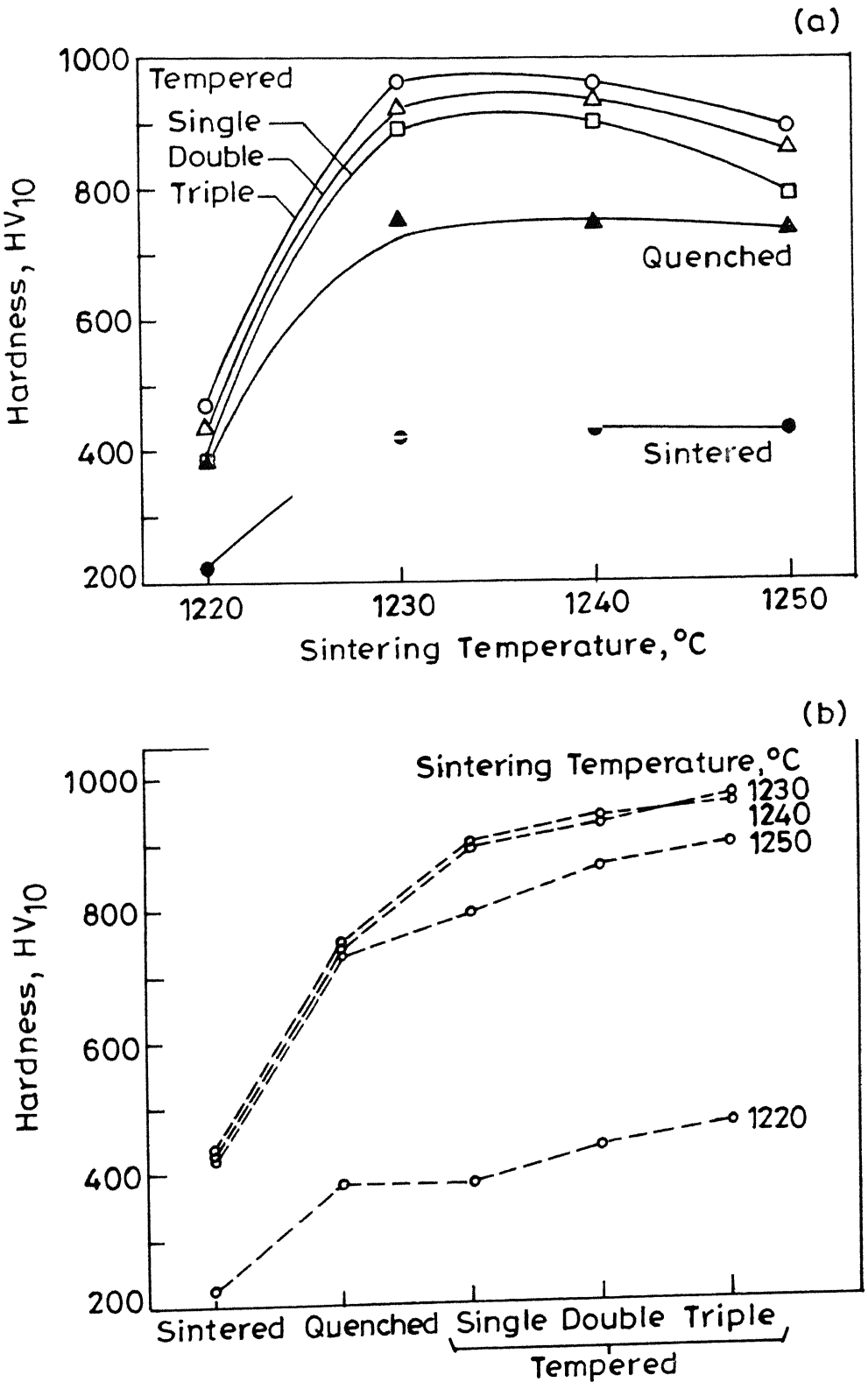

Fig. 3.6 Hardness variation of T42 HSS with respect to (a) Sintering temperature (b) Various treatments.

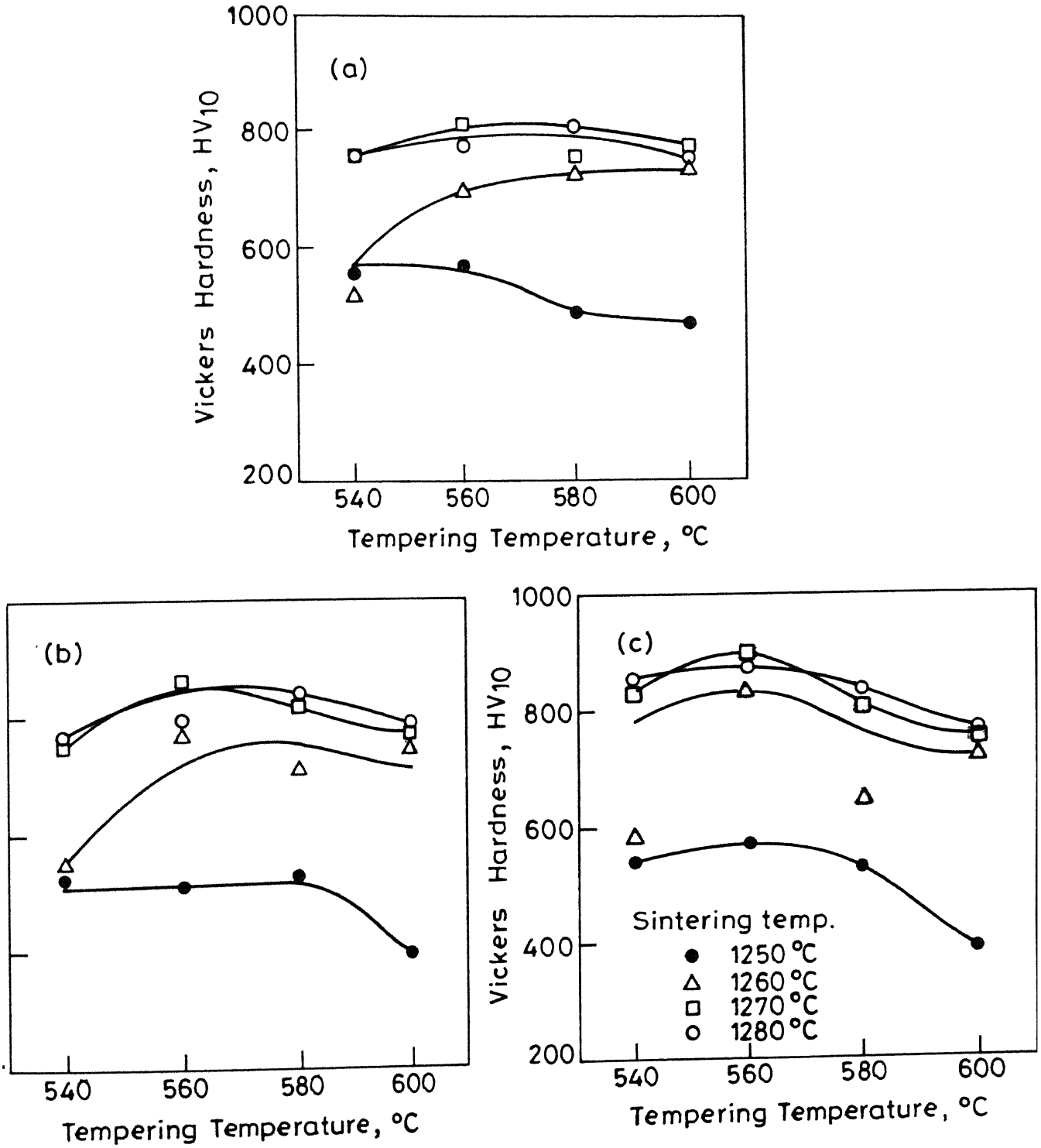

Fig. 3.7 Vickers hardness vs tempering temperature of successively tempered T15HSS with respect to sintering temperature:
(a) Single tempered (b) Double tempered (c) Triple tempered.

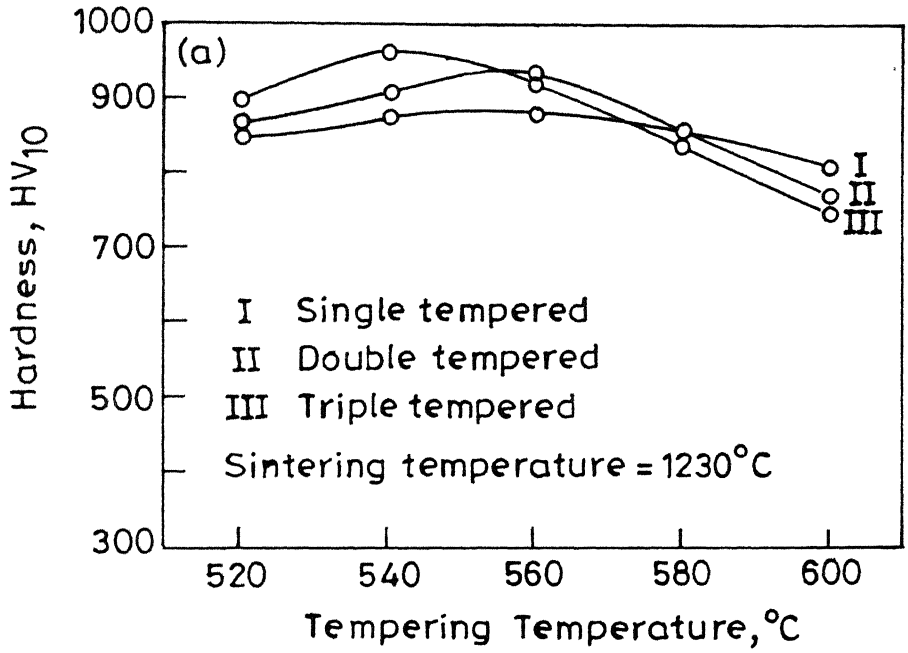

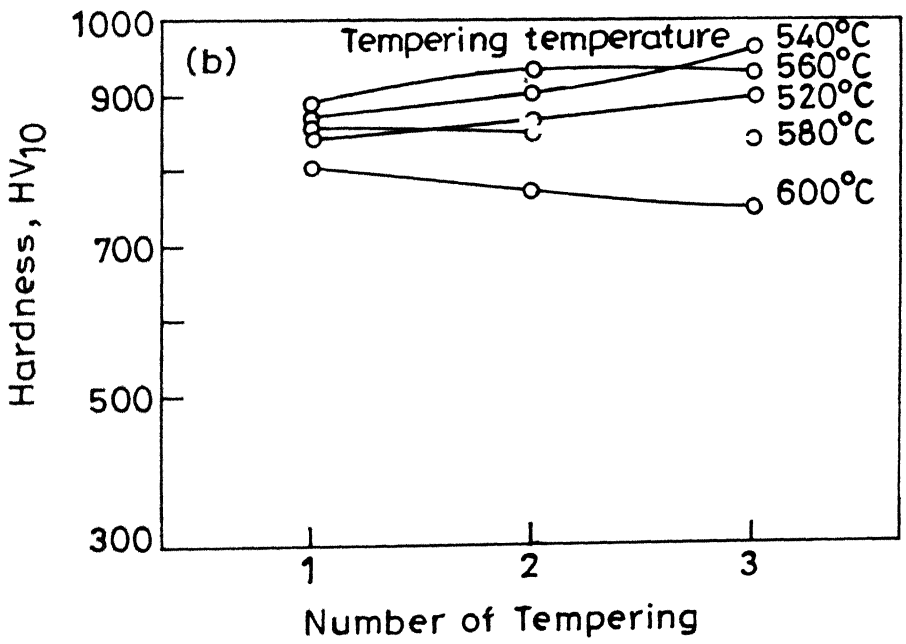

Fig. 3.8 Tempered hardness varations of T 42 HSS w.r.t.
(a) Tempering temperature
(b) Number of tempering

III.2.4. Transverse Rupture Strength (TRS):

The TRS variation with respect to the sintering temperature for T15 (HSS) is shown in Figure 3.2c, which follows a similar trend to that of densification. The as sintered TRS of T15 and T42 HSS are 1500 MPa and 1800 MPa respectively and the TRS in triple tempered condition for T15 and T42 HSS are 1950 MPa and 1300 MPa respectively (not shown). The sintered TRS of T15 is lower than that of T42 whereas the reverse is true in case of the triple tempered TRS.

III.2.5. Compressive Yield Strength:

The room and elevated temperature compressive yield strengths of T15 and T42 HSS are shown in Figure 3.9. It is evident that 0.2% offset compressive yield strength for T42 HSS is higher than the corresponding of T15 HSS at any testing temperature. In both the cases, there was rapid fall in the yield strength beyond 500^{o}C.

III.2.6. X-ray Diffraction Analysis:

The results of X-ray diffraction analysis for monitoring the transformation of retained austenite during tempering are shown in Table III.2. The increase in the ratio of the peak intensities for martensite (110) and austenite (111) from the first to the third tempering indicate the increasing transformation of retained austenite to martensite in any grade of HSS. However, owing to the

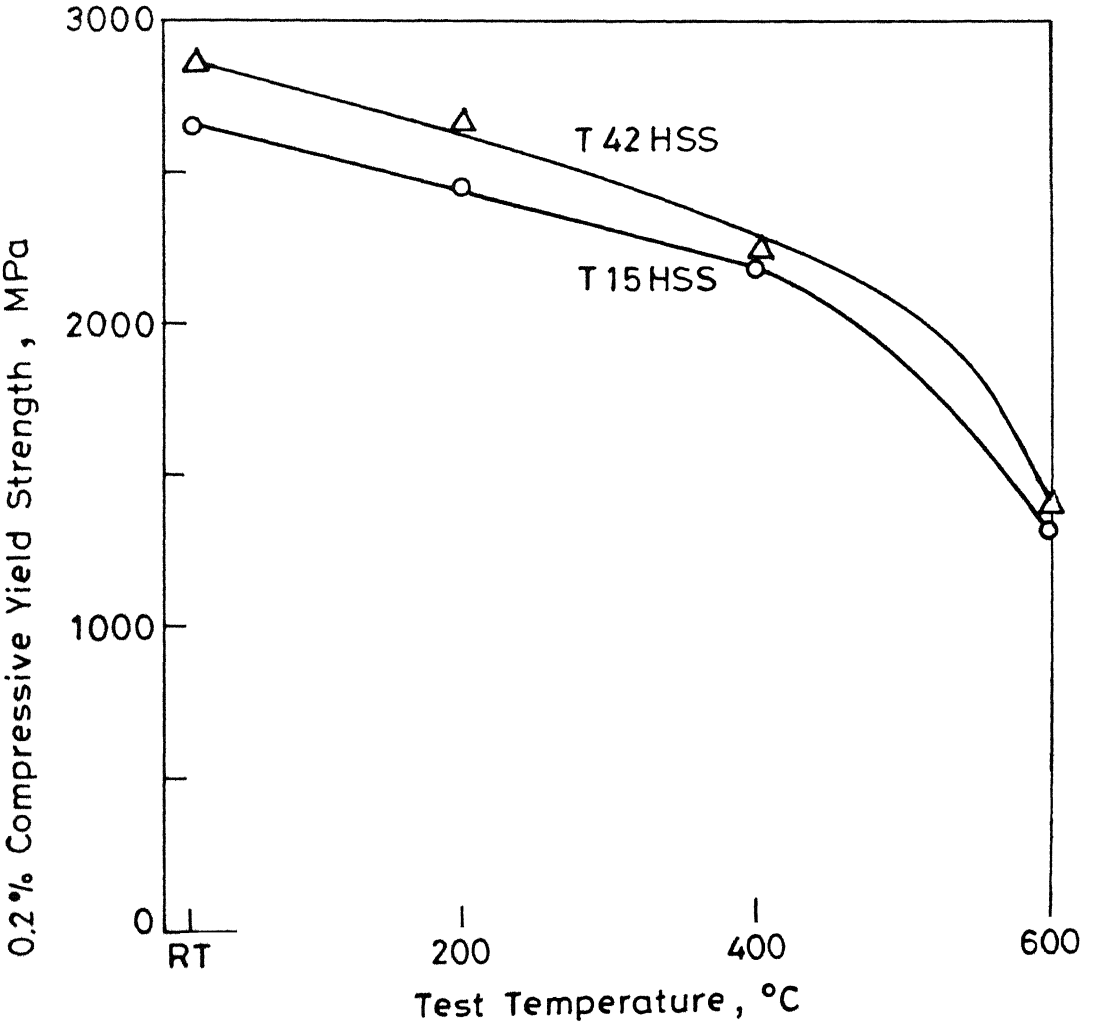

Fig.3.9 Compressive yield strength (0.2% offset) of fully heat treated T15 and T42 HSS at different testing temperatures.

Table III.2: X-ray diffraction study of retained austenite to martensite transformation during tempering.

HSS grade	$\frac{I_{Martensite\ (110)}}{I_{Austenite\ (111)}}$
T15 HSS:	
- Single tempered	1.00
- Double tempered	1.90
- Triple tempered	6.62
T42 HSS:	
- Single tempered	1.07
- Double tempered	2.52
- Triple tempered	4.00

difference in their compositions and carbide contents, a comparison between these two grades of HSS viz. T15 and T42 could not be done.

III.2.7. Microstructural Analysis:

The optical microstructures of T15 HSS sintered at various temperatures are shown in Figure 3.10. Sintering at 1250°C resulted in only 85% of theoretical density and many large pores could be observed (Figure 3.10a). The porosity gradually decreased when the sintering temperature was increased to 1260°C (Figure 3.10b). Samples sintered either at 1270°C or 1280°C showed a microstructure virtually free from pores. The microstructure of samples sintered at the optimum sintering temperature i.e. 1270°C (Figure 3.10c) is well developed with fine grain matrix and carbides. At 1280°C, coarsening of the matrix as well as carbides could be observed (Figure 3.10d). The optical microstructures of T42 HSS sintered at various sintering temperatures are shown in Figure 3.11. The progressive change in the microstructure with sintering temperature in case of T42 HSS was similar to that observed for T15 HSS. Samples sintered at temperature lower than the optimum temperature i.e. at 1220°C showed many large pores (Figure 3.11c). Sintering at the optimum sintering temperature i.e. 1230°C resulted in uniform microstructures with few isolated pores (Figure 3.11b). At higher sintering temperatures, both matrix and carbide coarsenings were noticed. Figure 3.12

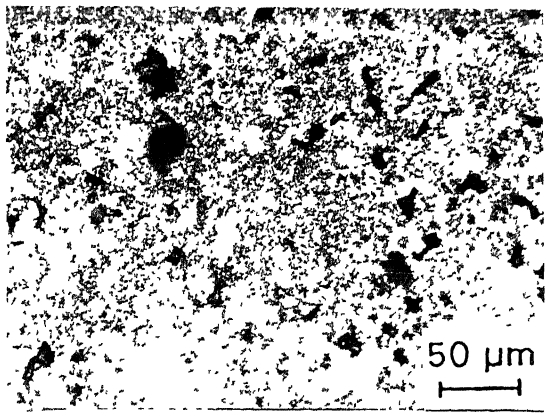

(a) 1250°C

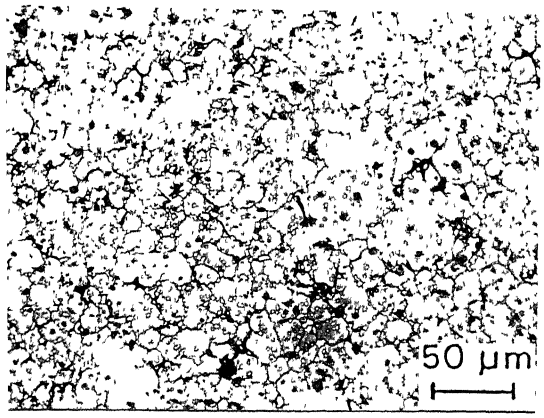

(b) 1260°C

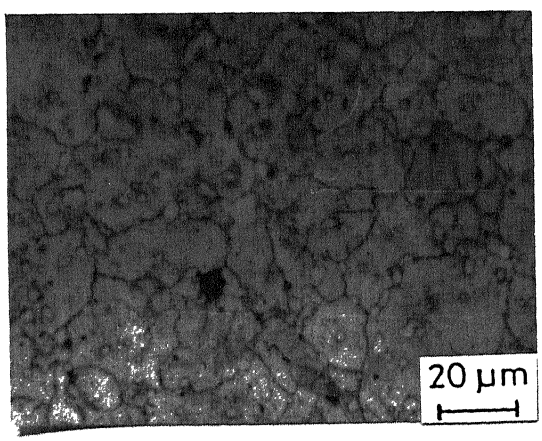

(c) 1270°C

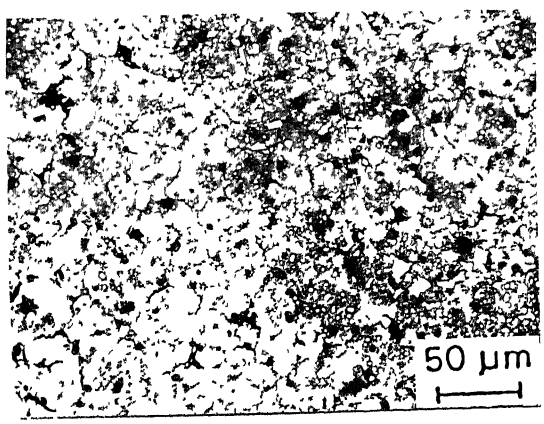

(d) 1280°C

Figure 3.10. Optical microstructures of sintered T15 HSS with respect to sintering temperature.

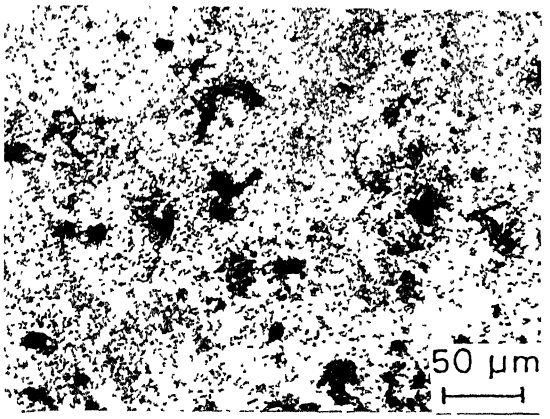

(a) 1220°C

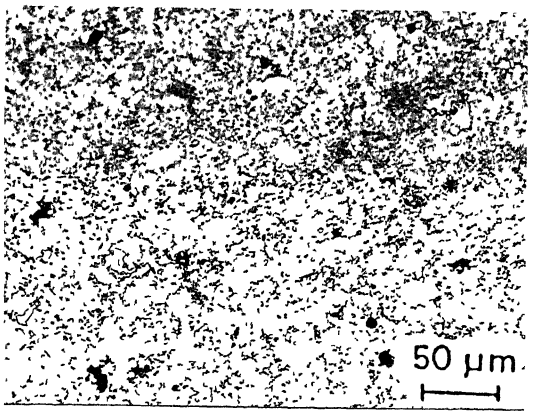

(b) 1230°C

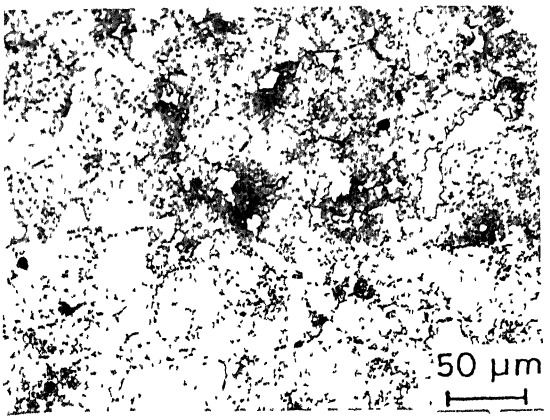

(c) 1240°C

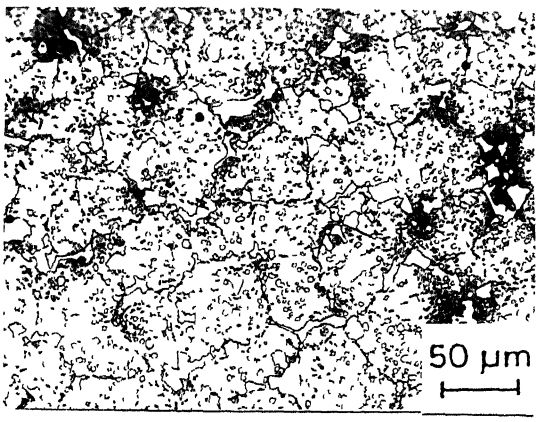

(d) 1250°C

Figure 3.11. Optical microstructures of sintered T42 HSS with respect to sintering temperature.

makes a direct comparison between the microstructures of T15 and T42 HSS after sintering at the optimum sintering temperatures, oil quenching from 1200°C and triple tempering at 550°C. It is observed that the sintered and triple tempered microstructures of T15 grade are coarser as compared to the corresponding of T42 HSS. But, in case of quenched microstructure, the reverse is true.

The volume fraction of primary carbides and their size distribution in sintered, transformation annealed (for T15 HSS)/quenched (for T42 HSS) and triple-tempered conditions for both the grades of HSS as determined by the image analysis are shown in Figure 3.13 and Figure 3.14 respectively. The volume fraction of primary carbides increased from the sintered to the triple tempered conditions in both the cases. In T15 HSS, the increase was from ~15% to ~24% whereas in T42, it was from ~15% to 20%.

In as sintered condition, the MC carbide content in T15 HSS was higher (8%) as compared to that of T42 HSS (6%). But the M_6C type carbide content in T42 HSS was higher (10%) than that of T15 HSS (7%). This prominence of MC carbide in T15 HSS and M_6C carbide in T42 HSS was true in triple tempered condition as well. The MC carbide content increased progressively from sintered condition to triple tempered condition in T15 HSS (Figure 3.13a) whereas in case of T42 HSS (Figure 3.14a) the change was minimal.

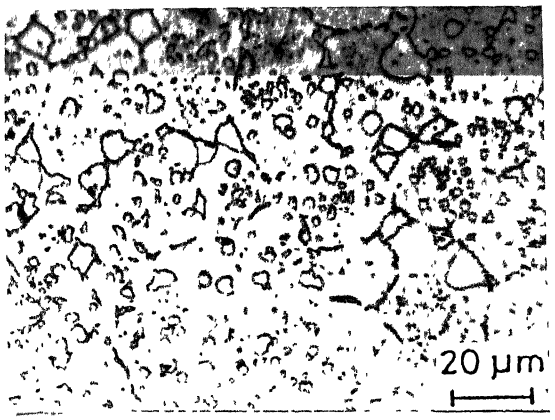

(a) Sintered

(b) Sintered

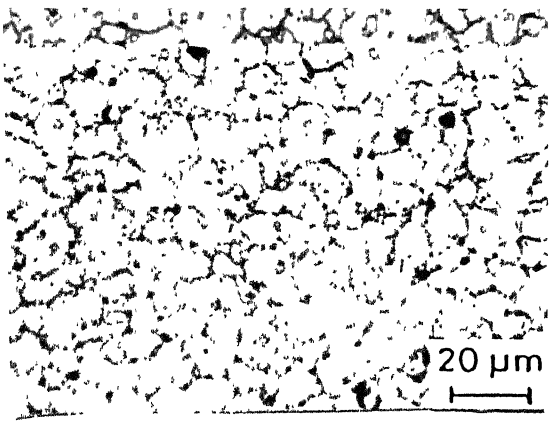

(c) Quenched

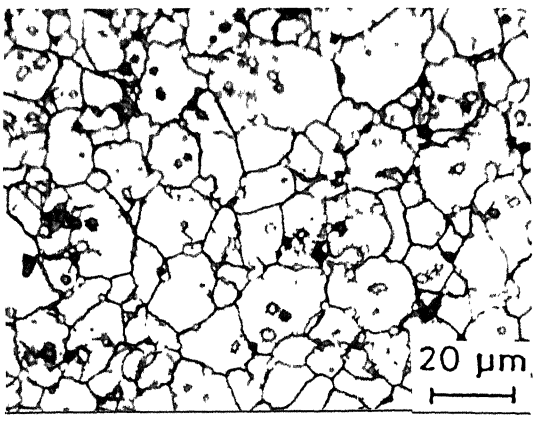

(d) Quenched

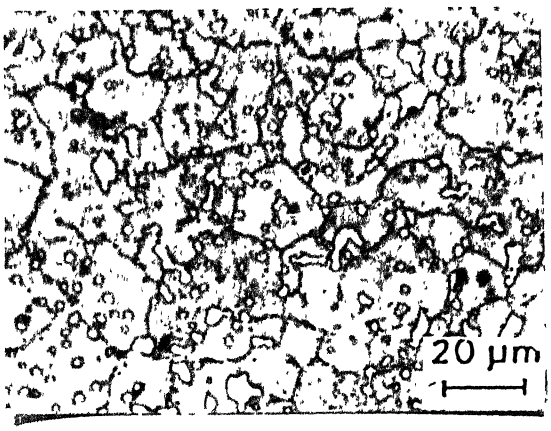

(e) Triple tempered

T15

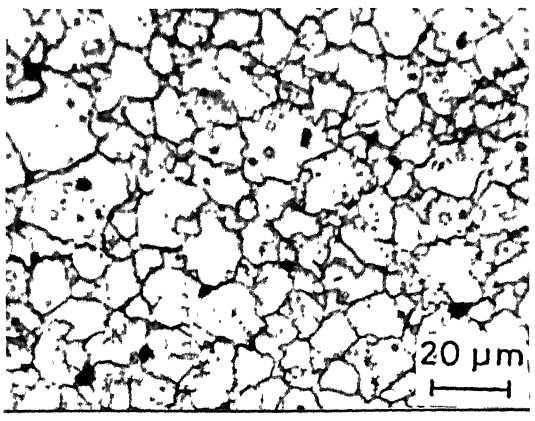

(f) Triple tempered

T42

Figure 3.12. Optical microstructures of T15 and T42 HSS with respect to various conditions.

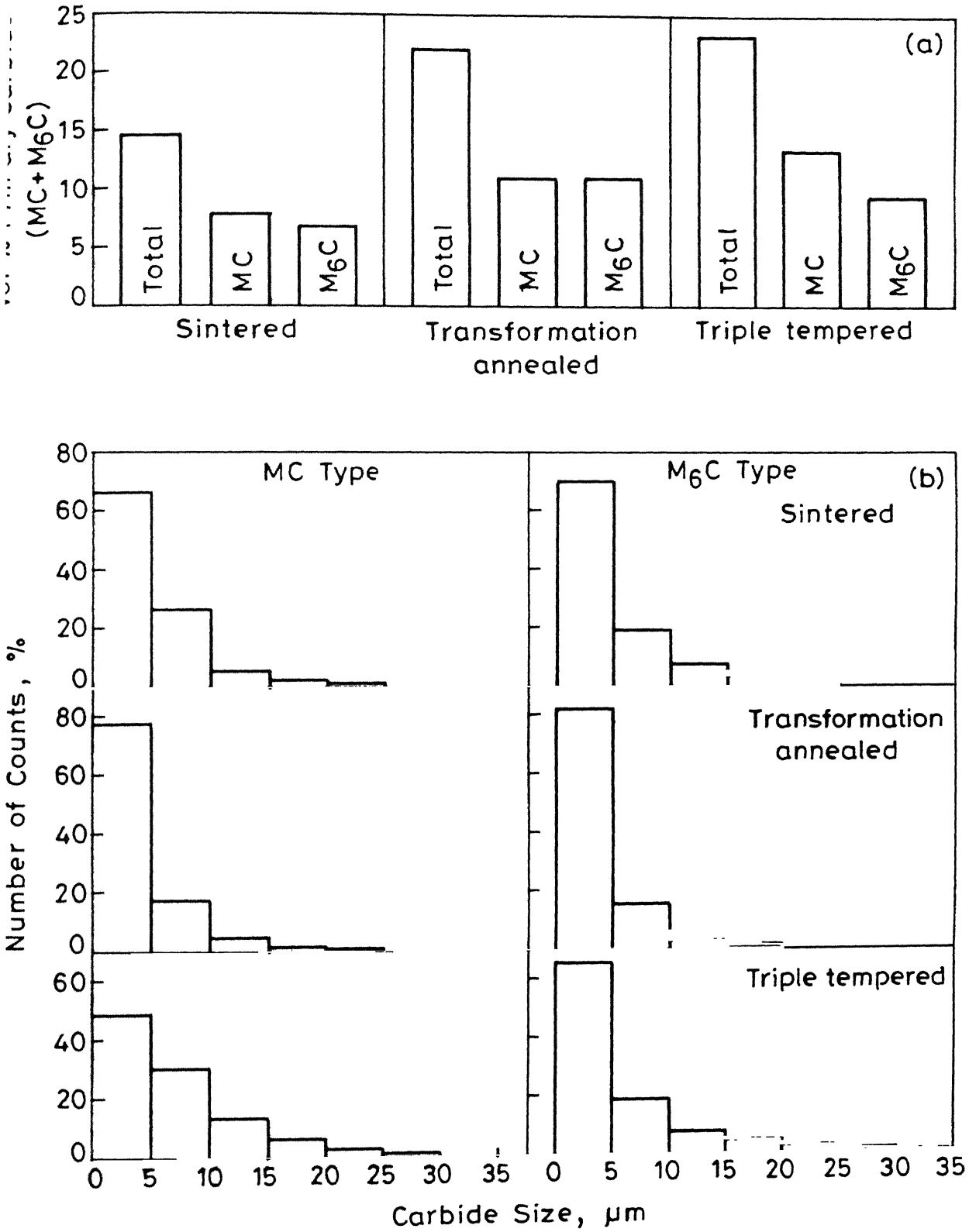

Fig.3.13 Primary carbides (MC + M_6C) in T15HSS in sintered, transformation annealed and triple tempered conditions:
(a) Volume %
(b) Size distribution

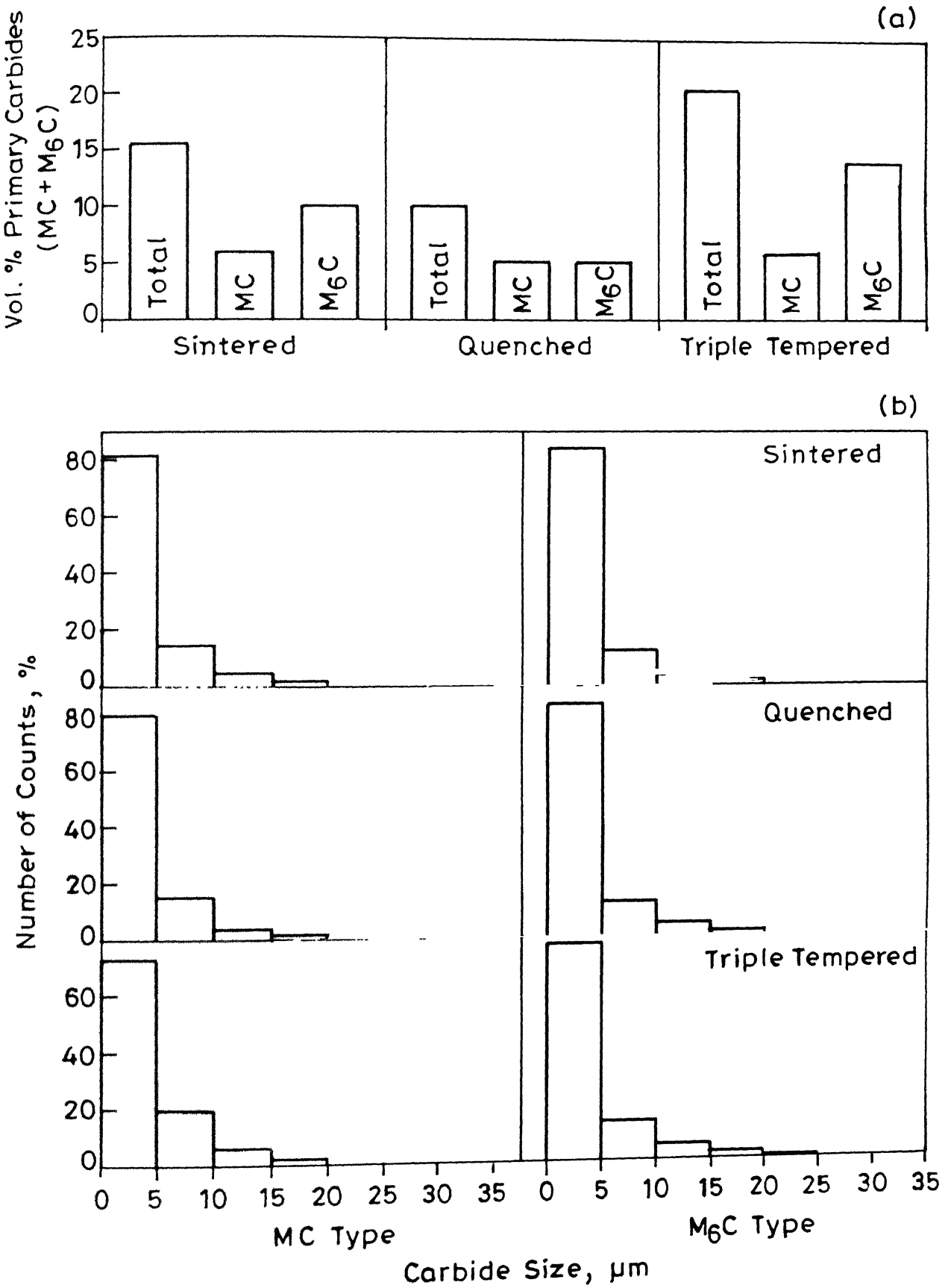

Fig. 3.14 Primary carbides (MC + M_6C) in T 42 HSS in sintered, quenched and triple tempered conditions (a) Volume % (b) size distribution.

From the size distribution of these two types of primary carbides (Figure 3.13b and Figure 3.14b), it was observed that there was coarsening of both the MC and M_6C carbides from sintered condition to the triple tempered condition. However, the degree of coarsening observed for MC carbides in T15 HSS (Figure 3.13b) was more as compared to the same for M_6C carbides, whereas, in case of T42 HSS (Figure 3.14b) the reverse was true.

Figure 3.15 shows the SEM micrographs of T15 HSS in various conditions. In comparison to the optical microscopy, SEM offers the unique combination of high magnification, greater resolution and high depth of focus which reveal more details of the various features present in the microstructure. In the sintered condition (Figure 3.15a), the microstructure consisted of primary carbides along the grain boundary and within the grains. The white phase was M_6C carbide and the grey phase was MC carbide as confirmed from the EDX analysis. In the annealed condition, the microstructure contained chromium rich $M_{23}C_6$ carbides in addition to the primary carbides (Figure 3.15c and d). $Cr_{23}C_6$ carbides were very fine and could be resolved only at magnifications above 5000X. In the quenched condition (Figure 3.15e and f), the secondary carbides and finer fractions of primary carbides had gone into solution leaving behind the larger primary carbides. The precipitation of proeutectoid M_6C carbides around larger MC carbide particles as satellites could be easily observed (Figure 3.15f). In the triple

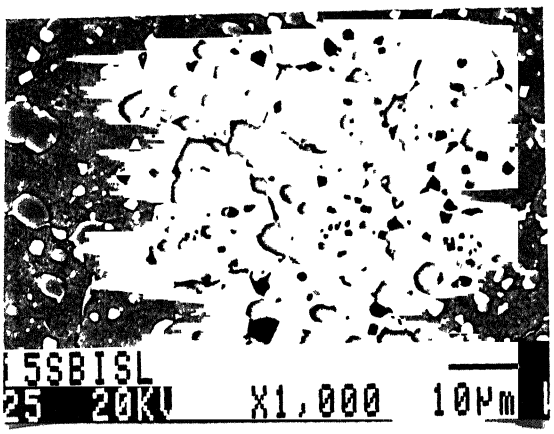

(a) Sintered

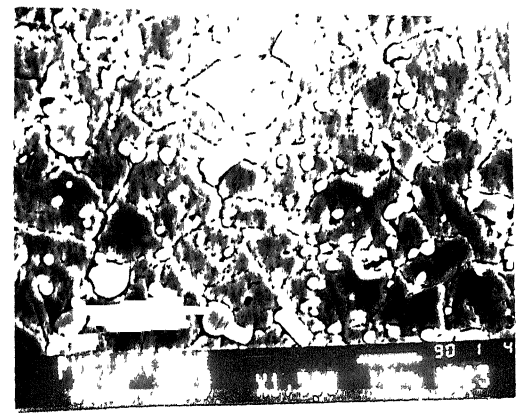

(b) Triple tempered

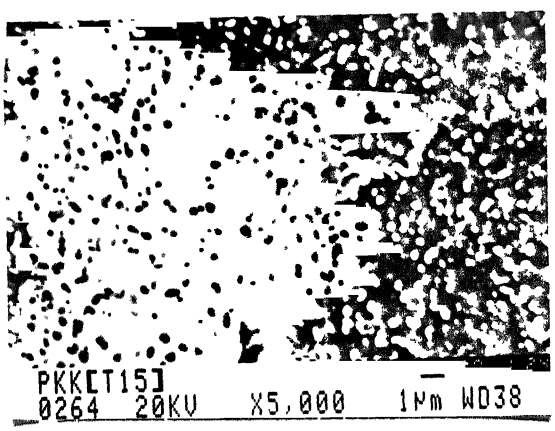

(c) Transformation annealed

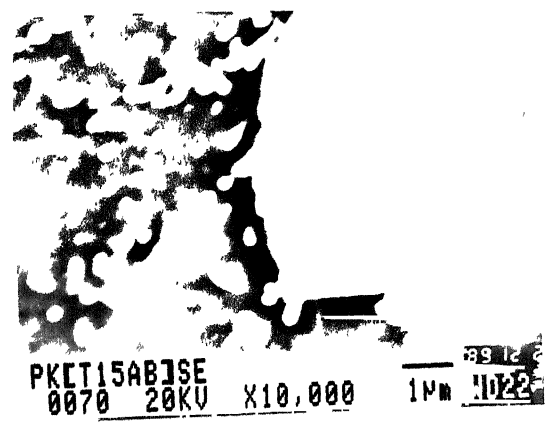

(d) Transformation annealed

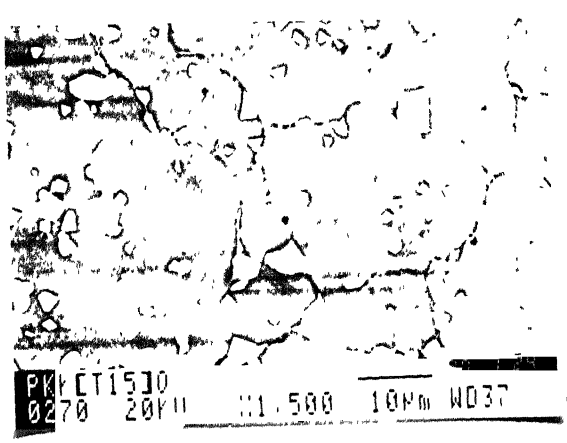

(e) Quenched

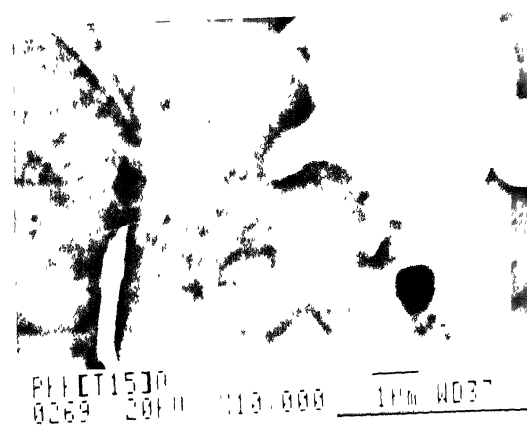

(f) Quenched

Figure 3.15. SEM photomicrographs of T15 HSS in various conditions.

tempered condition (Figure 3.15b), the microstructure consisted of carbides in a tempered martensite matrix. Only the primary carbides on and within prior austenite grains could be observed as the secondary carbides could not got yet resolved on SEM. Here again, the two types of carbides viz. MC and M_6C could be distinguished from their colour.

Figure 3.16 shows the SEM micrographs of T42 HSS in various conditions. The sintered microstructures (Figure 3.16a) consisted of primary carbides (MC and M_6C) on and within the prior austenite grains similar to that observed in T15 HSS. The EDX analysis also confirmed that the white phase was M_6C whereas the grey phase MC. The microstructure after transformation annealing (Figure 3.16c and d) showed the presence of chromium rich carbide ($Cr_{23}C_6$) uniformly distributed in the structure along with the primary carbides. The primary carbides in annealed T42 HSS were fine and more uniformly distributed as compared to that of T15 HSS. The microstructures after the first two temperings (Figure 3.16e and f) contained primary carbides and martensite. As compared to the first, the acicularity of the martensite decreased in the second tempering and small rounded carbides were noticed. In the triple tempered condition (Figure 3.16b) similar to that of T15 HSS, the martensite in T42 HSS was fully tempered one.

Table III.3 gives the chemical composition of various phases as determined by the SEM-EDX analysis for T15 and T42 HSS. In both the cases, the grey phase was MC

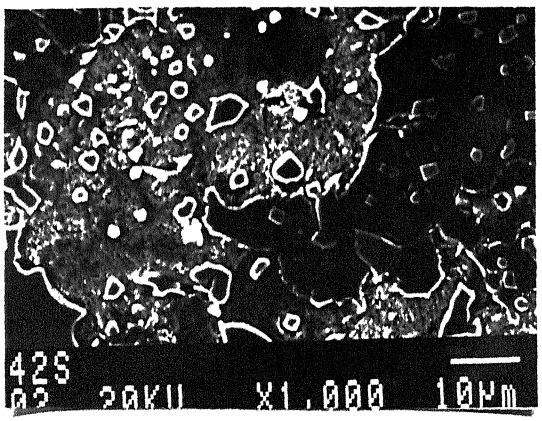

(a) Sintered

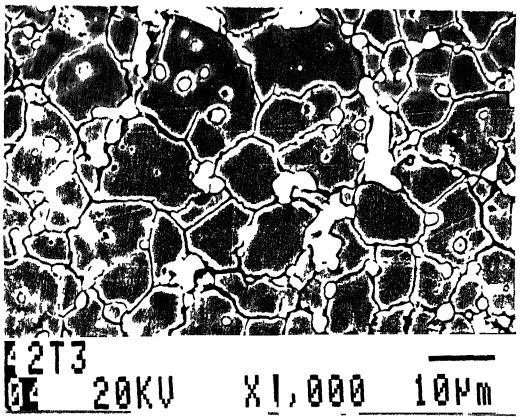

(b) Triple tempered

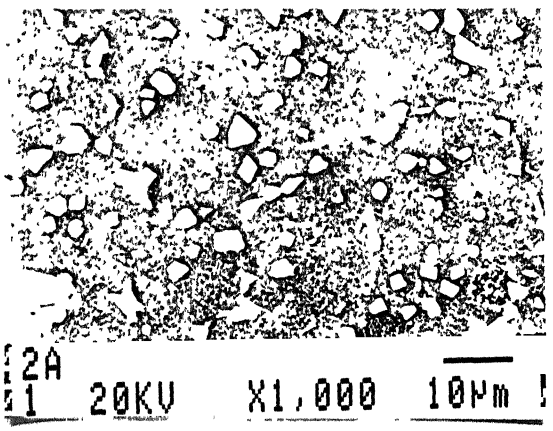

(c) Transformation annealed

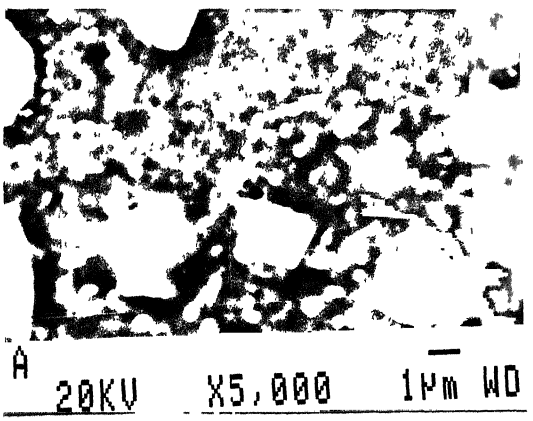

(d) Transformation annealed

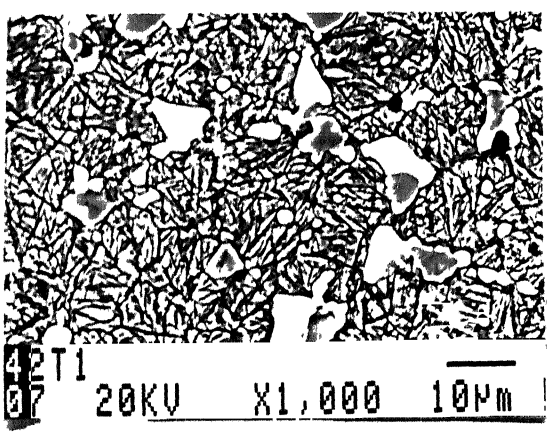

(e) Single tempered

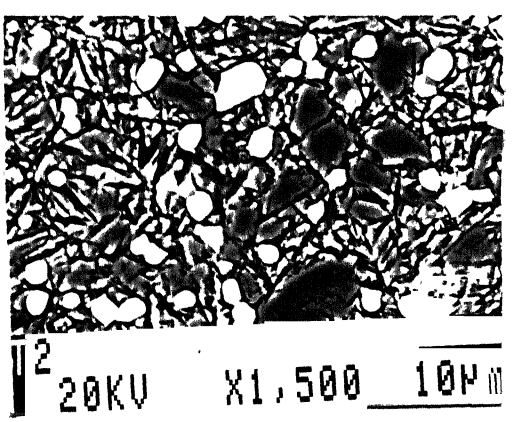

(f) Double tempered

Figure 3.16. SEM photomicrographs of T42 HSS in various conditions.

Table III.3: EDX analysis of various phases in T15 and T42 HSS.

HSS grade	Description of phase	Mass % chemical analysis						Assigned phase
		Fe	Cr	Co	Mo	V	W	
T15 HSS (Sintered)	Matrix	79.31	3.97	4.80	0.41	2.78	8.73	Matrix
	Grey phase	19.18	-	-	-	48.80	32.02	MC type carbide
	White phase	31.62	-	-	-	-	68.37	M_6C type carbide
T15 HSS (Triple tempered)	Matrix	83.02	4.32	8.95	-	1.80	1.93	Matrix
	Grey phase	4.82	12.10	1.34	2.66	52.28	26.80	MC type carbide
	White phase	35.23	5.41	4.21	4.15	6.64	44.37	M_6C type carbide
T42 HSS (Sintered)	Matrix	74.69	5.08	13.36	0.77	0.83	5.27	Matrix
	White phase	35.42	5.66	6.90	13.55	3.80	34.67	M_6C type carbide
T42 HSS (Triple tempered)	Matrix	73.47	4.25	11.22	4.02	1.62	5.42	Matrix
	Grey phase	3.49	9.72	0.11	1.88	54.16	30.64	MC type carbide
	White phase	34.46	4.96	3.38	1.48	7.21	48.50	M_6C type carbide

type carbide which was rich in vanadium, while the white phase, M_6C type carbide was rich in tungsten and iron. The matrix was naturally rich in elements which did not participate in the formation of primary carbides i.e. Fe and Co.

Figure 3.17 shows the SEM-fractographs taken on the fracture surfaces of the broken TRS test pieces of T15 and T42 HSS. Both T15 and T42 HSS showed similar nature of crack propagation.

III.2.8. Magnetic Property:

The magnetic property (coercivity) variations of T15 and T42 HSS in sintered, quenched and triple tempered conditions are shown in Figure 3.18. The coercivity observed for T42 was higher in case of quenched and triple tempered conditions, whereas there was practically no difference in the coercivity values for either grades of HSS in as sintered condition.

III.2.9. Tool Life:

Tool life data of both T15 and T42 HSS as determined from the cutting test is shown in Table III.4. T42 HSS had a longer tool life of 30 minutes as compared to 21 minutes for T15 HSS under identical test conditions.

Table III.4 : Tool life of T15 and T42 HSS

(Cutting conditions: Speed = 70 M/min, feed = 0.1 mm/rev. depth of cut = 1.0 mm, no lubricant/coolant used)

HSS grade	Tool life, minutes
T15 HSS	21.5
T42 HSS	30.5

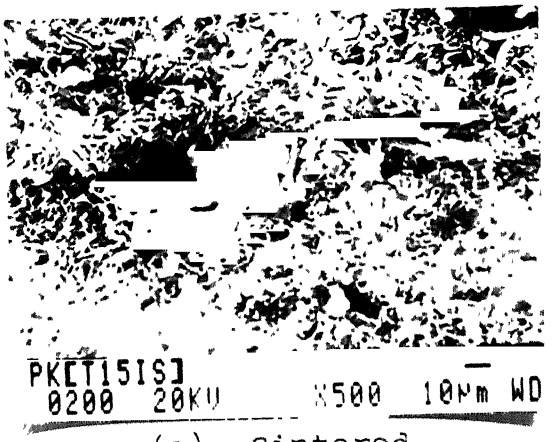

(a) Sintered

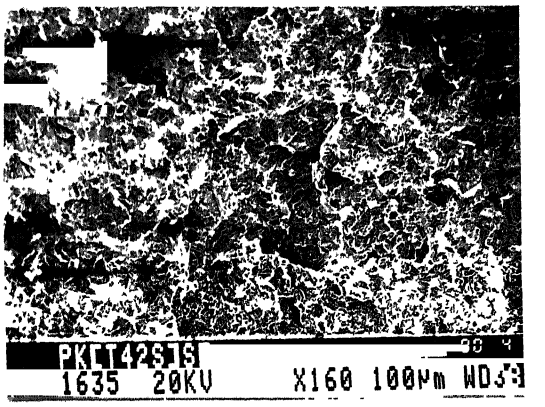

(b) Sintered

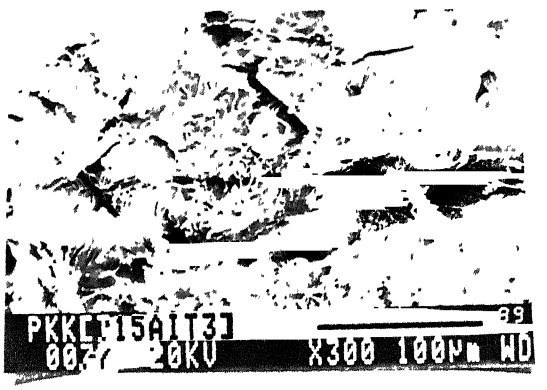

(c) Triple tempered

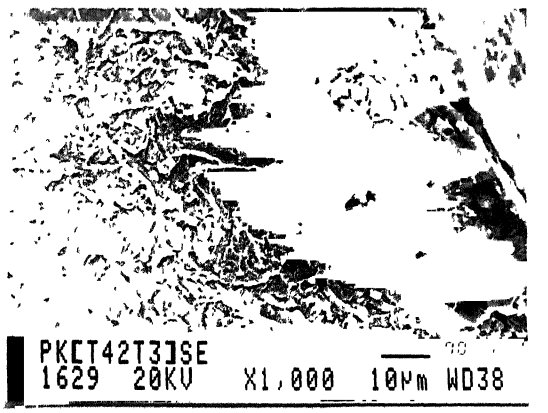

(d) Triple tempered

(e) Triple tempered

T15

(f) Triple tempered

T42

Figure 3.17. SEM fractographs of T15 and T42 HSS in sintered and triple tempered conditions.

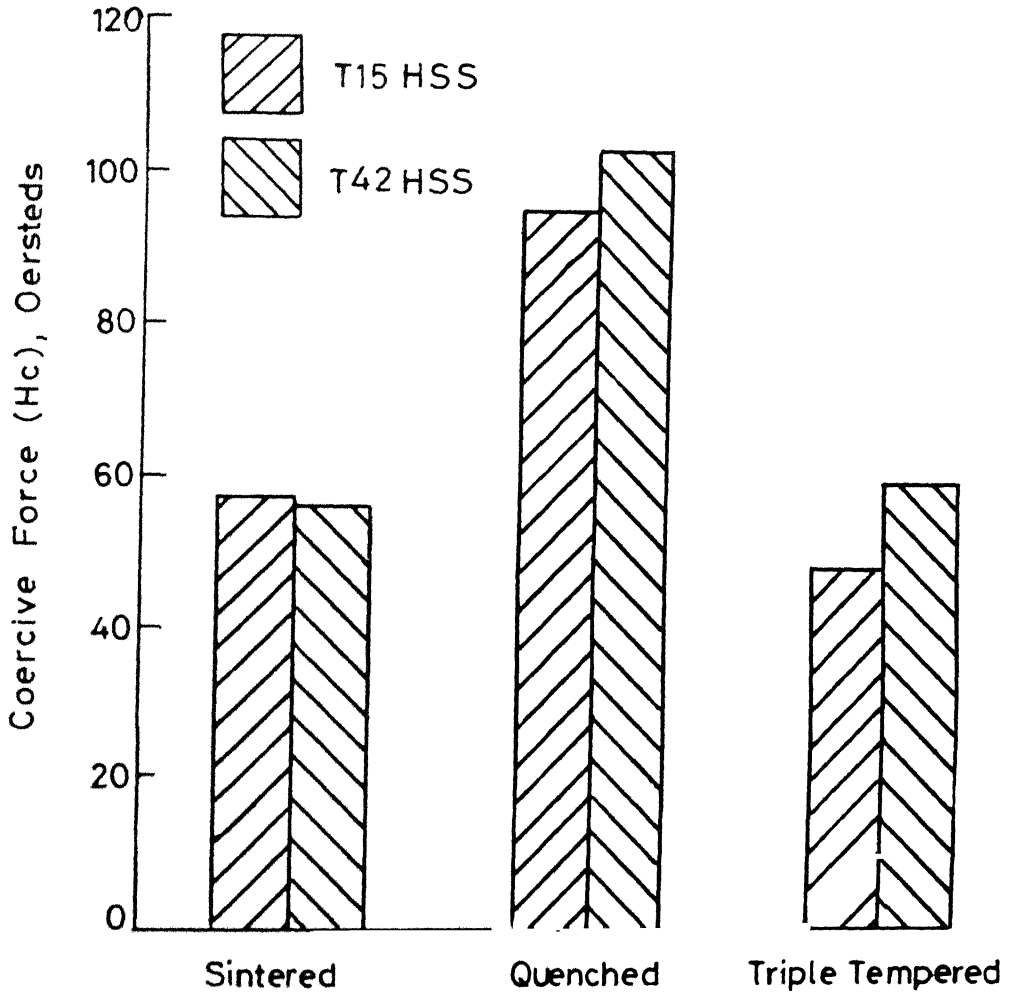

Fig. 3.18 Coercivity variation of T15 and T42 HSS in various conditions.

III.3. HSS COMPOSITES CONTAINING TiC:

III.3.1. Densification:

The densification behaviour of T15 HSS containing 0-8 mass % TiC is shown in Figure 3.19. T15 HSS (belonging to Source-I) achieved full density at 1270°C which is the optimum sintering temperature for this grade, but the densities achieved by the composites were lower. The marginal increase in the sintered density with the increase in the sintering temperature was lower for higher TiC content in the composites. The temperature at which rapid densification starts got shifted to higher values for composites containing higher TiC contents and correspondingly higher sintering temperatures were required for achieving full densities. The effect of TiC addition on the sintered density and the optimum sintering temperatures to achieve full density (>98% Th.) is shown in Figure 3.21. At 1270°C (optimum temperature for straight composition), the decrease in the sintered density is inversely proportional to the TiC content in the composite (Figure 3.21a). Composite containing 8 mass % TiC could not be fully sintered even at a relatively high temperature of 1320°C (Figure 3.19).

Figure 3.20 shows the densification behaviour of T42 HSS composites containing 0-8 mass % TiC. Similar to the T15 HSS composites, the composites of T42 HSS required higher sintering temperature to achieve full density with the increase in the TiC content. The marginal increase in the

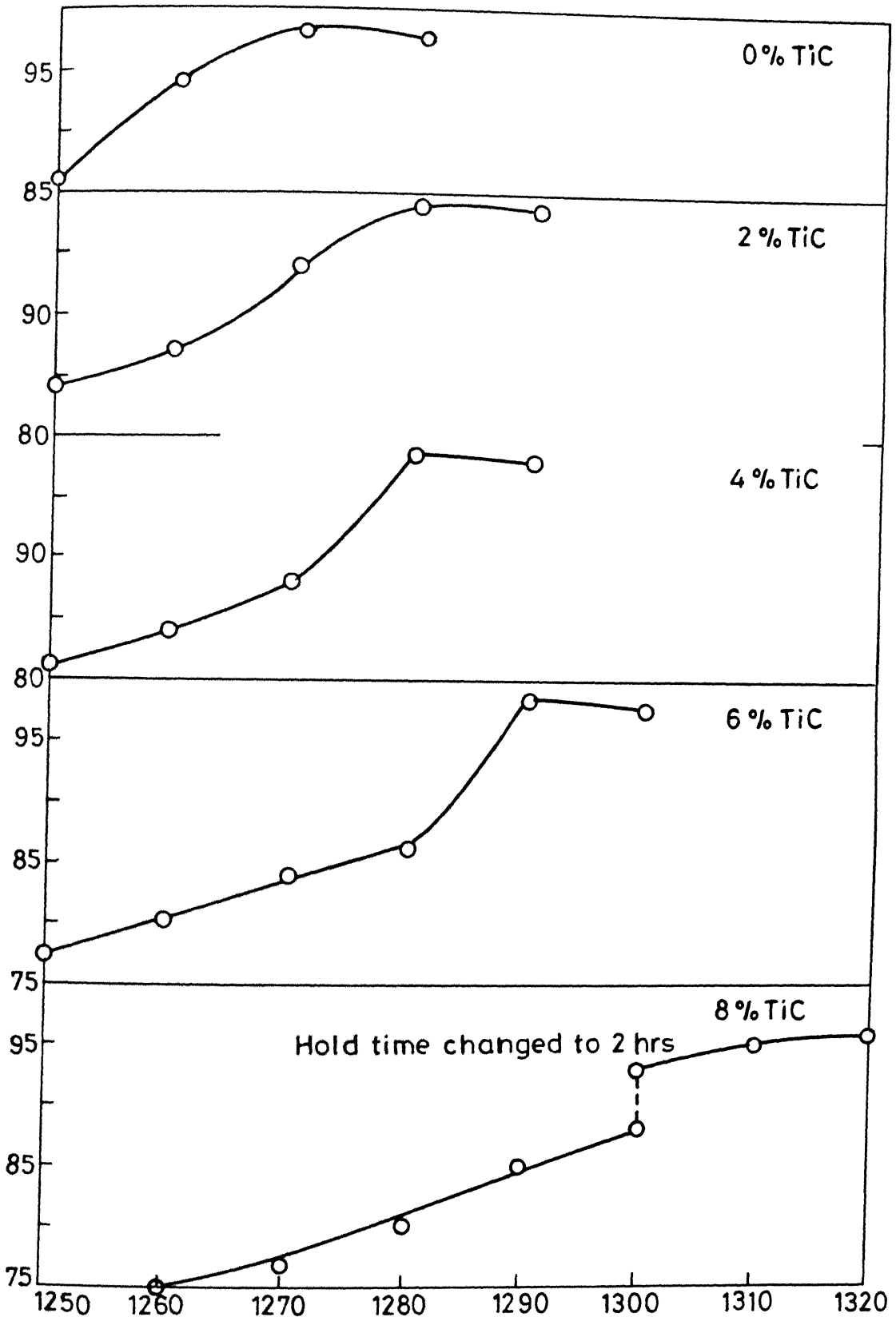

Fig.3.19 Densification behaviour of T15 HSS-TiC composites with respect to sintering temperature.

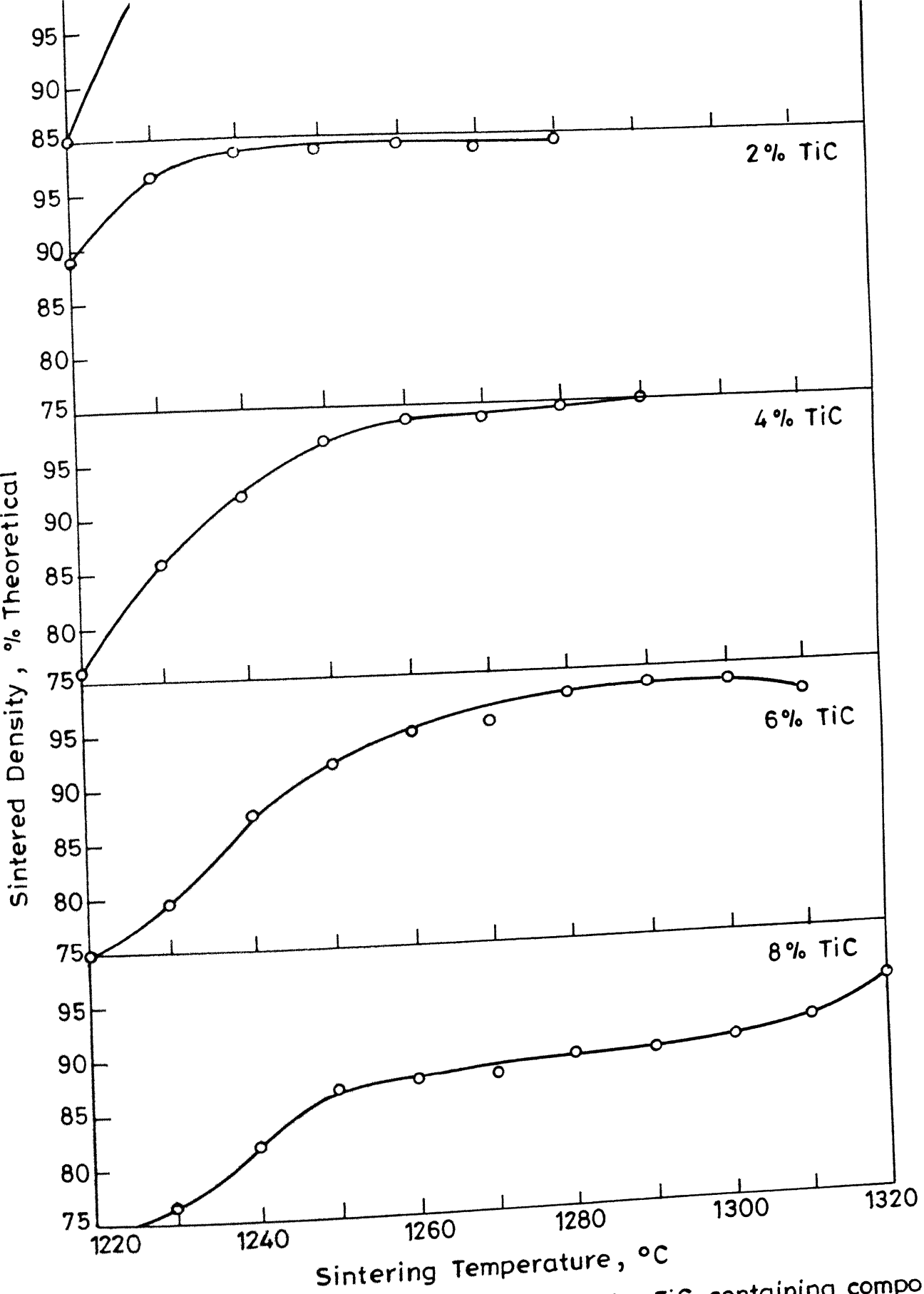

Fig. 3.20 Desification behaviour of T42 HSS and its TiC containing composites w.r.t. sintering temperature.

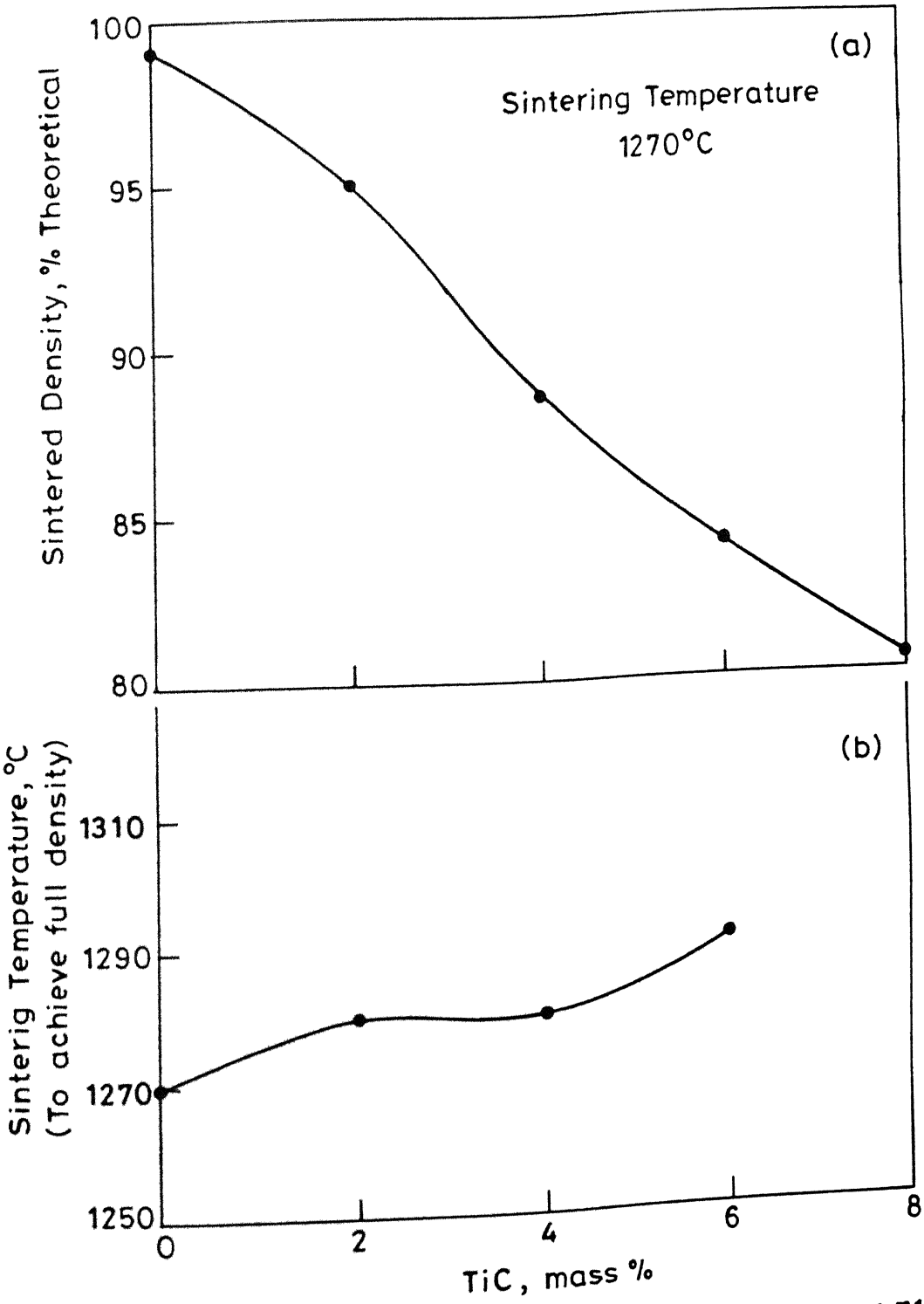

Fig. 3.21 (a) Effect of TiC addition on sintered density of T15 HSS sintered at 1270°C, Time 1.5 hrs,
(b) Effect of TiC addition in T15 HSS on sintering temperature (to achieve full density)

sintered density with sintering temperature is little higher than that observed for the composites of T15 HSS (Figure 3.19). Figure 3.22a shows the sintered densities achieved for T42 HSS and TiC composites when sintered at 1230°C. At 1230°C, straight composition achieved full density whereas the TiC rich composites achieved lower densities. The sintering temperature required to achieve full density with respect to TiC addition is shown in Figure 3.22c. The optimum sintering temperatures for composites containing 2, 4 and 6 mass % TiC were 1240°C, 1260°C and 1290°C respectively whereas composite containing 8 mass % TiC could not be sintered to full density even at 1320°C.

III.3.2. Hardness:

The sintered and triple tempered hardness variation with respect to TiC addition in T15 and T42 HSS is shown in Figure 3.23 and Figure 3.24 respectively. The sintered hardness increased with the increase in TiC content up to 4 mass % in T15 and T42 HSS. There was a decrease in the hardness value for any further addition of TiC beyond 4 mass %. T15 HSS composite containing 4 mass % TiC achieved a maximum sintered Vickers hardness of 650 whereas for T42 HSS composite containing 4 mass % TiC the value was 600. Similar to the sintered hardness variation, a peak was observed for triple tempered hardness for either T15 or T42 HSS based composites containing 4 mass % TiC. The Hardness variation

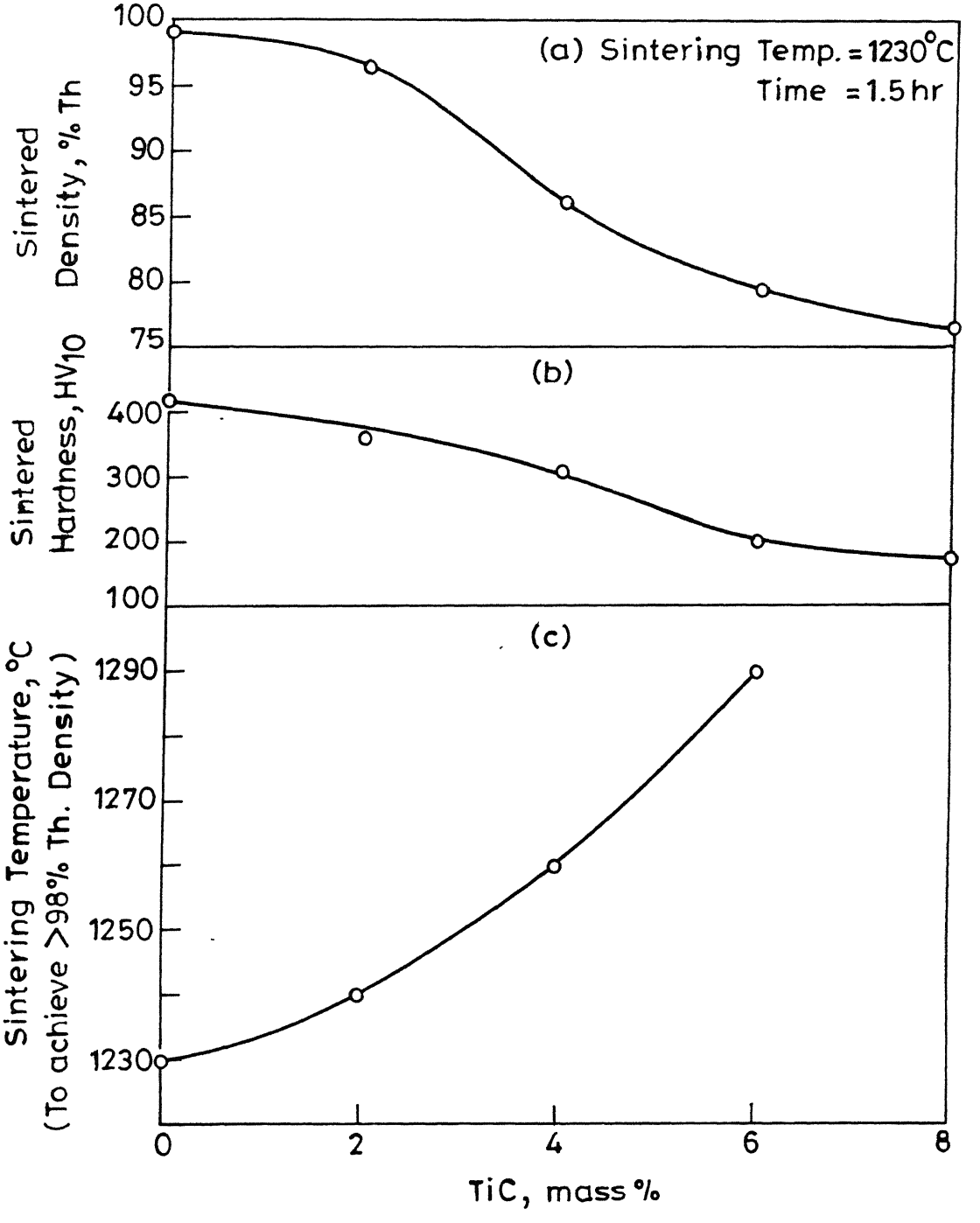

Fig. 3.22 Effect of TiC addition in T42 HSS on (a) Sintered density (b) Sintered hardness (c) Sintering temp. to achieve >98% Th. density.

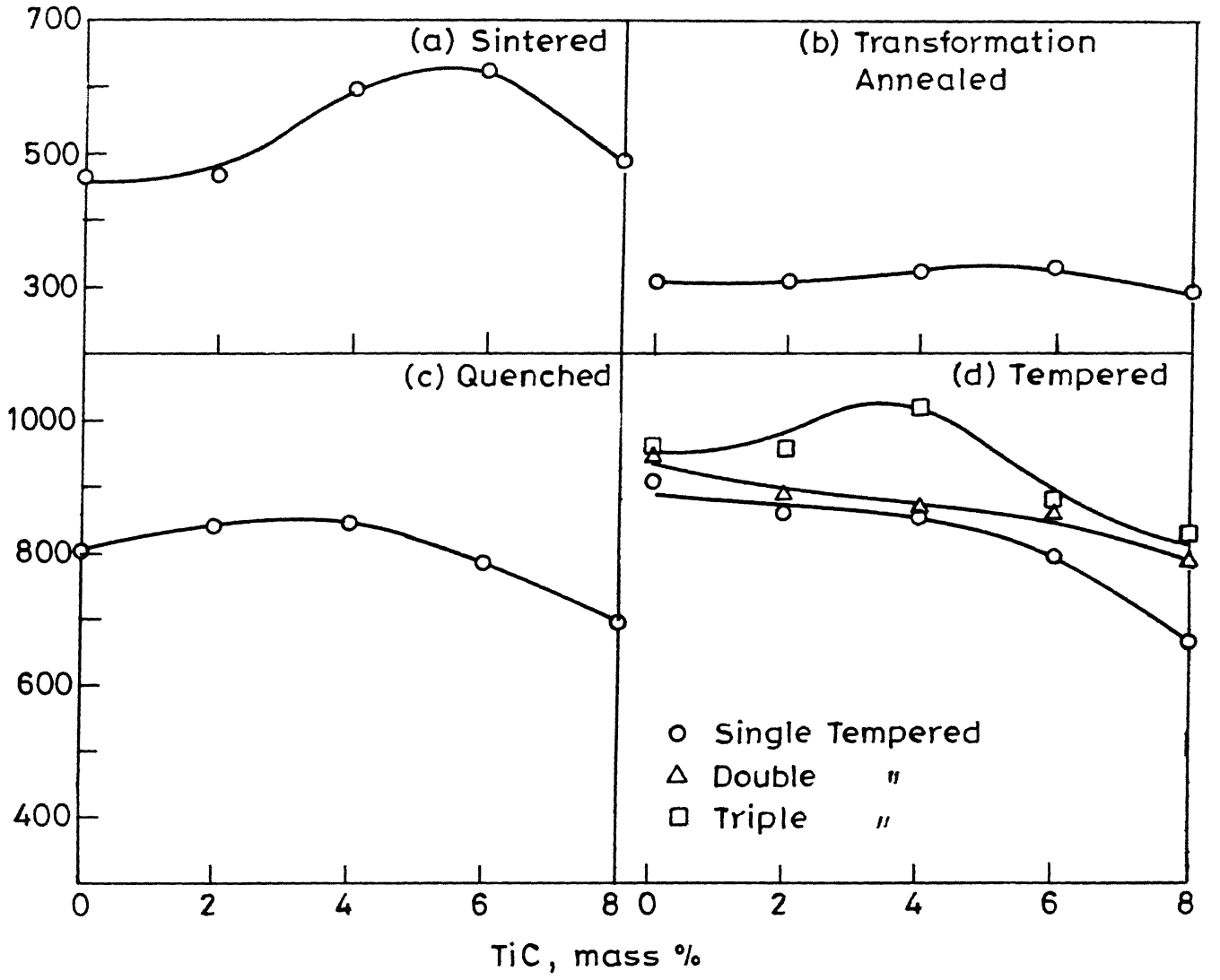

3.23 Hardness variation of T42 HSS and its TiC containing composites in various conditions: (a) Sintered (b) Transformation annealed (c) Quenched (d) Tempered.

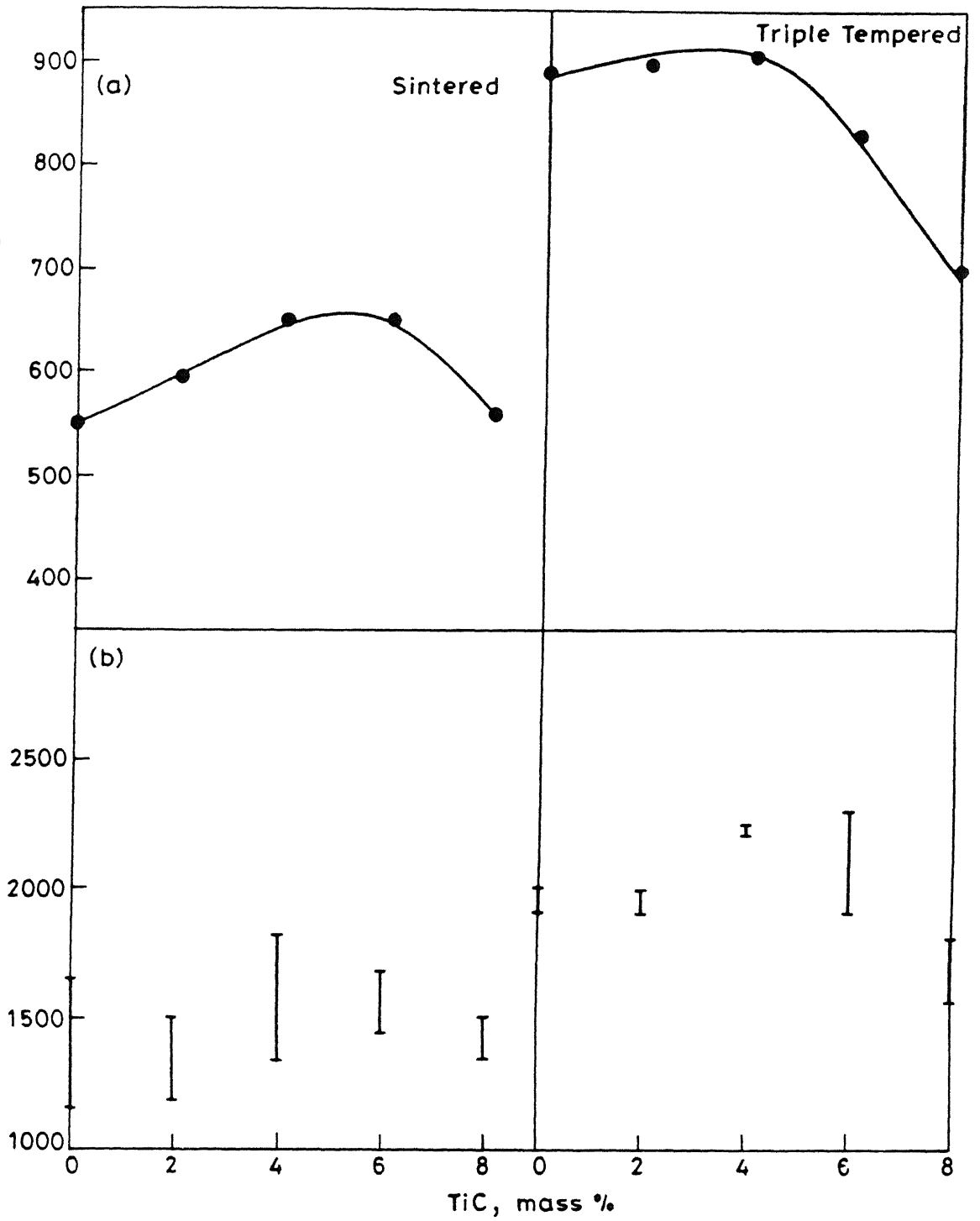

Fig.3.24 (a) Effect of TiC addition on sintered and triple tempered hardness of T15 HSS ; (b) Effect of TiC addition on TRS of sintered and Triple tempered T15 HSS.

conditions is shown in Figure 3.25. Peak hardness was obtained for composites containing 4 mass % TiC in any of the heat treatment conditions for either grades of HSS.

III.3.3. Transverse Rupture Strength (TRS):

The TRS variation with respect to TiC addition of sintered and triple tempered T15 and T42 HSS is shown in Figure 3.24 and Figure 3.25 respectively. Similar to the hardness variation, there exists a peak TRS value for composites containing 4 mass % TiC in either condition. In case of T15 HSS based composites (Figure 3.24), the triple tempered TRS was higher than the sintered TRS, whereas in case of T42 HSS based composites, the reverse was observed.

III.3.4. Compressive Yield Strength:

The room and elevated temperature compressive yield strength variation of composites of T15 and T42 HSS containing TiC are shown respectively in Figures 3.26, 3.27 and 3.28. In any composite, with the increase in the testing temperature, there was a continuous fall in the yield strength and beyond 500^{o}C, the fall was rapid. For either HSS, composites containing 4 mass % TiC gave the highest compressive yield strength at any testing temperature. In case of T15 HSS composites, a gain of 22% in room temperature compressive yield strength for composites containing 4 mass % TiC (3250 MPa) above that of the straight composition was obtained. Similarly, for T42 HSS composites, the gain in

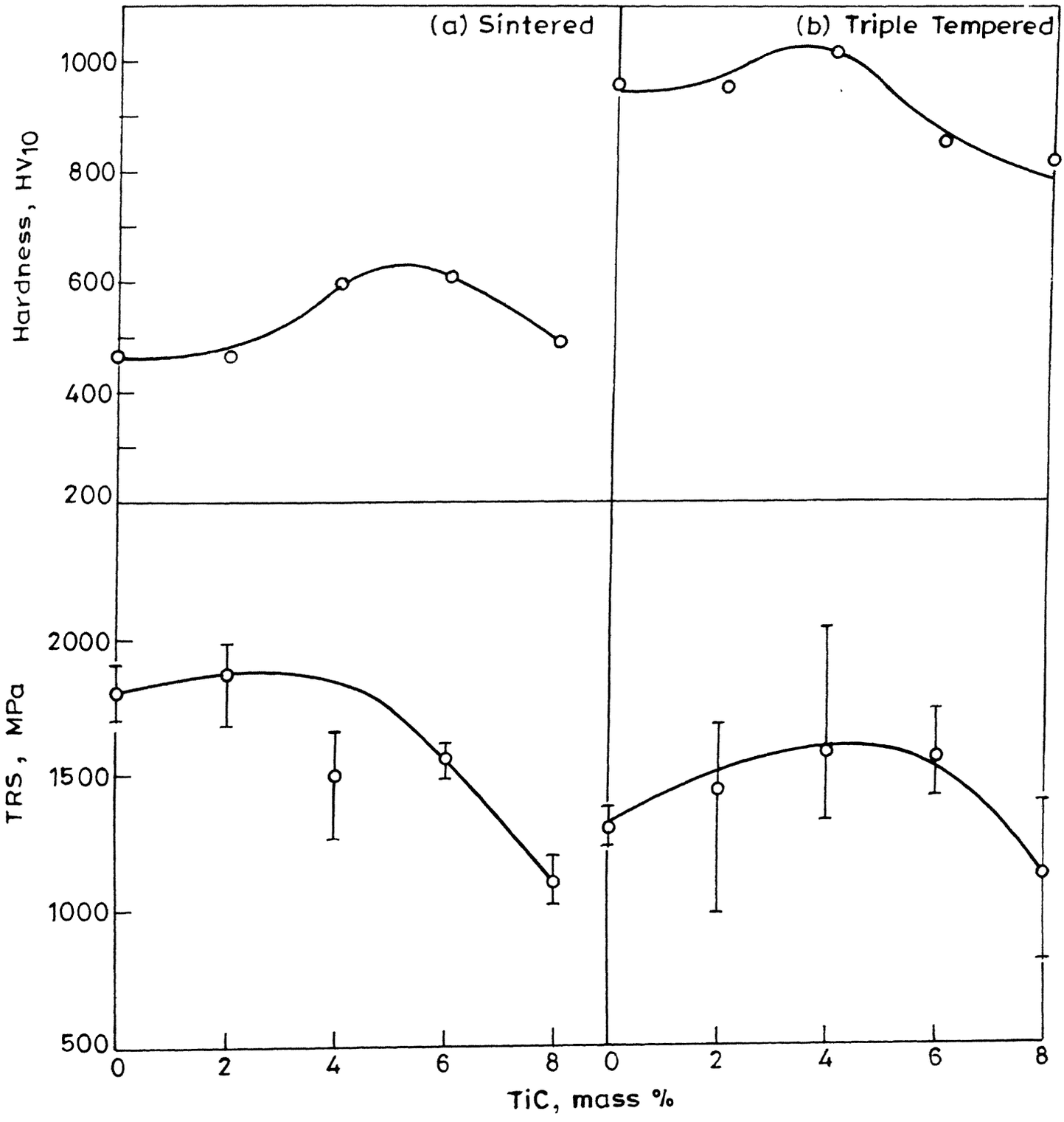

Fig.3.25 Effect of TiC addition on hardness and TRS of T42 HSS in (a) Sintered (b) Triple tempered conditions.

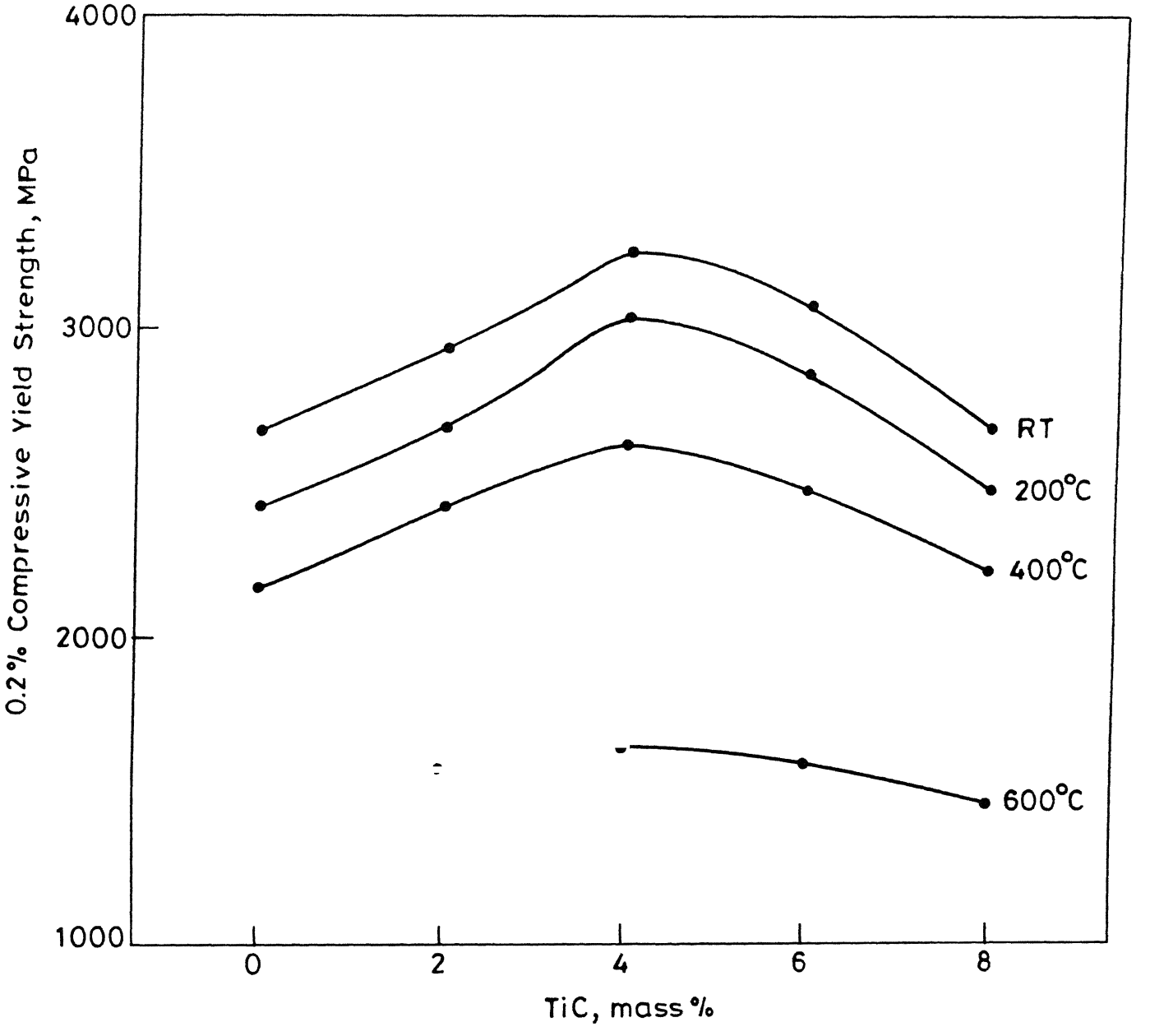

Fig.3.26 0.2% compressive yield strength variation of T15 HSS and its TiC containing composites tested at various temperatures.

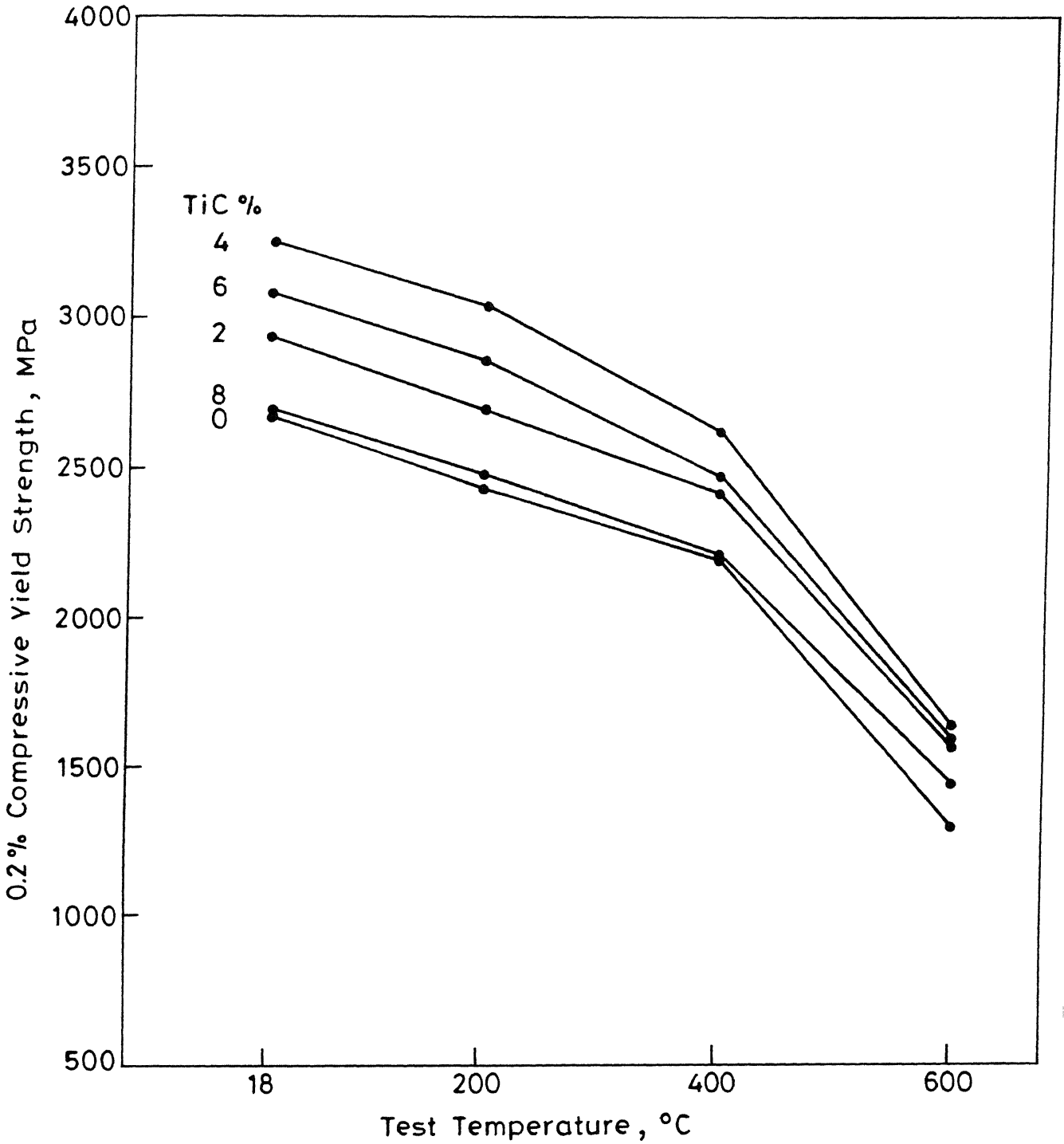

Fig. 3.27 0.2% Compressive yield strength variation of T15 HSS and its TiC containing composites with temperature.

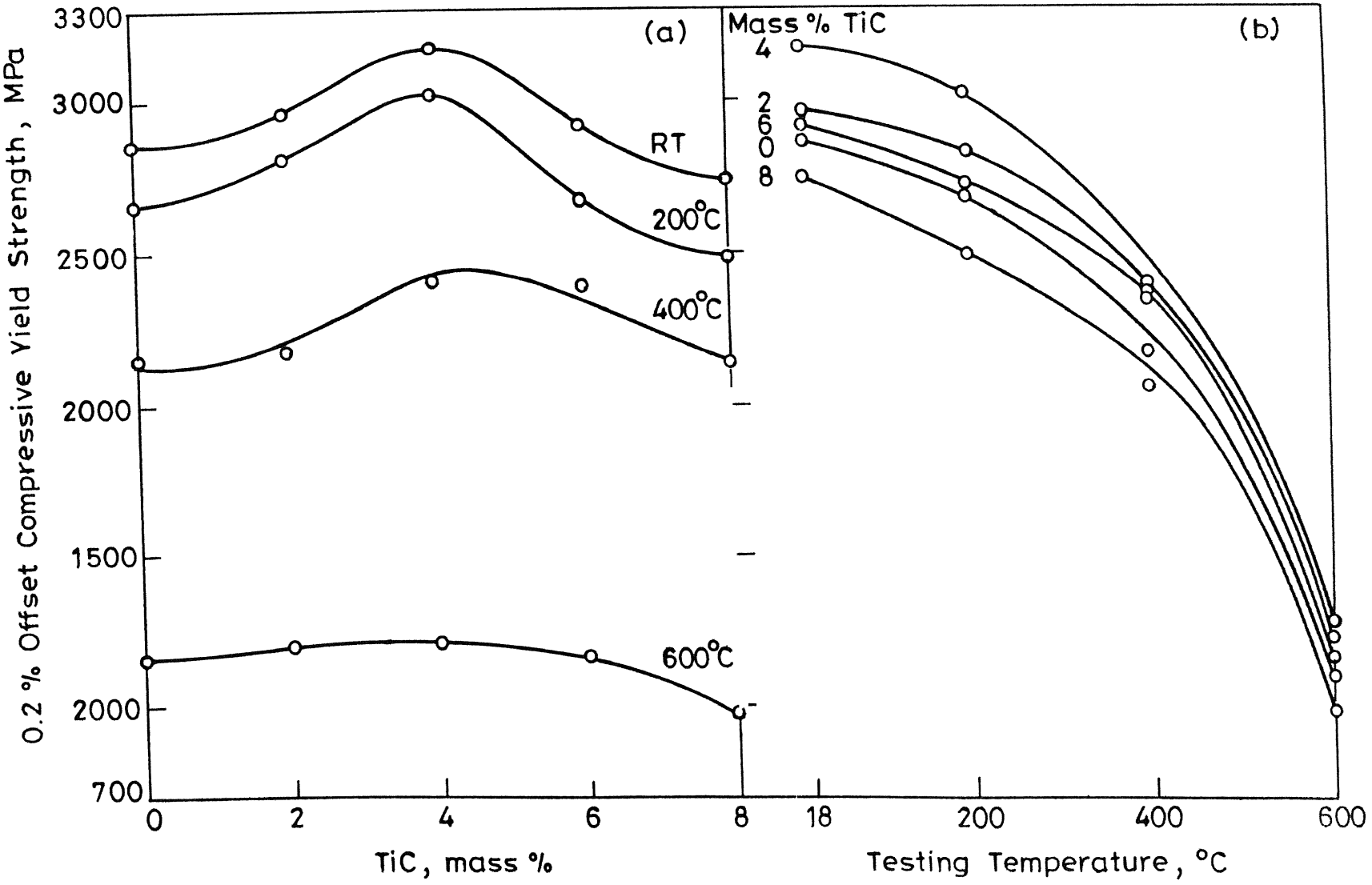

Fig.3.28 0.2% offset compressive yield strength of fully heat treated T42 HSS and its TiC containing composites w.r.t. (a) TiC addition (b) Testing temperature.

compressive yield strength was only 11% for the composite containing 4 mass % TiC (3180 MPa) above that for the straight composition. Comparing between the composites of any constant refractory compound (TiC or TiN) content, composites based on T15 HSS showed higher compressive yield strength than those based on T42 HSS, although the difference was marginal.

III.3.5. Microstructural Analysis:

Figure 3.29 and Figure 3.30 show the optical microstructures respectively for T15 and T42 HSS composites containing TiC in sintered and triple tempered conditions. In either case, there was no observable porosity indicating that the steel was fully dense. The sintered microstructure consisted of primary carbides on and within the grains. The TiC particles were to some extent aglomerated due to their nonuniform dispersion during processing. The microstructures in case of T42 HSS based composites were similar to those based on T15 HSS. The microstructure of 6 mass % TiC containing composite was coarser as compared to that containing 4 mass % TiC.

Figures 3.31 and 3.32 show the nature of the MC type of primary carbide in TiC containing T15 or T42 HSS based composites respectively. The MC type of the carbide was dark in colour. TiC particles were greyish in colour and were clustered around the primary MC carbides. The nature of

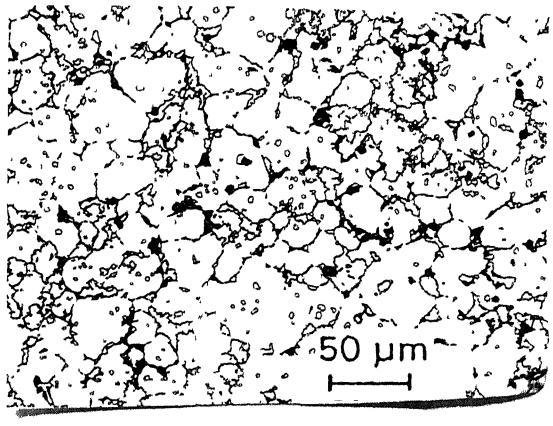

(a) Sintered

(b) Sintered

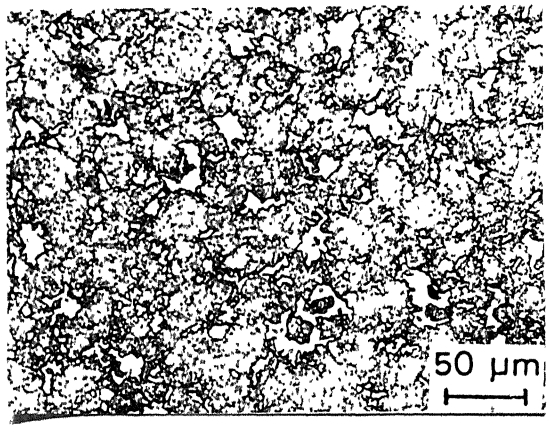

(c) Triple tempered
4 mass % TiC

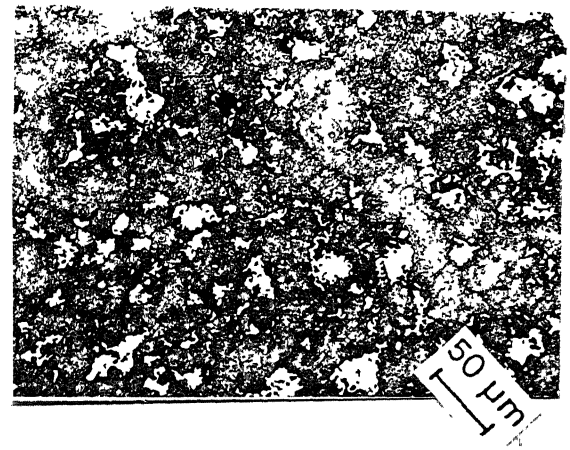

(d) Triple tempered
6 mass % TiC

Figure 3.29. Optical microstructures of T15 HSS containing TiC.

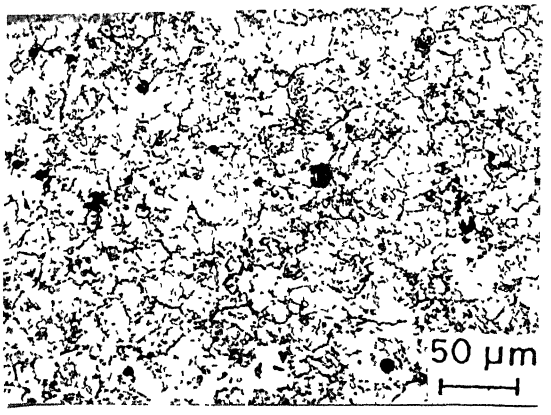

(a) Sintered

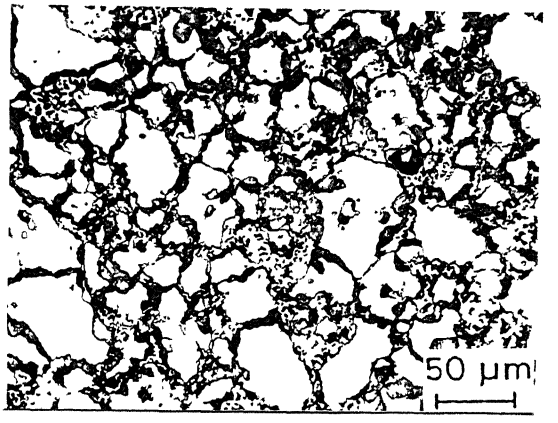

(b) Sintered

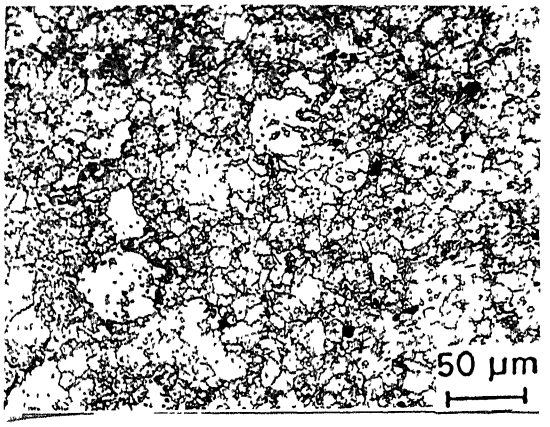

(c) Triple tempered
4 mass % TiC

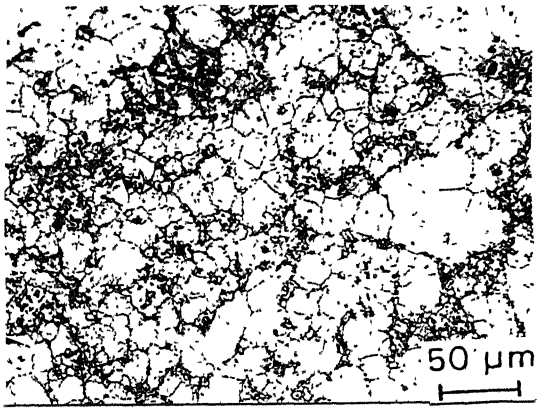

(d) Triple tempered
6 mass % TiC

Figure 3.30. Optical microstructures of T42 HSS containing TiC.

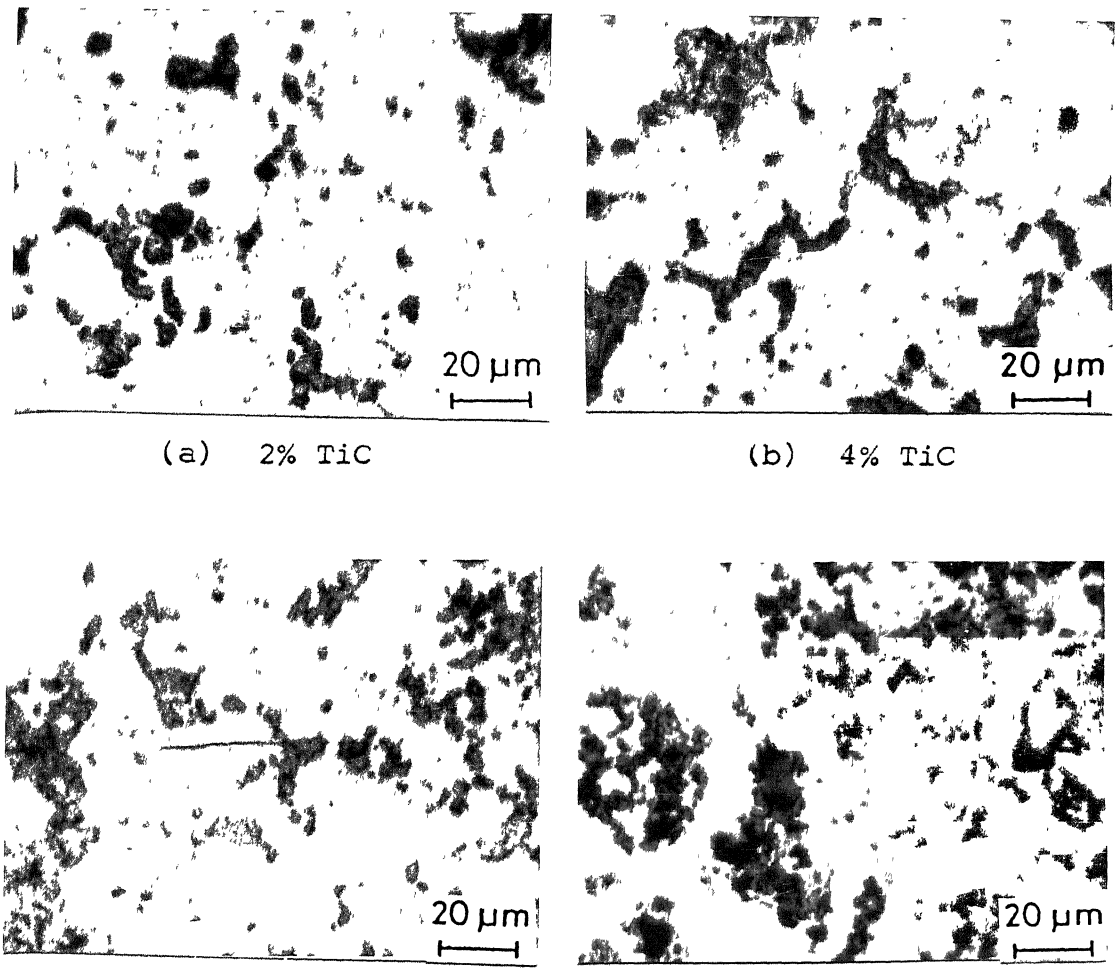

(a) 2% TiC (b) 4% TiC

(c) 6% TiC (d) 8% TiC

Figure 3.31. MC type primary carbide in T15 HSS-TiC composites in sintered condition.

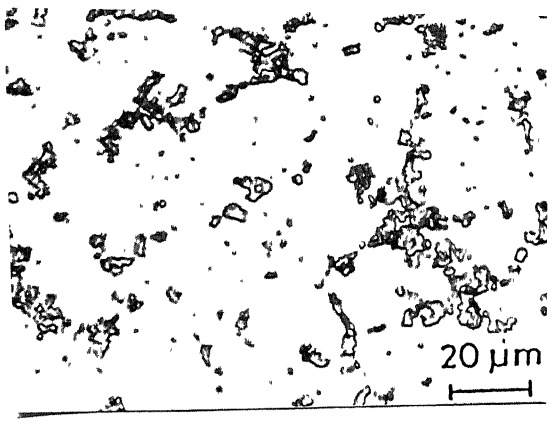

(a) Sintered

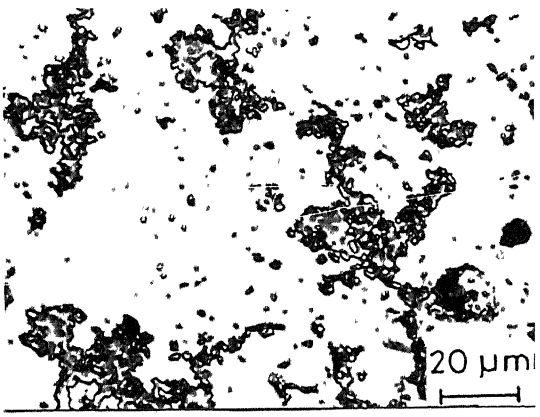

(b) Sintered

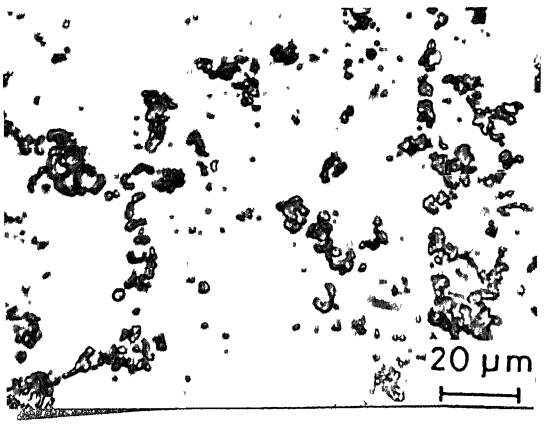

(c) Triple tempered
4% TiC

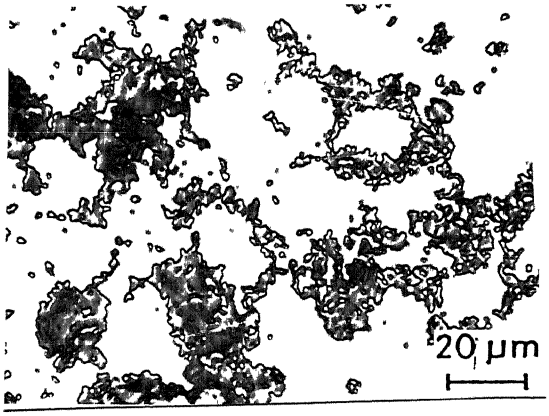

(d) Triple tempered
6% TiC

Figure 3.32. MC type primary carbide in T42 HSS-TiC composites in sintered and triple tempered conditions.

the microstructure for either T15 or T42 HSS was identical and remained unchanged in any condition viz. sintering, hardening or tempering.

The grain size variation with respect to TiC addition in T15 and T42 HSS is shown in Figure 3.33 and Figure 3.34 respectively. In both the cases, the grain size increased with the increase in the TiC content in the composite. The grain size in the sintered condition was higher than that in the triple tempered condition. In case of T15 HSS based composites (Figure 3.33), the largest grain size observed was 35 μm for the composite containing 8 mass % TiC in the sintered condition. This value got reduced to 15 μm size after transformation annealing/triple tempering. In case of T42 HSS based composites (Figure 3.34), the largest grain size of 16 μm was obtained for composite containing 8 mass % TiC in sintered condition. After transformation annealing/ triple tempering, this got reduced to 7 μm. The grain size of any T42 HSS based composite in any condition was lower than the corresponding T15 HSS based composite.

The volume fraction variation of primary carbides (MC and M_6C) for T15 or T42 HSS based composites measured quantitative metallographically is shown in Figure 3.35 and Figure 3.36 respectively. The volume fraction of MC carbide in both the cases increased gradually corresponding to the increase in TiC content. For any composite, the MC volume fraction also increased when the condition changed from

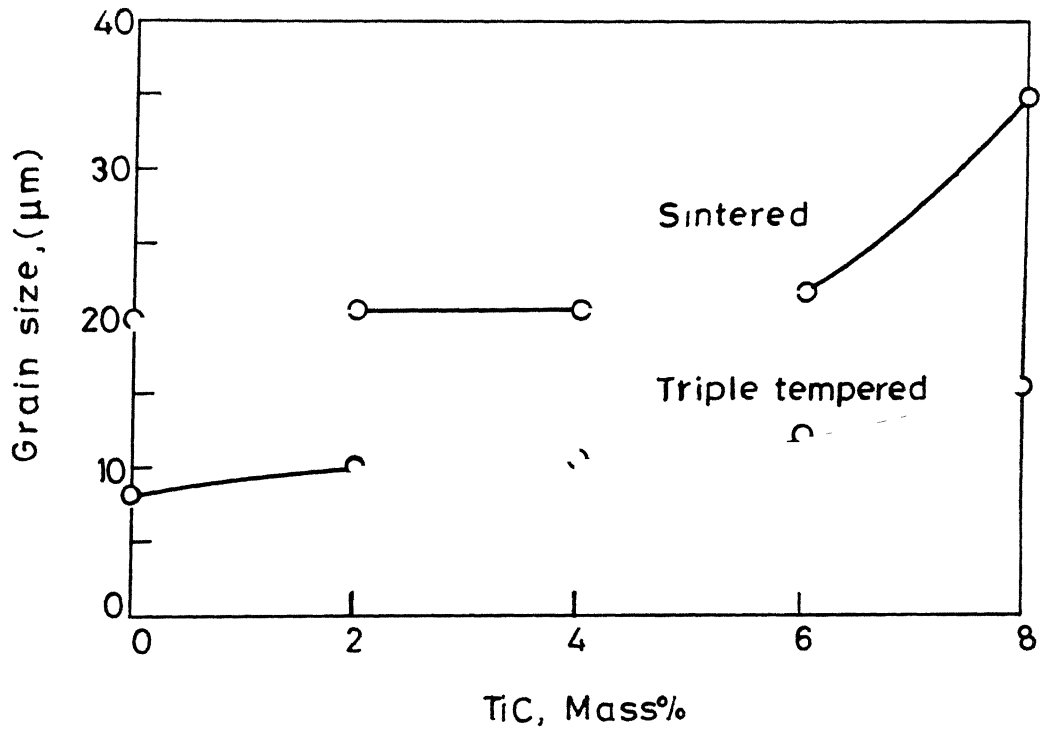

Fig.3.33 Effect of TiC addition on grain size of T15 HSS (sintered at different optimised temperature).

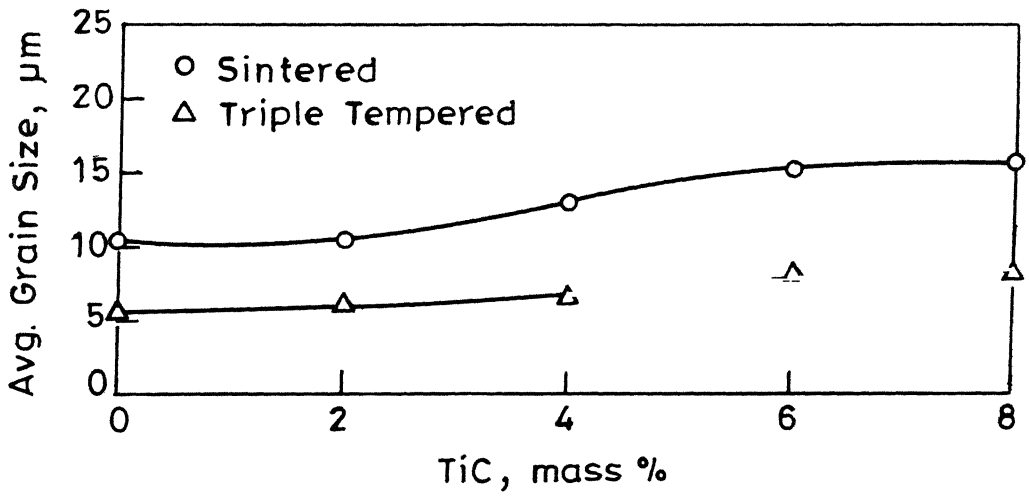

Fig. 3.34 Effect of TiC addition on grain size of T42 HSS (sintered at different optimised temperatures).

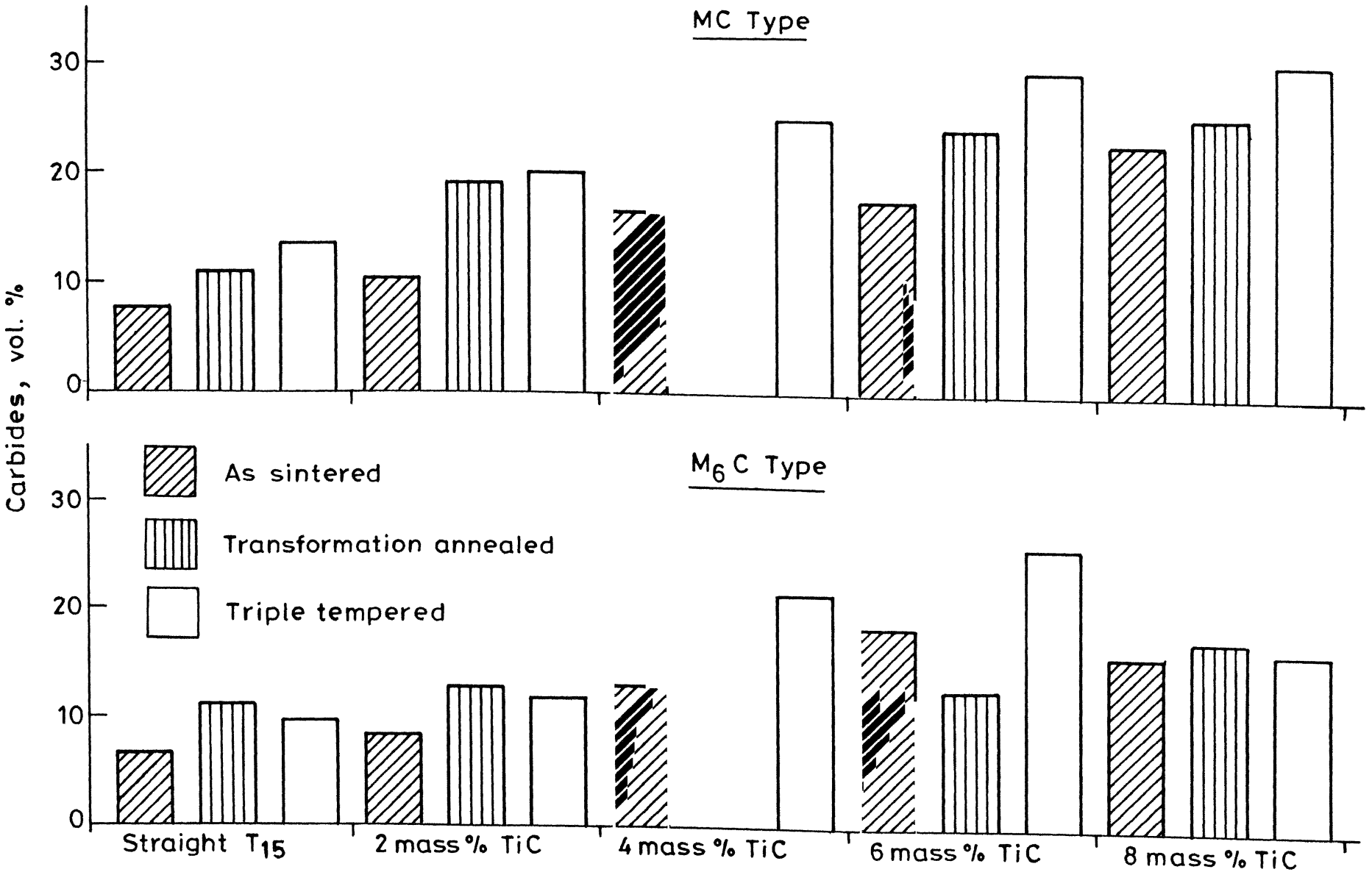

Fig.3.35 Volume fraction of MC and M_6C type carbides in as sintered, transformation annealed and triple tempered T15 HSS and its TiC containing composites

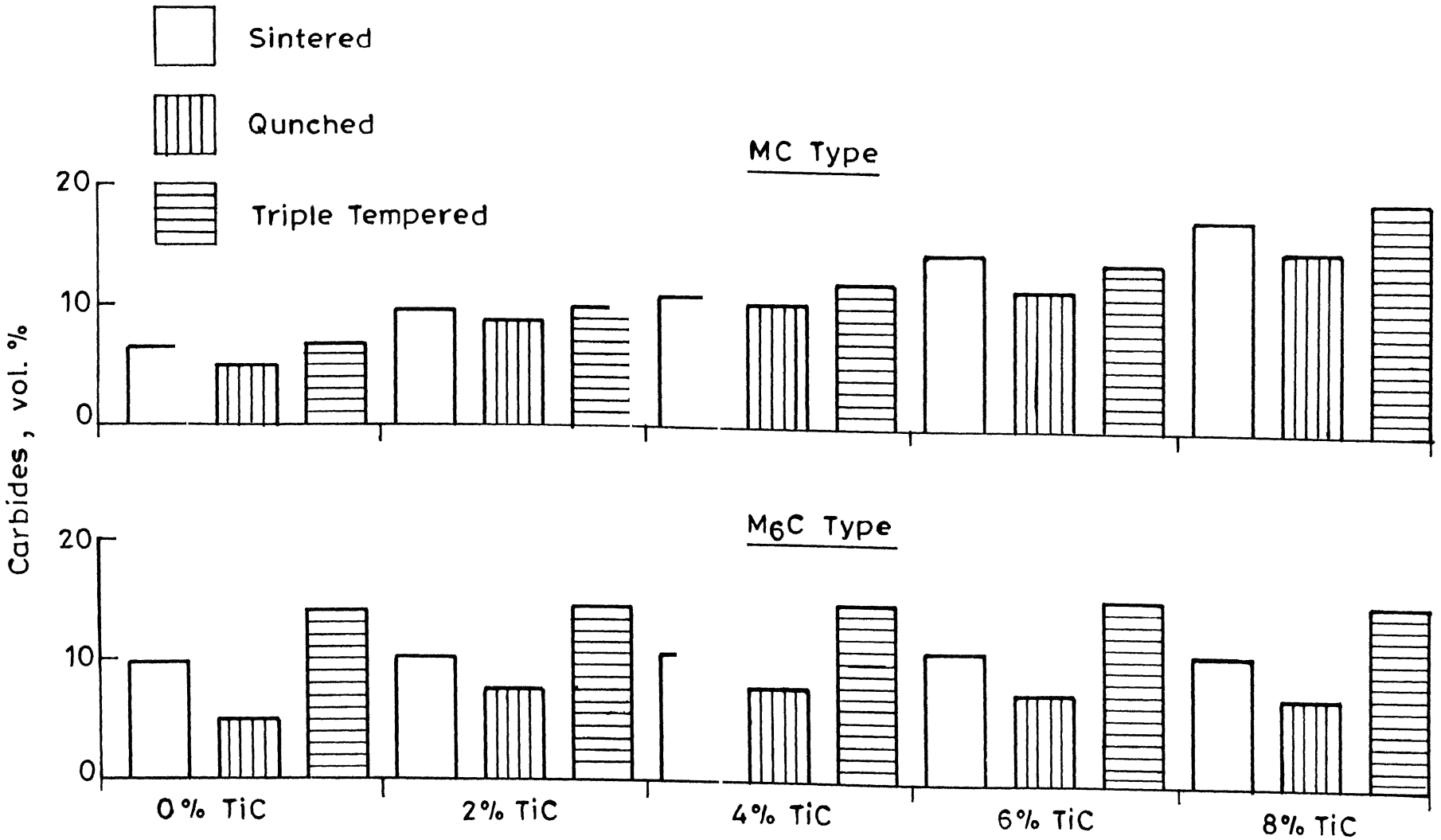

Fig. 3.36 Volume fraction of MC and M_6C type carbides w.r.t. TiC addition in T42 HSS.

sintered to triple tempered condition. The highest MC volume fraction noticed was 30% for T15 HSS containing 8 mass % TiC in triple tempered condition, whereas in case of similar T42 HSS based composite, the highest MC content noticed was 19%. The volume fraction of M_6C carbide in case of T15 HSS based composites increased gradually with the increase in TiC content, whereas this remained nearly unchanged in case of T42 HSS based composites. Figure 3.37 and Figure 3.38 show the size distribution of primary carbides for the TiC containing composites based on T15 and T42 HSS respectively. In either case, the composites containing higher TiC content contained coarser primary carbides after any heat treatment. Comparing between similar composites of T15 and T42 HSS, it is seen that the composites based on T15 HSS contained larger fraction of coarse carbides as compared to that of T42 HSS based.

Figure 3.39 shows the SEM micrographs of T42 HSS based composites containing 4 mass % TiC in various heat treatment conditions. TiC particles were black and uniformly distributed throughout the matrix. Their identity was confirmed from the EDX analysis (Table III.5). It was also noticed that the matrix contained no titanium which indicate about the stability of TiC particles in HSS matrix.

Figure 3.40 shows the SEM fractographs taken on the fracture surfaces of broken TRS test pieces of T42 HSS containing 4% TiC. The fractograph in sintered condition contains dimples indicative of the ductile nature of the fracture.

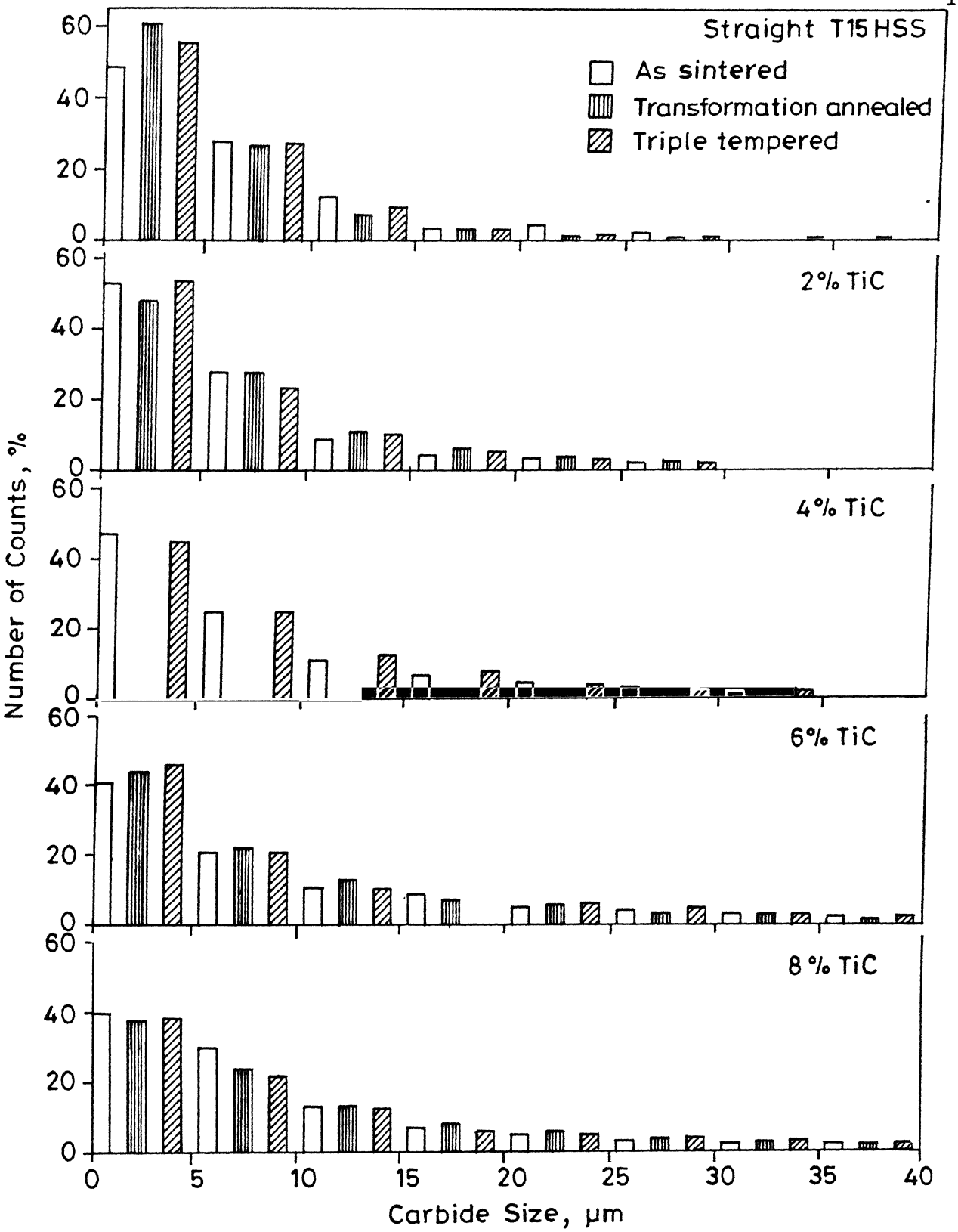

Fig.3.37 Carbide size distribution in T15 HSS and its TiC containing composites in as sintered, transformation annealed and triple tempered conditions.

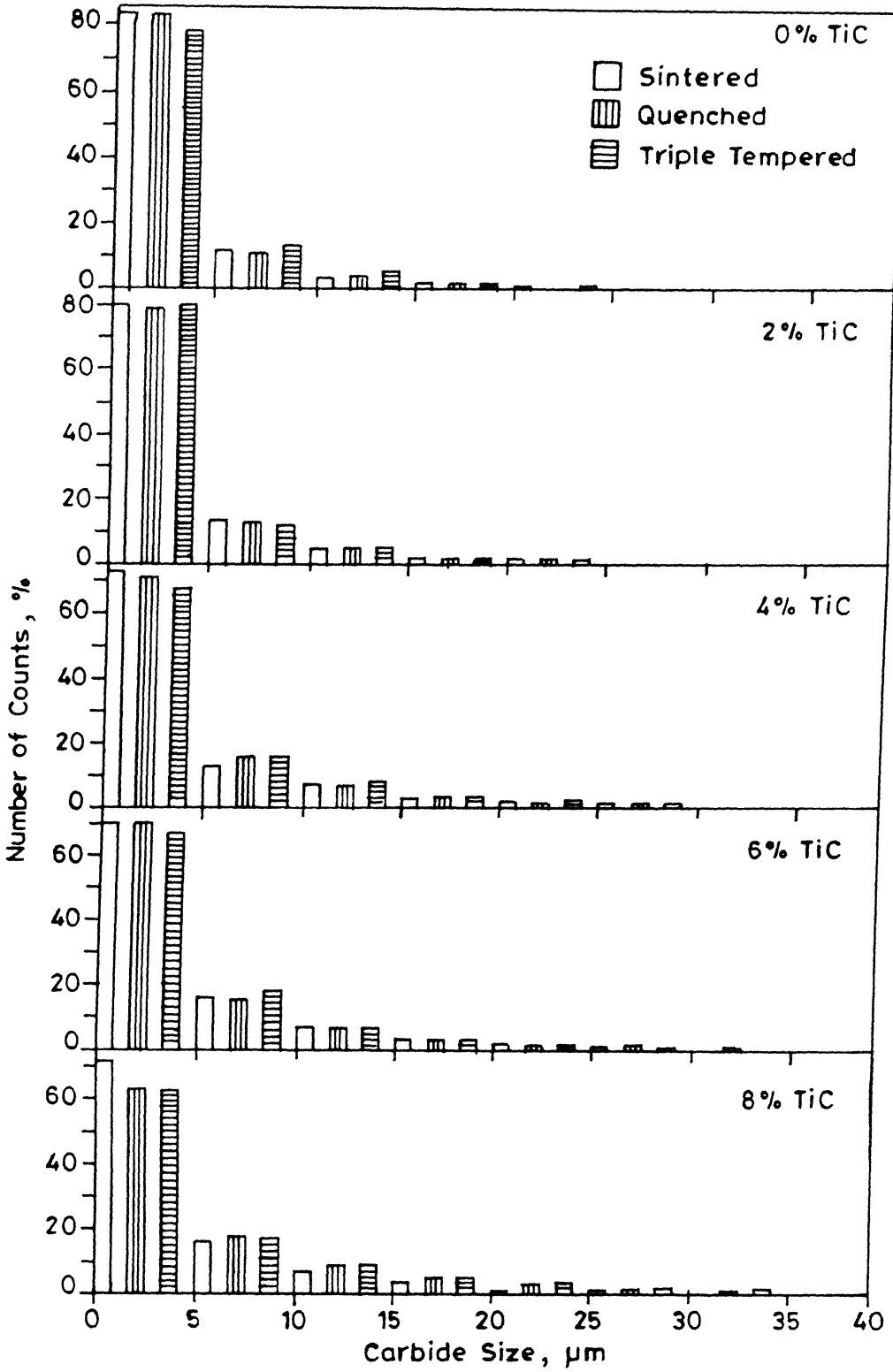

Fig.3.38 Size distribution of primary carbides in T42 HSS and its TiC containing composites.

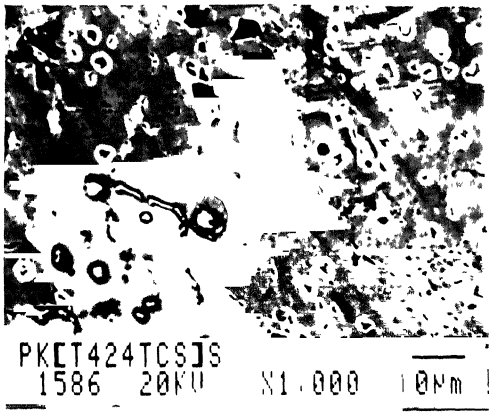

(a) Sintered

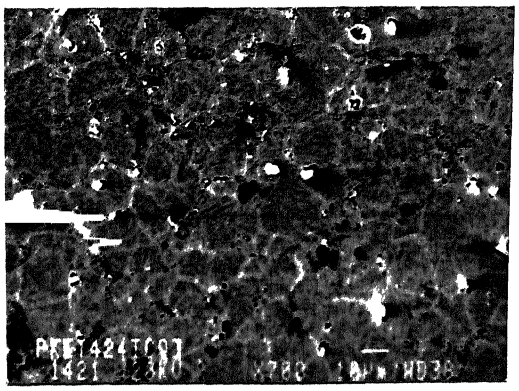

(b) Quenched

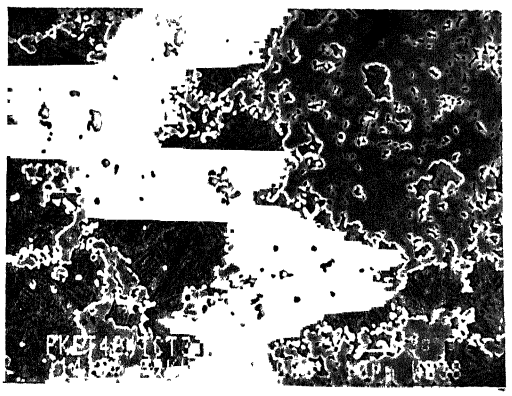

(c) Triple tempered

Figure 3.39. SEM photomicrographs of T42 HSS containing 4% TiC.

Table III.5: EDX analysis of various phases of T15 and T42 HSS containing TiC.

HSS composite	Description of phase	Mass % chemical analysis							Assigned phase
		Fe	Cr	Co	Mo	V	W	Ti	
T15 - 4% TiC Sintered	Matrix	79.32	3.72	5.60	1.71	2.75	6.90	-	Matrix
T15 - 4% TiC Sintered	Dark phase	4.70	0.50	0.40	0.20	0.05	1.00	92.96	TiC particle
T15 - 4% TiC Triple tempered	Matrix	81.94	4.93	4.84	0.66	1.78	5.86	-	Matrix
T15 - 4% TiC Triple tempered	Dark phase	4.17	0.48	0.34	0.21	0.08	1.65	92.86	TiC particle
T15 - 4% TiC Triple tempered	Grey particle	4.65	1.61	0.53	3.38	31.48	38.18	20.14	MC type carbide
T42 - 4% TiC Sintered	Grey phase	14.48	3.10	1.38	16.19	35.18	29.65	-	MC type carbide
T42 - 4% TiC Sintered	Dark phase	9.20	0.91	0.92	0.92	0.10	1.95	86.00	TiC particle
T42 - 4% TiC Triple tempered	Dark phase	2.47	0.45	1.03	0.23	-	2.58	93.45	TiC particle
T42 - 4% TiC Triple tempered	Dark phase in cluster form	4.57	4.23	9.01	3.62	19.82	1.41	57.34	MC carbide in TiC cluster

(a) Sintered

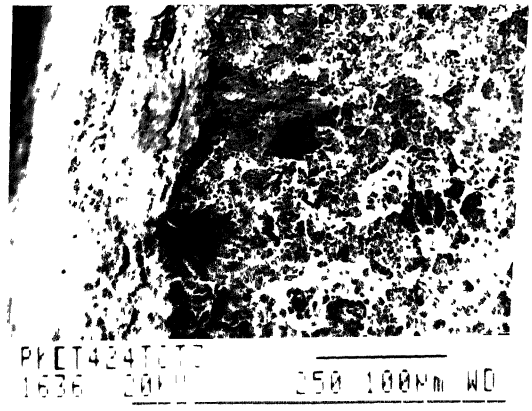

(b) Triple tempered

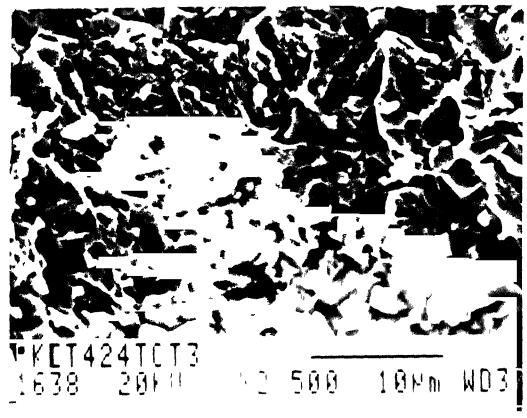

(c) Triple tempered

Figure 3.40. SEM fractographs of T42 HSS containing 4% TiC.

The fracture in triple tempered condition appears to be of quasi cleavage nature.

III.3.6. Magnetic Property:

The magnetic property in terms of coercivity of T15 and T42 HSS and their TiC containing composites is shown in Figure 3.41. There is a noticeable peak at 4 mass % TiC content in sintered condition for composites based on either T15 or T42. However, the coercivity of triple tempered samples remained more or less unchanged. The coercivity values obtained for any T42 HSS based composites in either sintered or triple tempered condition were higher than those obtained for T15 HSS based composites.

III.3.7. Tool Life:

Figure 3.42 shows the tool life variation of T15 and T42 HSS based composites containing TiC. The tool life increased with the increase in the TiC content for both the grades of HSS. An increase in the tool life of 25% and 65% above the base composition for composites containing 2% and 4% TiC respectively is noticed for T15 HSS, whereas the increase in tool life for the corresponding T42 HSS based composite compositions are 16 and 40% respectively. However, a direct comparison of these tool lives between the composites of T15 and T42 HSS base cannot be done due to the difference in the tool cross section.

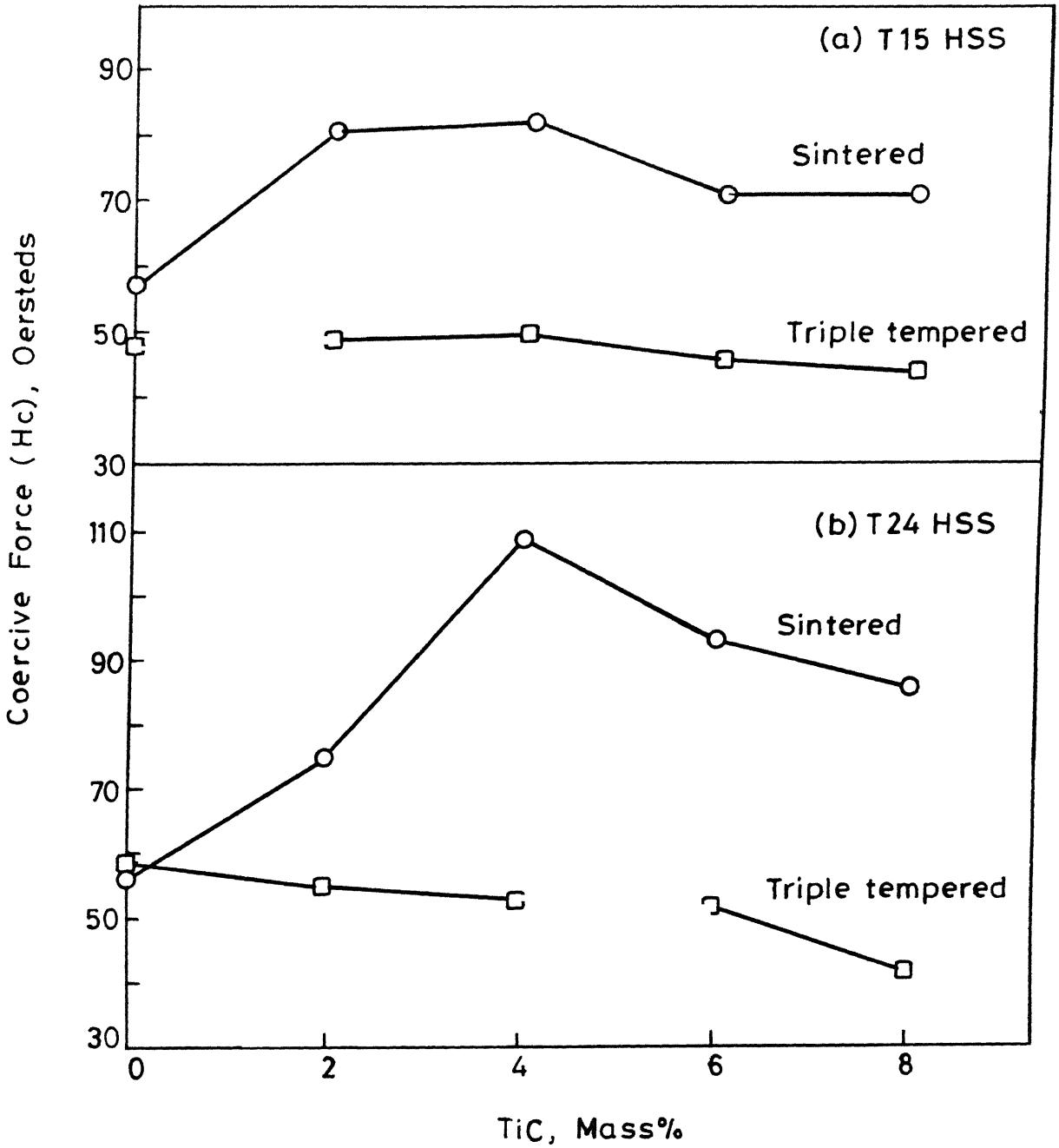

Fig.3.41 Variation of coercivity with respect to TiC addition in (a) T15 HSS (b) T42 HSS.

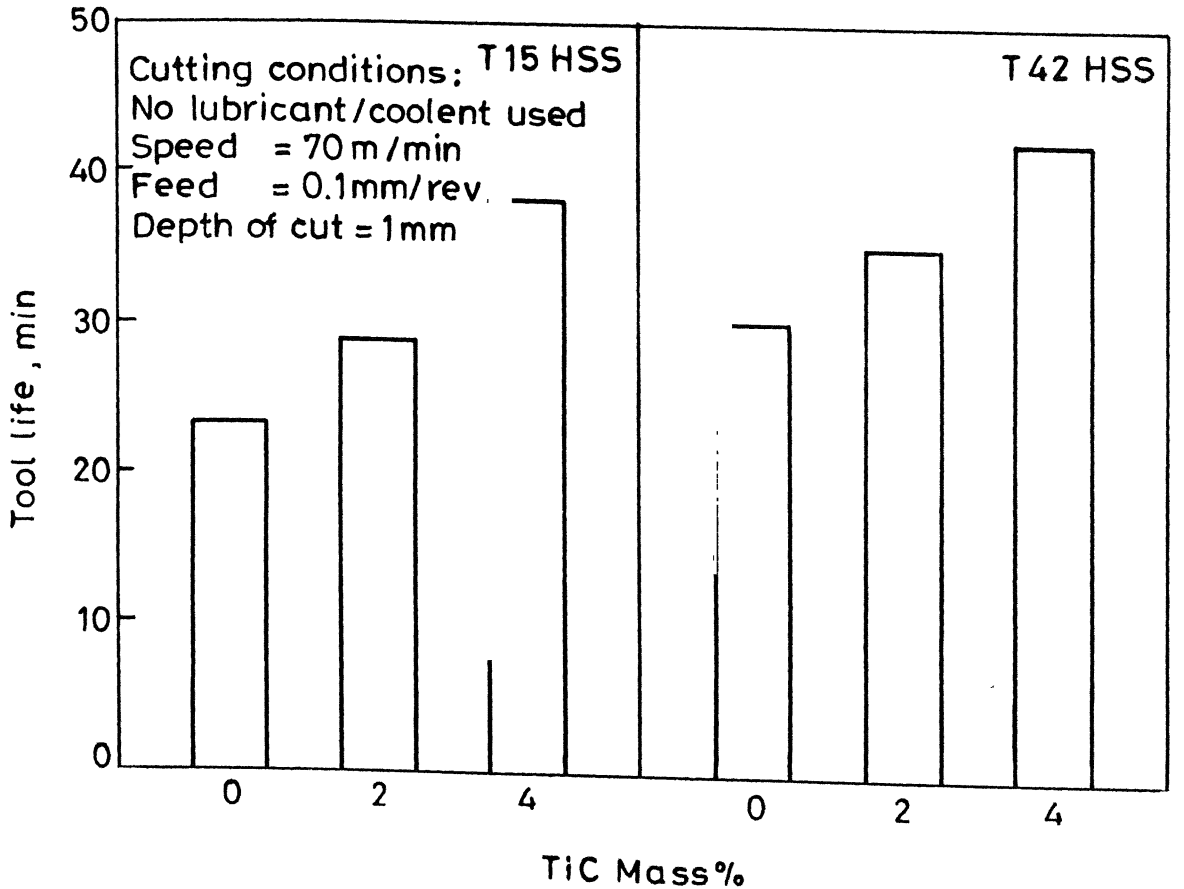

Fig.3.42 Tool life variation with TiC content in the composites of T15 and T42 HSS.

III.4. HSS COMPOSITES CONTAINING TiN:

III.4.1. Densification:

The densification behaviour of T15 HSS containing 0-8 mass % TiN is shown in Figure 3.43. At 1260°C, straight composition (belonging to Source-II) achieved full density whereas composites containing TiN achieved lower densities. The increase in the sintered density of either HSS at any sintering temperature was less for TiN rich HSS. Figure 3.45 shows the effect of TiN addition in T15 HSS on sintered density and also on the sintering temperature to achieve full density. The optimum sintering temperature for achieving full density increased with the increase in TiN content.

Figure 3.44 shows the densification behaviour of T42 HSS composites containing 0-8 mass % TiN. Similar to the T15 HSS composites, the T42 HSS based composites required higher sintering temperature to achieve full density for TiN rich composites. For any T15 HSS composites, the marginal increase in the sintered density with the increase in sintering temperature was lower than the corresponding T42 HSS based composites. Figure 3.46 shows the effect of TiN addition on the densification behaviour and the optimum sintering temperature to achieve full density for the TiN containing T42 HSS composites. The optimum temperatures required for full dense processing increased with the increase in TiN content (Figure 3.46c).

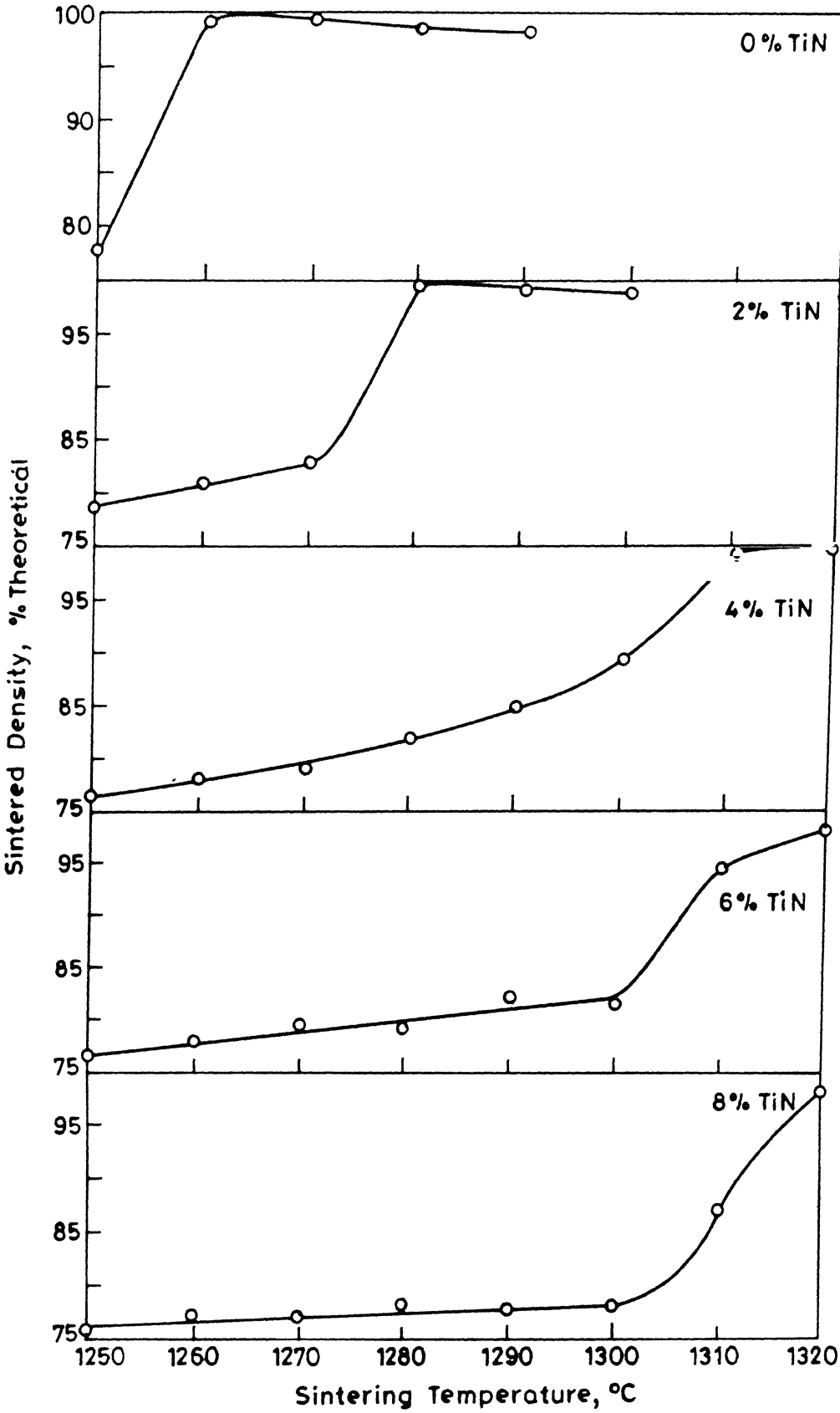

Fig. 3.43 Densification behaviour of T15 HSS and its TiN containing composites w.r.t. sintering temperature.

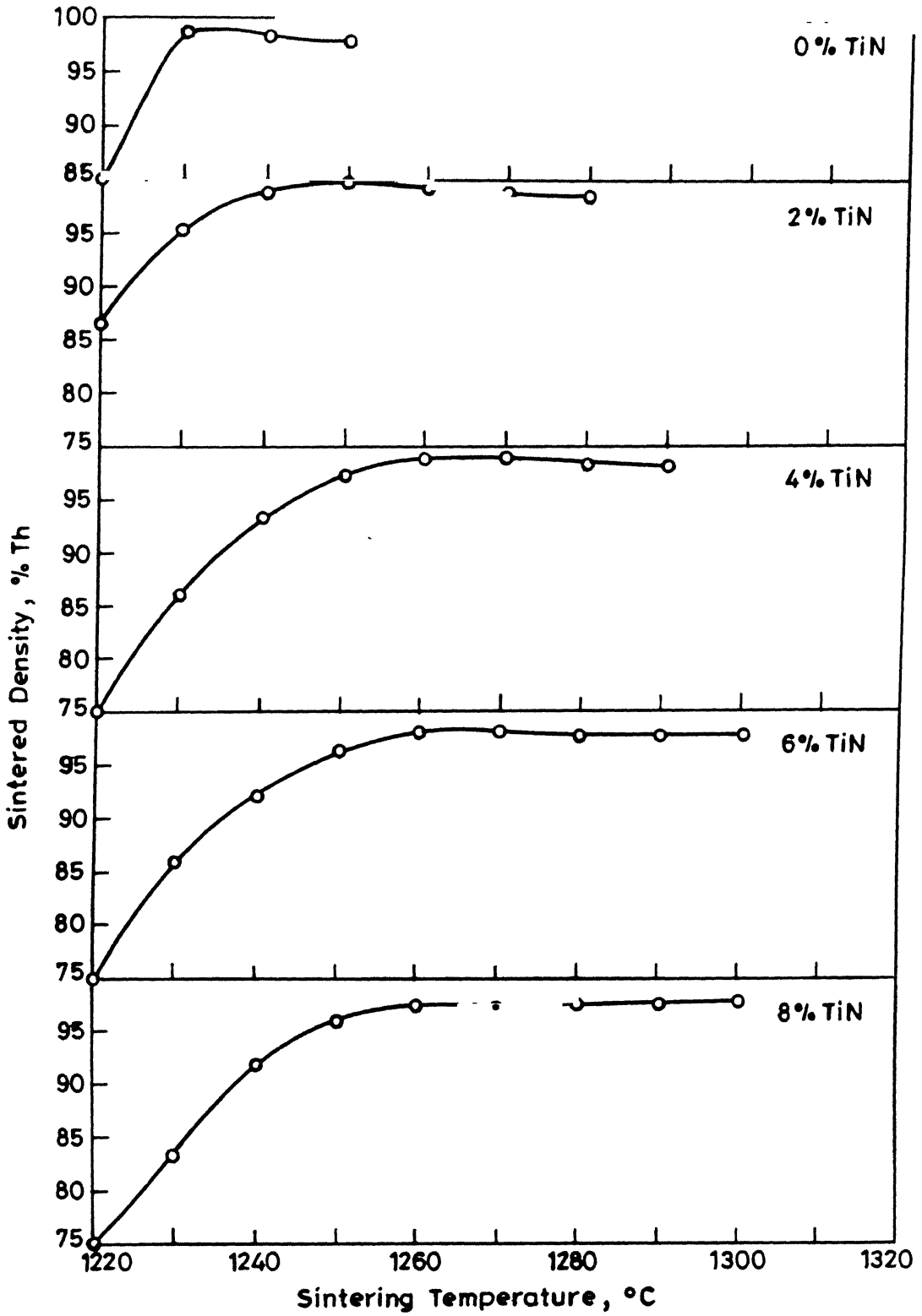

Fig. 3.44 Densification behaviour of T42 HSS and its TiN containing composites w.r.t. sintering temperature.

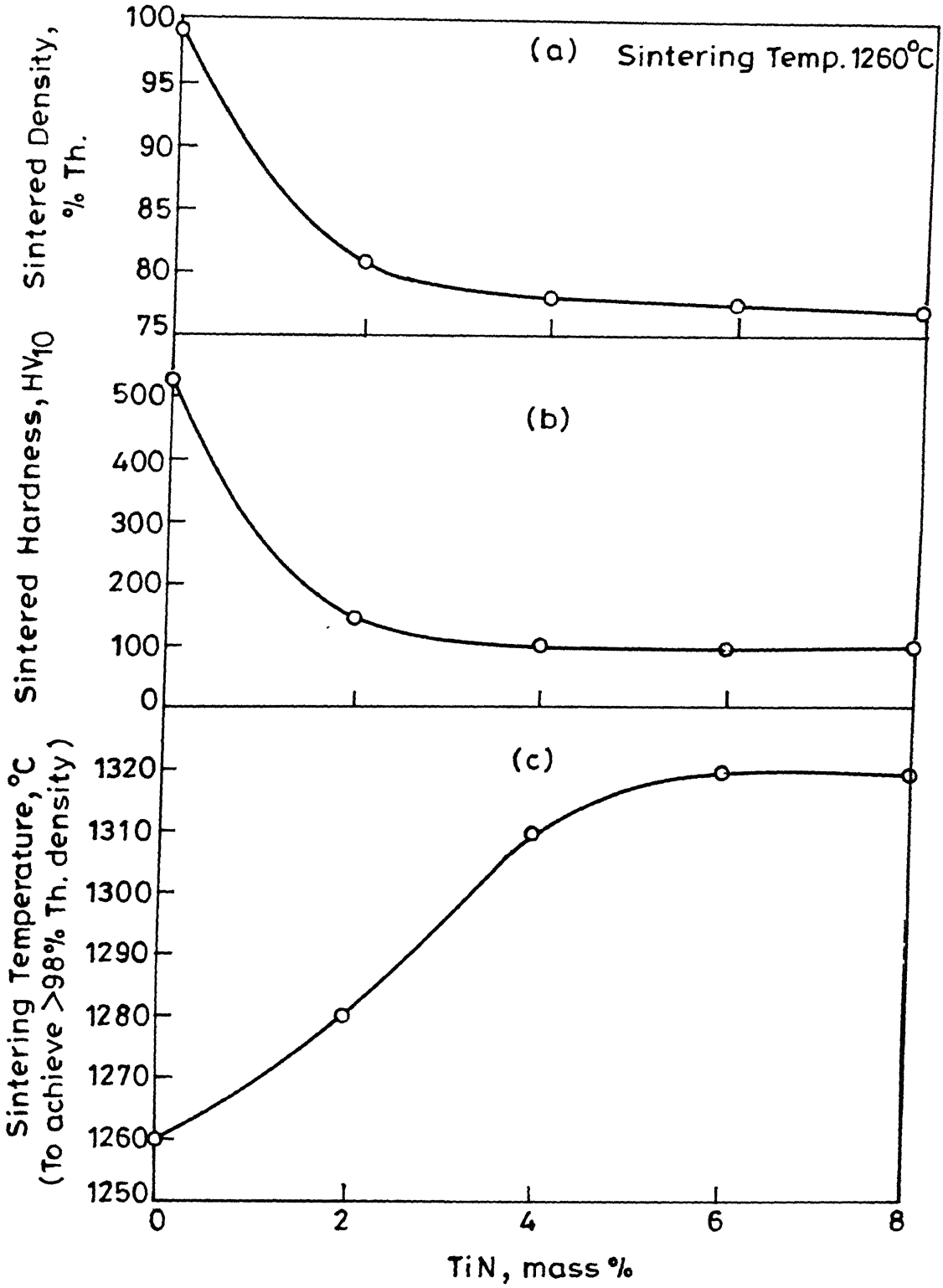

Fig. 3.45 Effect of TiN addition in T15 HSS on
(a) Sintered density, (b) Sintered hardness and
(c) Sintering temerature to achieve >98% Th. density.

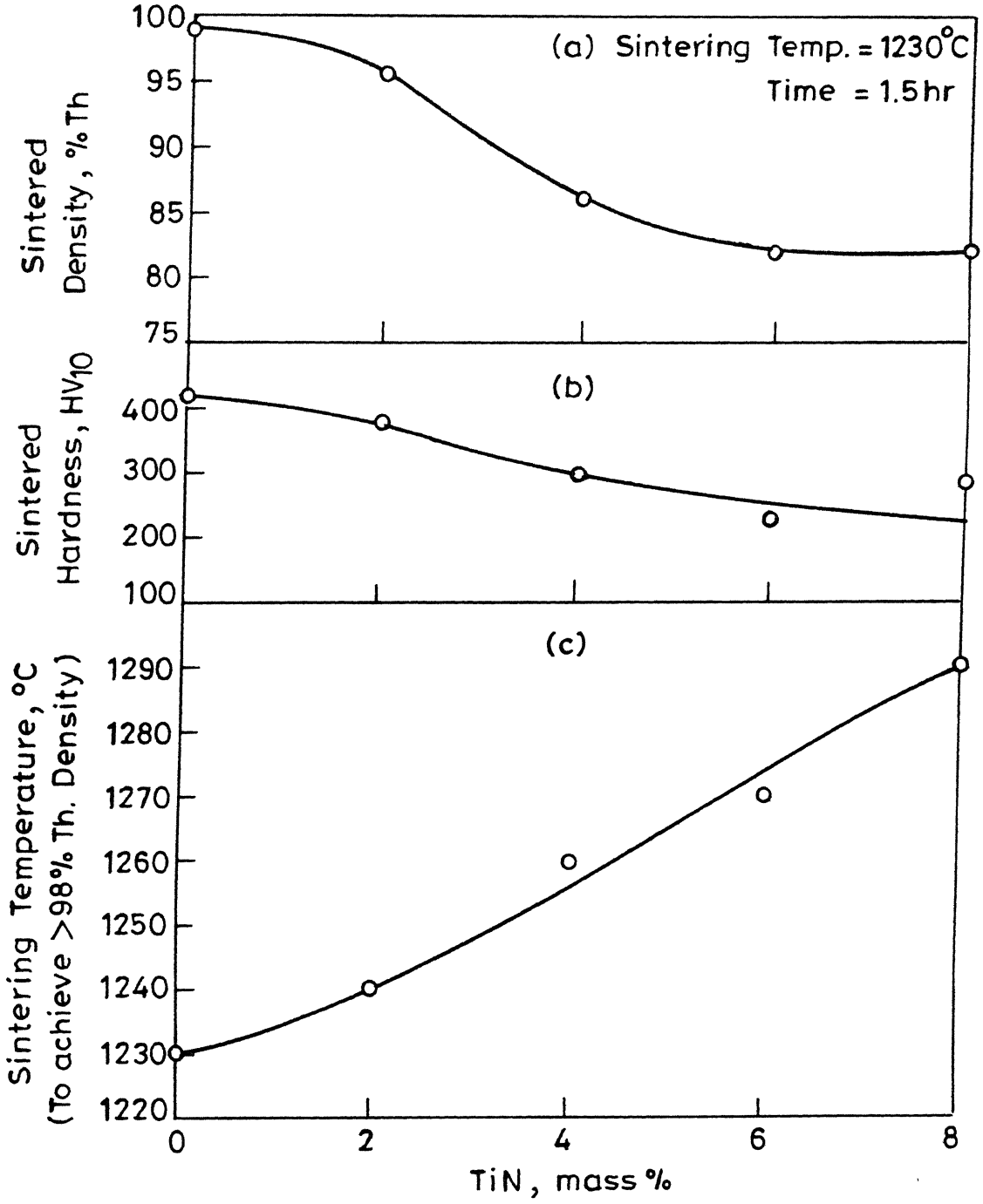

Fig.3.46 Effect of TiN addition in T42 HSS on (a) Sintered density (b) Sintered hardness (c) Sintering temp. to achieve >98% Th. density .

III.4.2. Hardness:

For either T15 or T42 HSS based composites containing TiN (Figures 3.45 and 3.46), sintered hardness follows a similar trend to that of densification with sintering temperature. The effect of TiN addition on the hardness of T15 HSS composites heat treated differently is shown in Figure 3.47. The hardness in any condition decreased with the increase in TiN content. Figure 3.48 shows the effect of TiN addition to T42 HSS on the hardness in sintered, transformation annealed, hardened and triple tempered conditions. Unlike the T15 HSS based composites (Figure 3.48), there exists a peak hardness value for the T42 HSS composite containing 4 mass % TiN in sintered, transformation annealed or triple tempered conditions. In case of T15 HSS based composites, the sintered hardness remained constant (Figure 3.47a) up to 6% TiN and then decreased with further TiN addition. In case of T42 HSS based composites, however, the sintered hardness increased with the increase in TiN content only up to 4%, followed with a decrement. Quenched and triple tempered hardness in case of T15 HSS based composites remained unchanged up to a TiN content of 2% followed by a decrement (Figure 3.47c and d). The triple tempered hardness of T42 HSS based composites remained unchanged up to 4% TiN content beyond which it decreased. The highest triple tempered hardness obtained was 880 HV_{10} for T15 HSS composite containing 2% TiN (Figure 3.49) in comparison to 950 HV_{10} for T42 HSS based composite containing 4 mass % TiN (Figure 3.50).

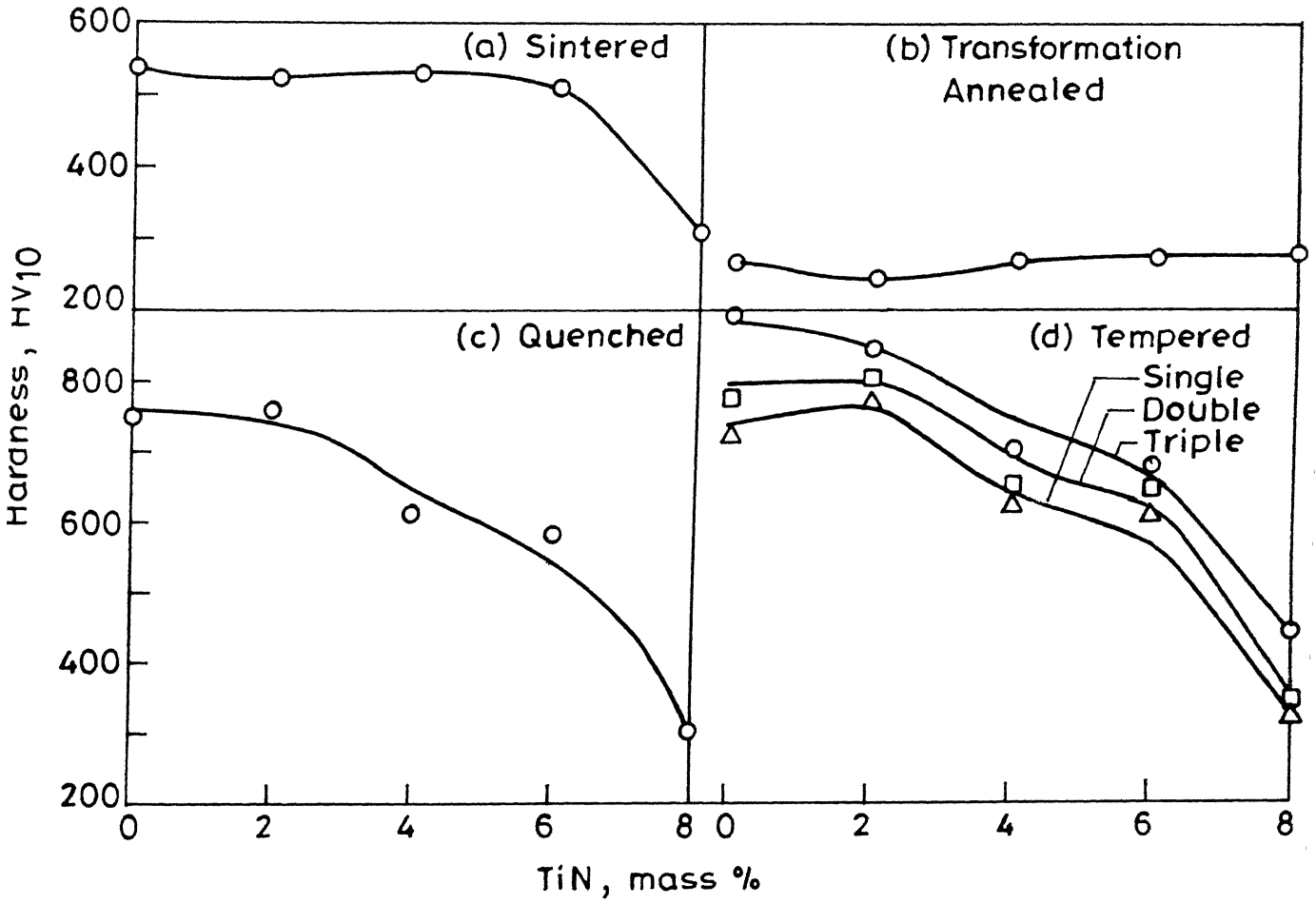

g.3.47 Hardness variation of T15 HSS and its TiN containg composites in various conditions : (a) Sintered (b) Transformation annealed (c) Quenched and (d) Tempered .

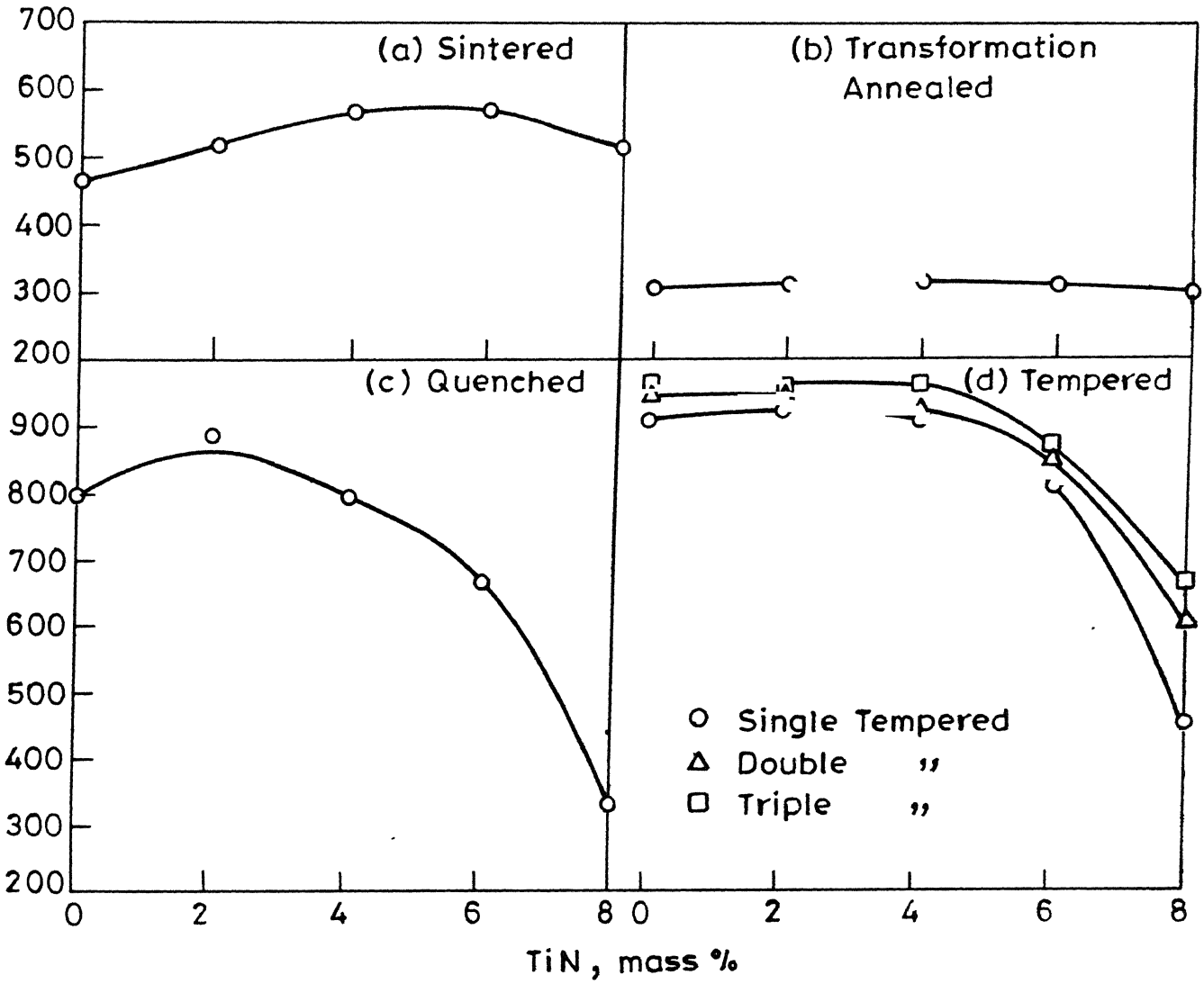

Fig.3.48 Hardness variation of T42 HSS and its TiN containing composites in various conditions: (a) Sintered (b) Transformation annealed (c) Quenched (d) Tempered .

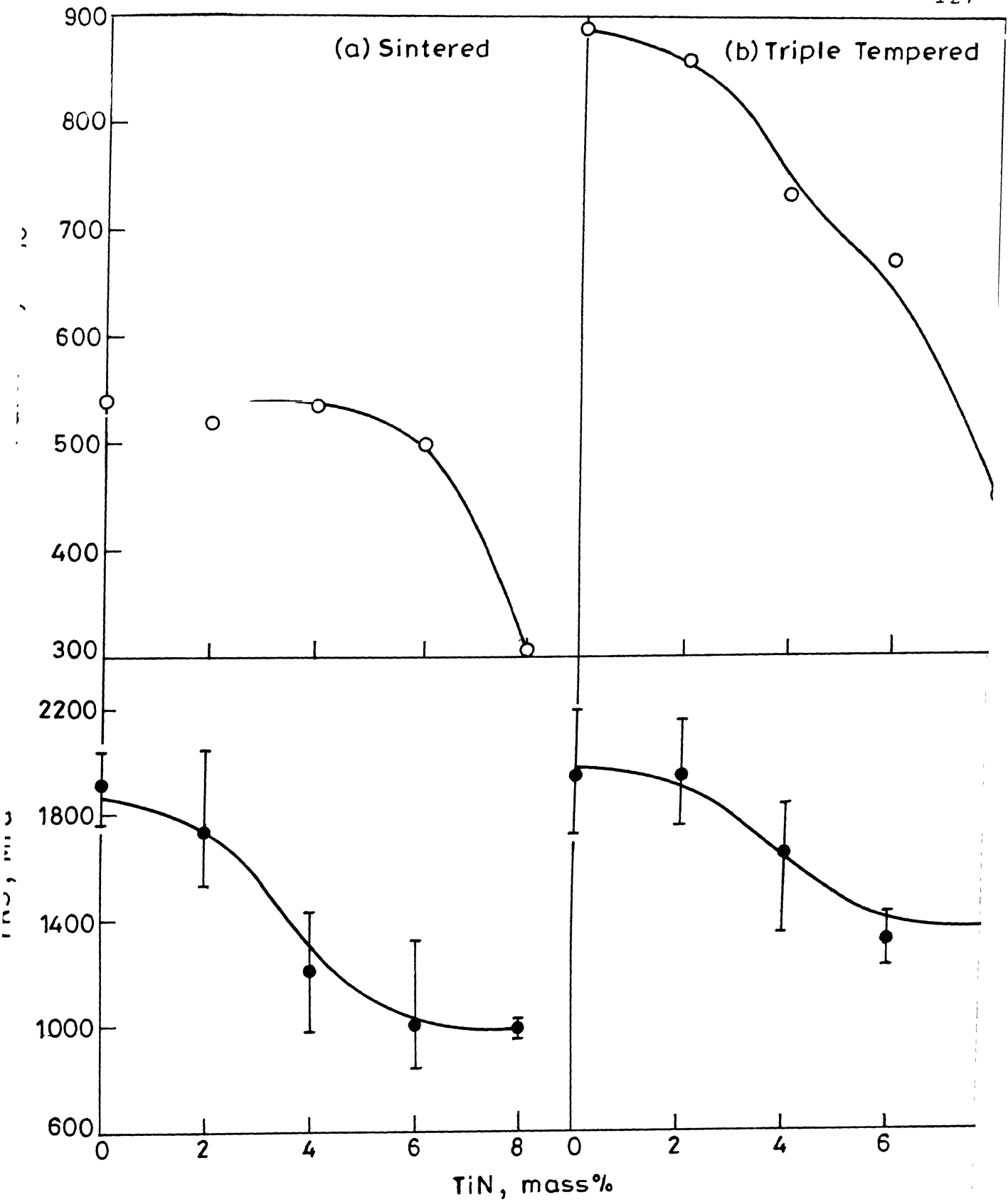

Fig.3.49 Effect of TiN addition on hardness and TRS of T15 HSS in (a) Sintered (b) Triple tempered condition.

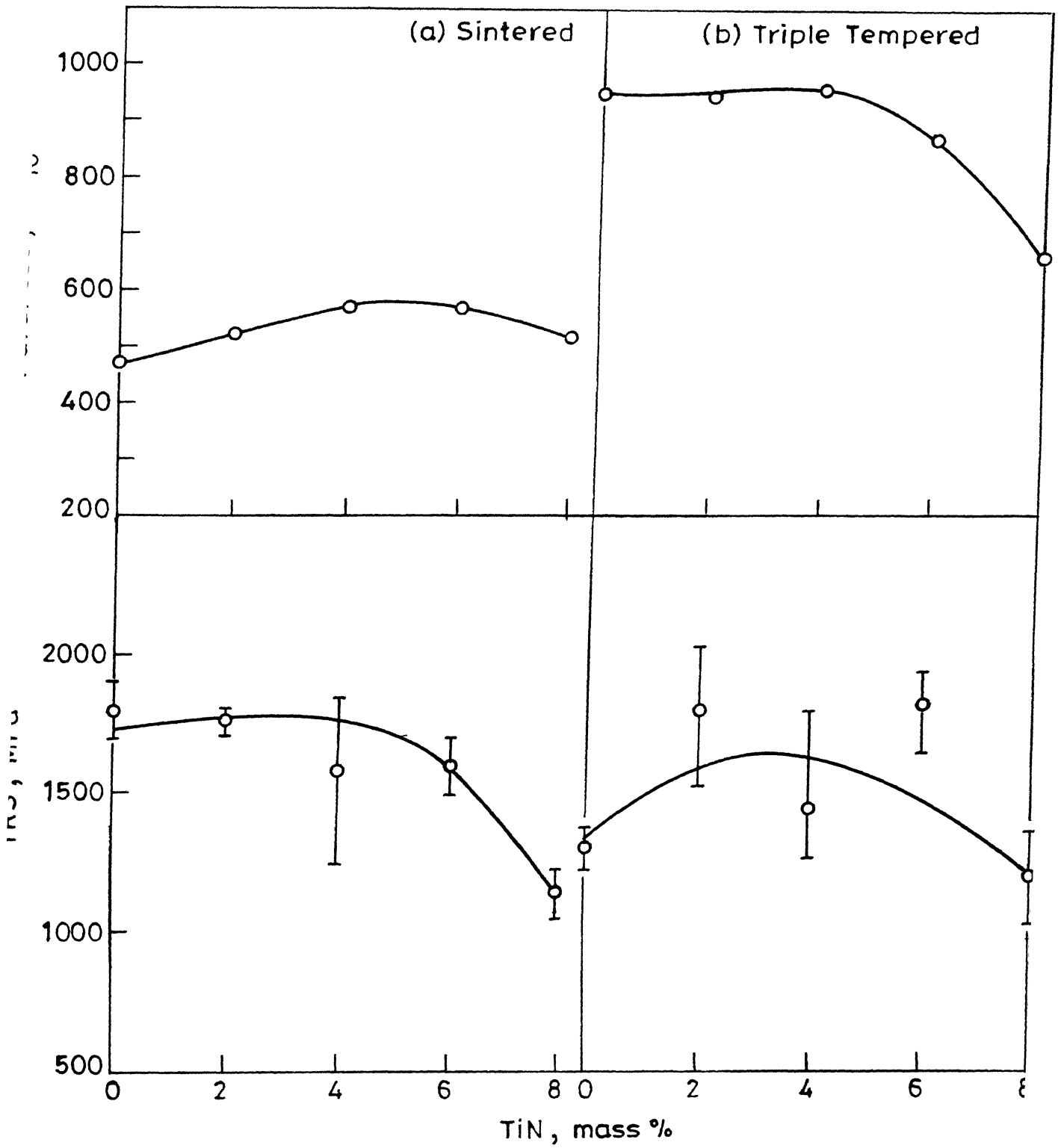

Fig.3.50 Effect of TiN addition on hardness and TRS of T42 HSS in (a) Sintered (b) Triple tempered conditions.

III.4.3. Transverse Rupture Strength (TRS):

The TRS variation with respect to TiN addition of sintered and triple tempered T15 and T42 HSS based composites are shown in Figures 3.49 and 3.50 respectively. In case of T15 HSS composites (Figure 3.49), TRS gradually decreased with the increase in TiN content in either sintered or triple tempered conditions. Highest TRS value of 2000 MPa was noted for straight T15 HSS after triple tempering. In case of T42 HSS based composites (Figure 3.50), however, there exists a peak TRS value for composites containing 4 mass % TiN in either sintered or triple tempered samples. The TRS value for T42 HSS composite was lower as compared to that of the corresponding T15 HSS based composite. The triple tempered TRS values of T15 HSS based composites were higher than the corresponding sintered values but, in case of T42 HSS composites, the reverse was true.

III.4.4. Elevated Temperature Compressive Yield Strength:

The room and elevated temperature compressive yield strength variation of T15 and T42 HSS composites containing TiN are shown in Figures 3.51 and 3.52 respectively. With the increase in the testing temperature, there is a continuous fall in the yield strength for any composite such that beyond about 500^{o}C, the fall is rapid. In case of T15 HSS composites (Figure 3.51b), the yield strength decreased with the increase in TiN content at any testing temperature.

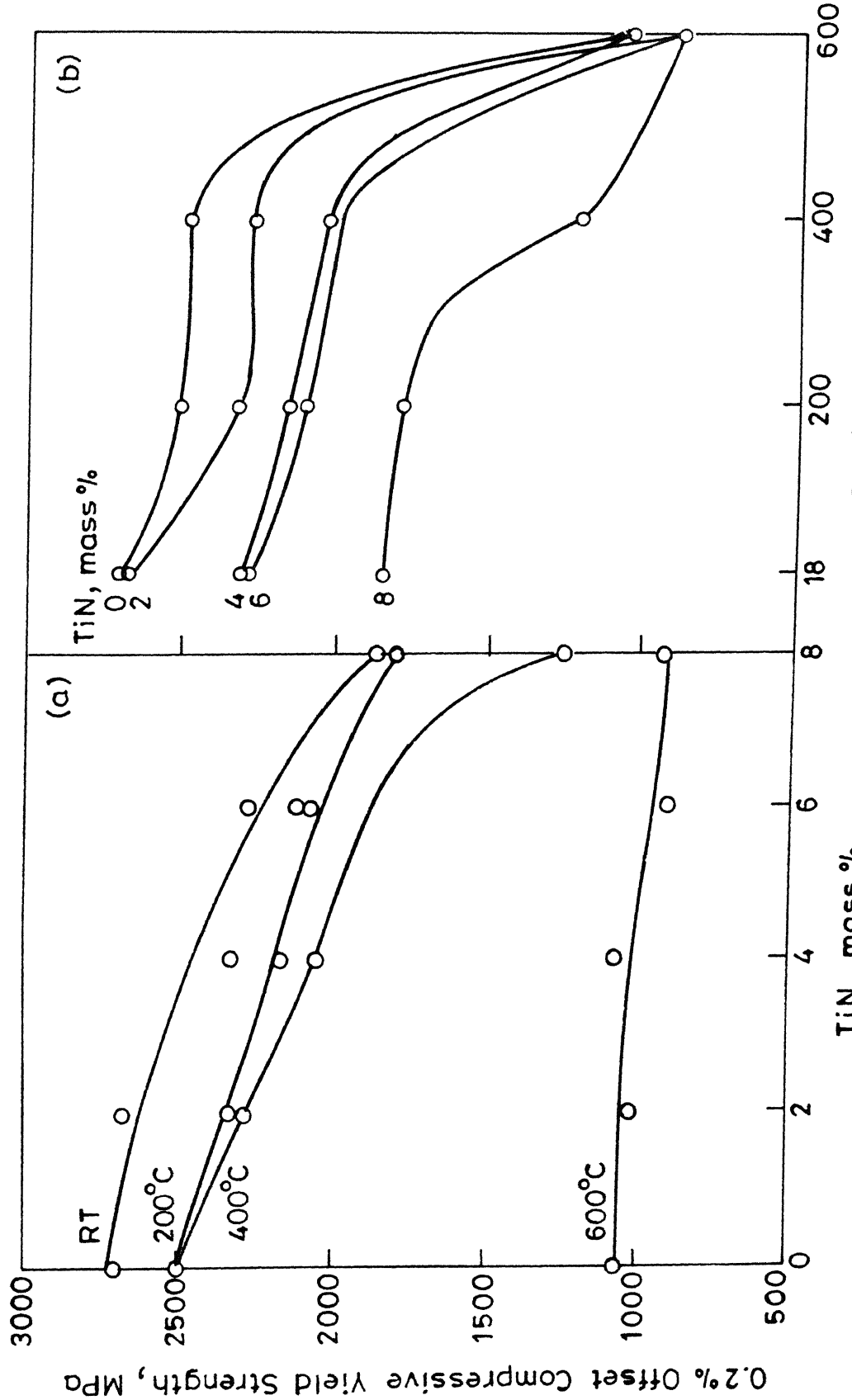

Fig.3.51 0.2% offset compressive yield strength of fully heat treated T15 HSS and its TiN containing composites w.r.t. (a) TiN addition (b) Testing temperature.

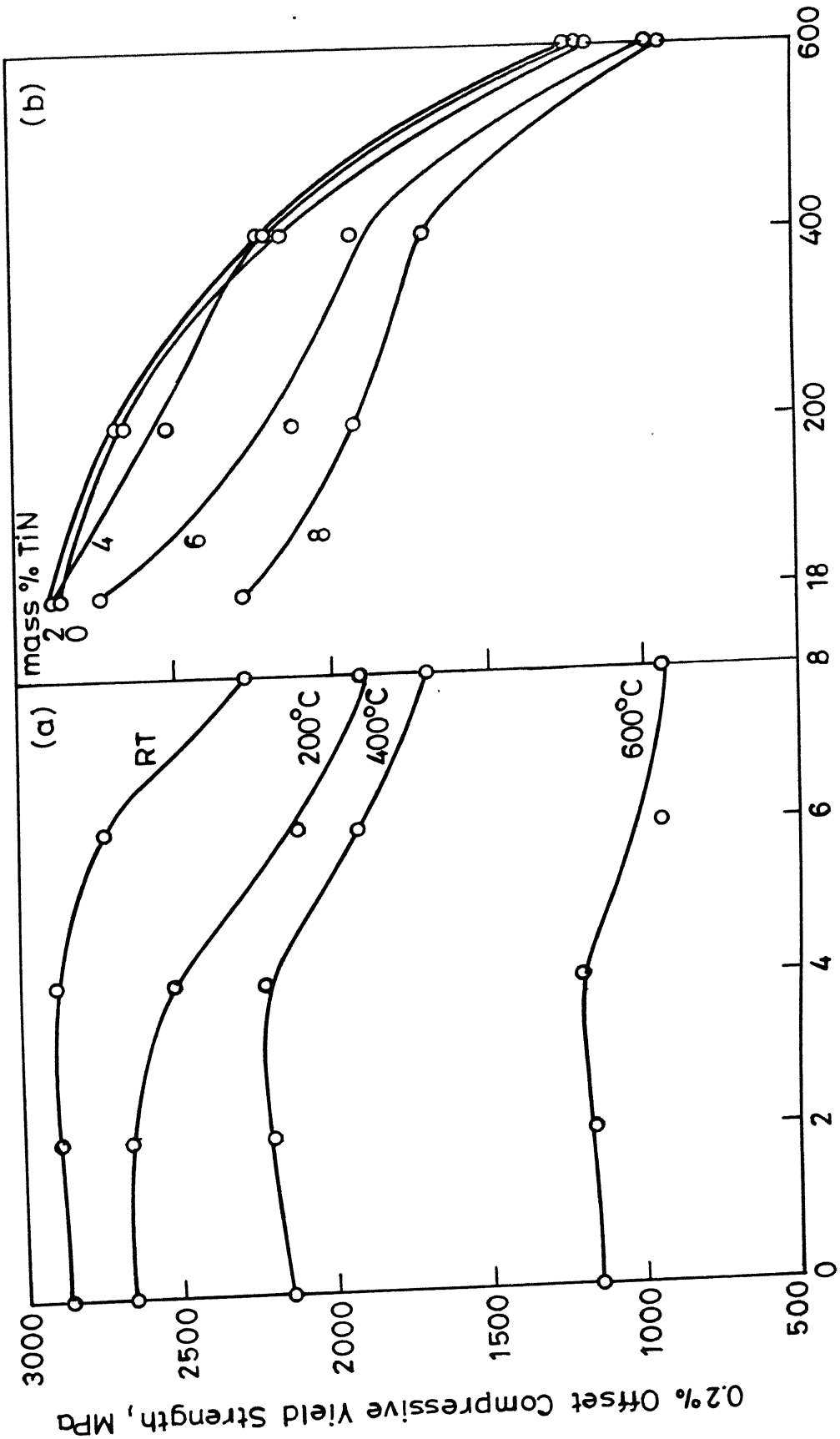

Fig.3.52 0.2% offset compressive yield strength of fully heat treated T42 HSS and its TiN containing composites w.r.t. (a) TiN addition (b) Testing temperature.

There was no gain on the yield strength in case of T15 HSS composites above the straight composition, whereas in case of T42 HSS (Figure 3.52), there was a marginal gain for the 2 or 4 mass % TiN containing composites above the straight composition at any testing temperature. For any composite containing fixed TiN content, the T42 HSS composites showed higher compressive yield strengths as compared to those based on T15 HSS.

III.4.5. Microstructural Analysis:

Figures 3.53 and 3.54 show the optical microstructures of T15 and T42 HSS based composites respectively containing TiN in the sintered, quenched or triple tempered conditions. The sintered structure for either composite showed no observable porosity, thus indicating achievement of full density. The sintered microstructure consisted of the primary carbides on and within the grains. The TiN particles at some places got agglomerated. Comparing between the microstructures of either HSS composites containing 4 and 6 mass % TiN, it is seen that the microstructure in case of 6 mass % TiN containing composite was coarser as compared to that of composite containing 4 mass % TiN. Some grain refinement was noticed after triple tempering. In general, the microstructures of T42 HSS based composites were similar, but finer than those corresponding to T15 HSS based composites.

Figures 3.55 and 3.56 shows the grain size variation with respect to TiN content in T15 and T42 HSS based composites

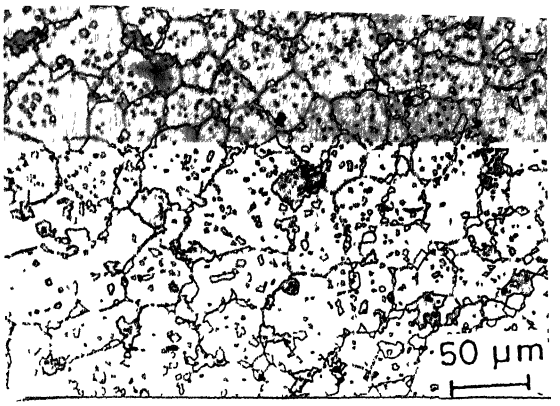

(a) Sintered

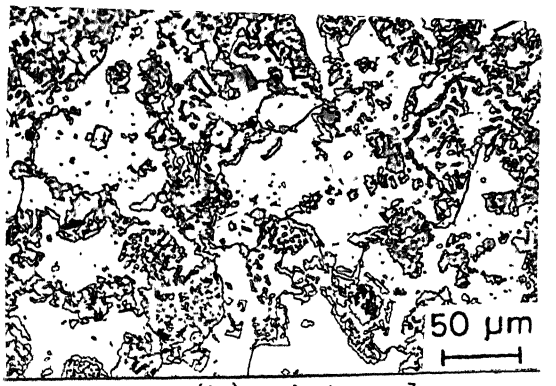

(b) Sintered

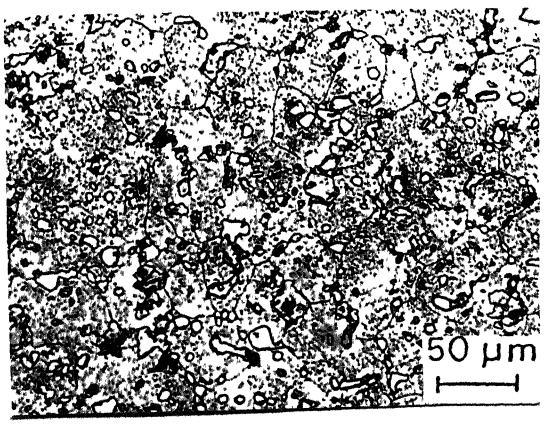

(c) Quenched

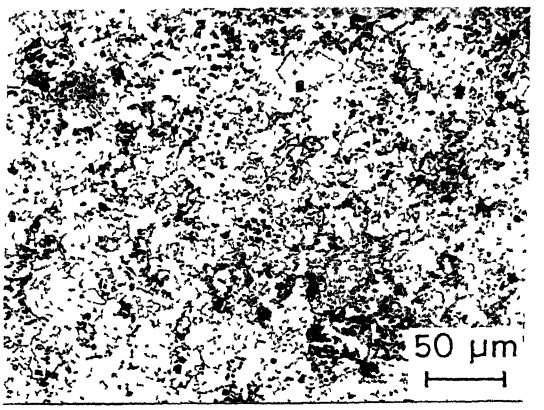

(d) Quenched

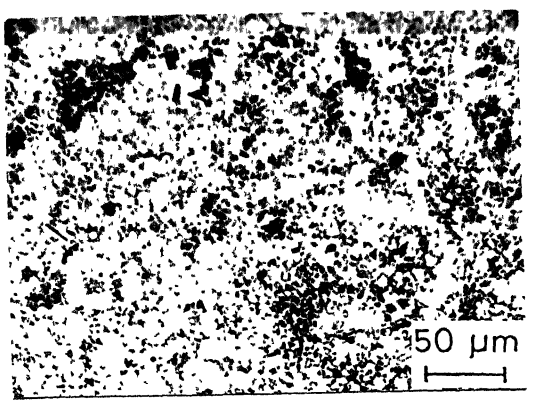

(e) Triple tempered
4% TiN

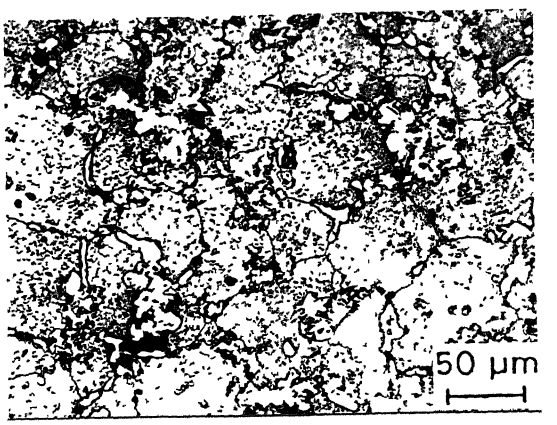

(f) Triple tempered
8% TiN

Figure 3.53. Optical microstructures of T15 HSS containing TiN in various conditions.

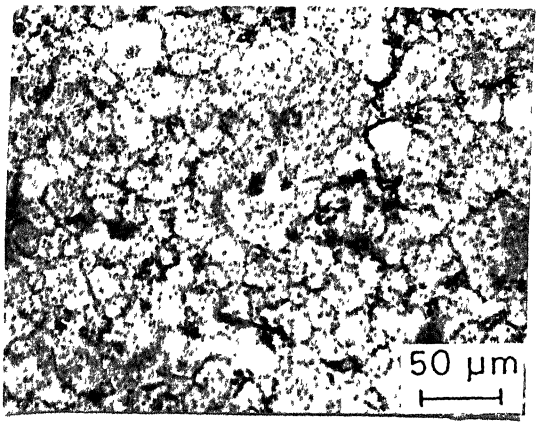

(a) Sintered

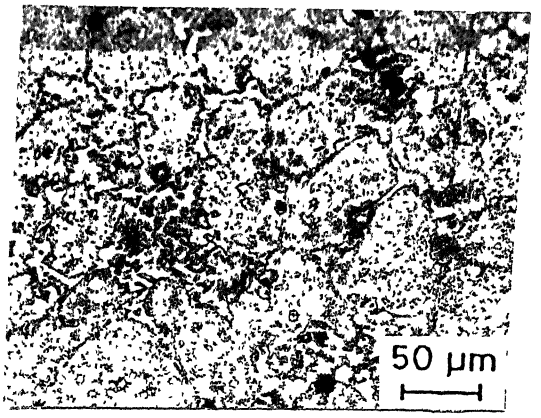

(b) Sintered

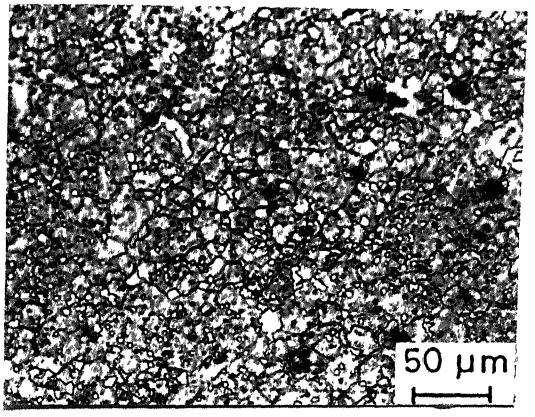

(c) Quenched

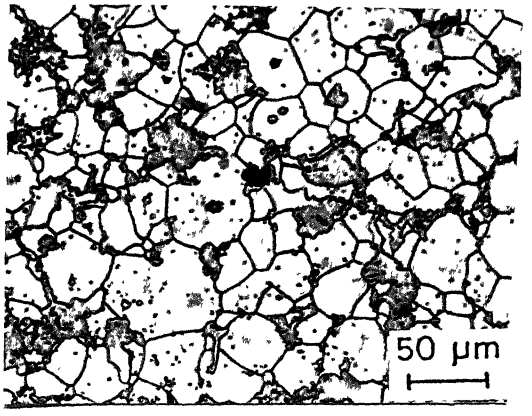

(d) Quenched

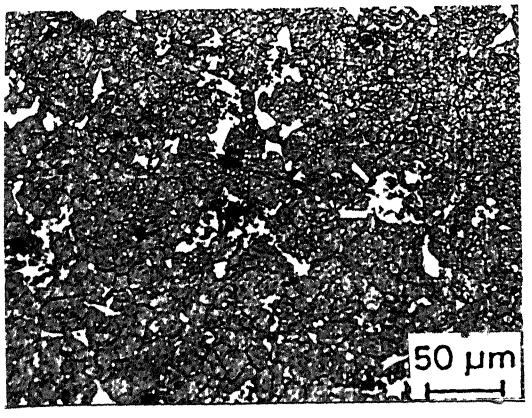

(e) Triple tempered
4% TiN

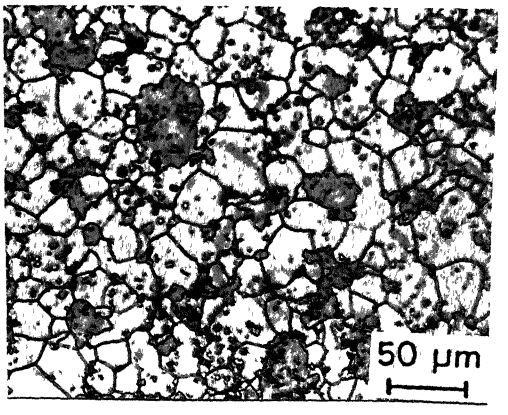

(f) Triple tempered
8% TiN

Figure 3.54. Optical microstructures of T42 HSS containing TiN in various conditions.

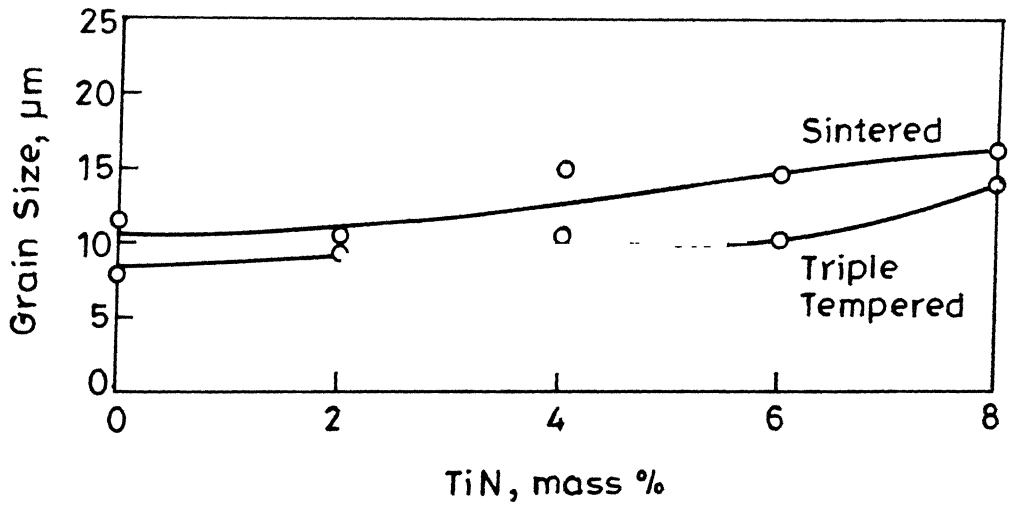

Fig.3.55 Effect of TiN addition on grain size of T15 HSS (sintered at different optimised temperatures).

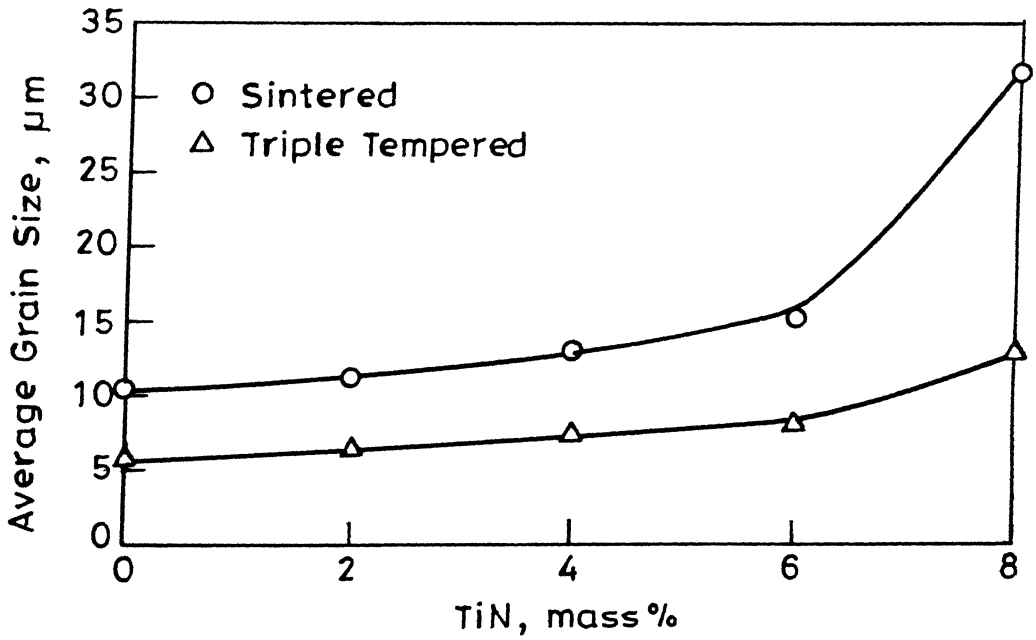

Fig. 3.56 Effect of TiN addition on grain size of T42 HSS (sintered at different optimised temperatures).

respectively. In both the cases, the triple tempered grain sizes were smaller than the sintered ones, indicating a grain refinement during transformation annealing prior to the actual hardening treatment. The sintered grain size up to an addition of 6% TiN in either T15 or T42 HSS were similar, but the 8 mass % TiN containing T42 HSS composite had a larger grain size (30 μm) as compared to similar T15 HSS based composite (18 μm). The grain size of any T42 HSS based composite composition after triple tempering was smaller than the value for corresponding T15 HSS based composite.

The volume fraction of primary carbides (MC and M_6C) as measured by the quantitative metallographic techniques are shown in Figures 3.57 and 3.58 respectively for T15 and T42 HSS based composites. In case of T15 HSS based composites, there was an increase in the volume fraction of either MC or M_6C carbides with the increase in TiN content, although the increase was rather marginal. For any composite composition, the volume fraction of either MC or M_6C carbides increased further after triple tempering. T42 HSS based composites also showed similar characteristics as regards the primary carbides, with the exception that for M_6C carbide, a substantial increase in the volume fraction with the increase in TiN content was observed. MC and M_6C carbides in T15 HSS composites were present in equal volumes, whereas in case of T42 HSS composites, M_6C carbide volume fraction was higher than the MC carbide fraction.

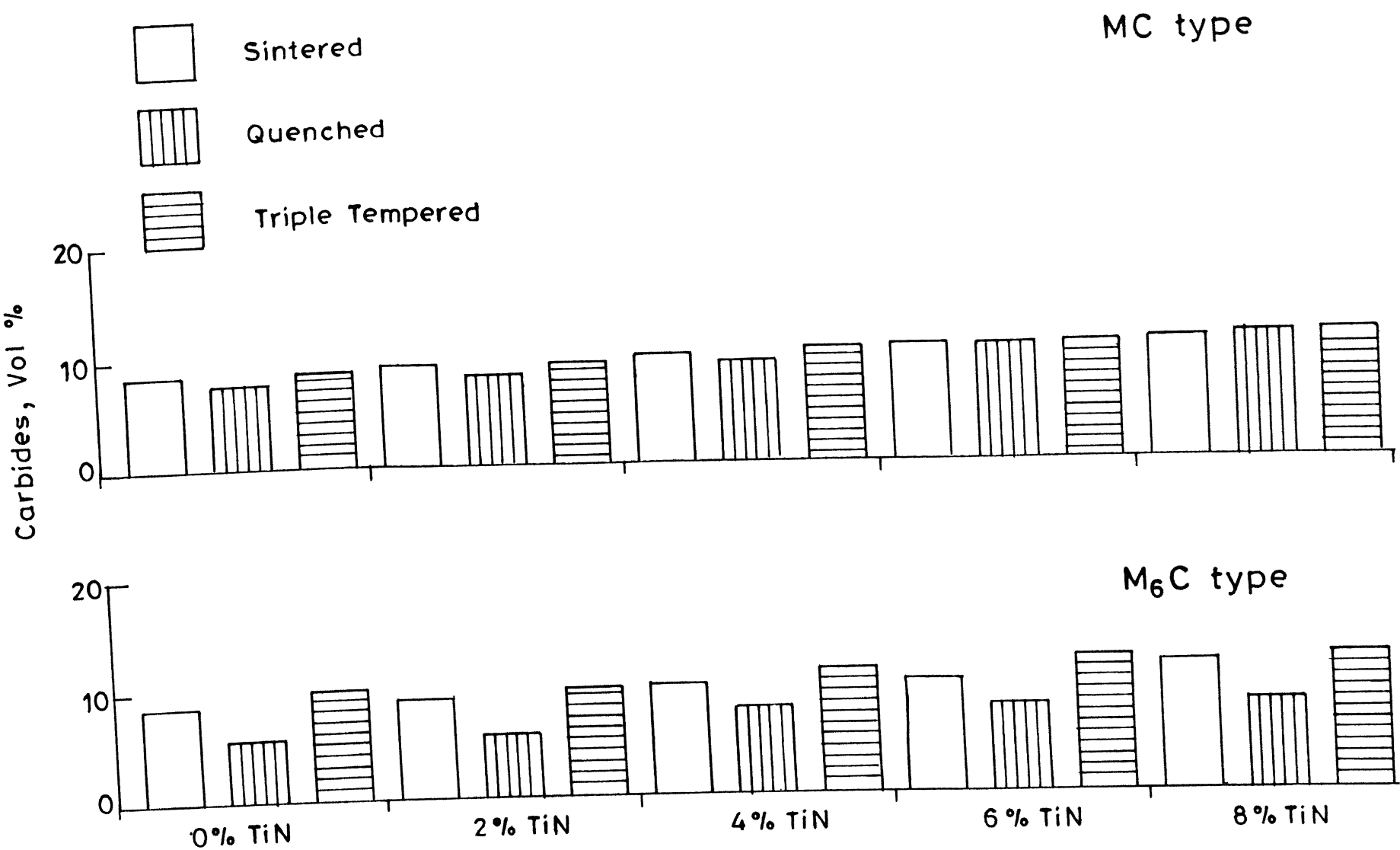

Fig.3.57 Volume fraction of MC and M_6C type carbides w.r.t. TiN addition in T15 HSS.

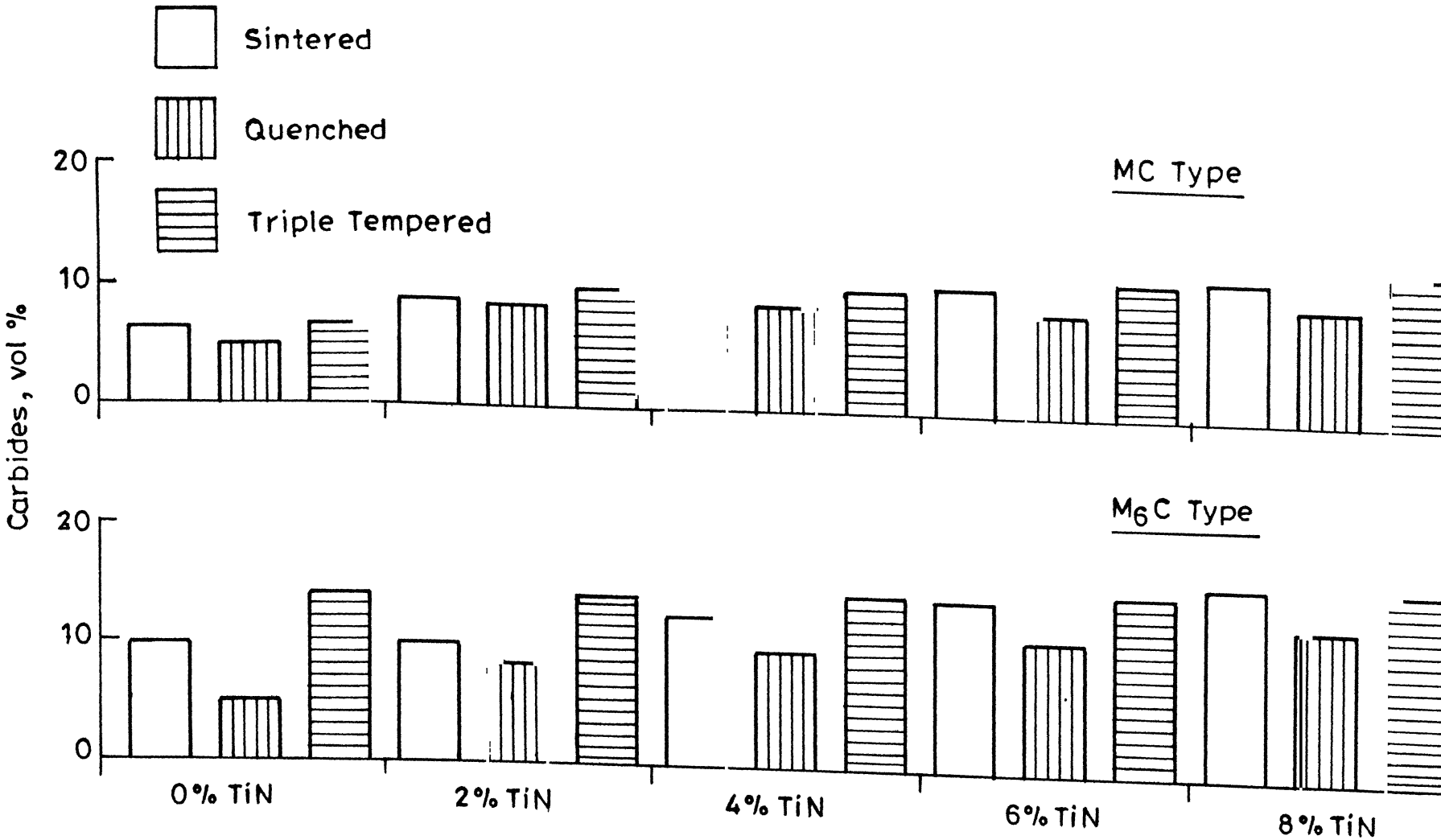

Fig. 3.58 Volume fraction of MC and M_6C type carbides w.r.t. TiN addition in T42 HSS.

The size distribution of primary carbides for the TiN containing composites of T15 and T42 HSS are shown in Figures 3.59 and 3.60 respectively. In either composite system, a coarsening of the primary carbides was noticed with increase in TiN content. In case of T42 HSS based composites, such a coarsening effect was greater as compared to that of T15 HSS based composites.

Figure 3.61 shows the SEM micrographs of T15 HSS containing 4 and 6 mass % TiN in sintered and triple tempered conditions. The microstructures similar to optical ones consisted of primary carbides and TiN particles. Individual stable cubic TiN particles were distinct even at higher magnifications (Figure 3.61c). In the triple tempered condition, finer primary carbides were present in addition to TiN particles. The SEM-EDX analyses of the different phases in T15 or T42 HSS based composites are shown in Table III.6. On the basis of the EDX analysis, the stability of the TiN particles could be gauged as matrix was free from titanium atoms.

III.4.6. Magnetic Property:

The magnetic property variation in terms of coercivity of T15 and T42 HSS based composites containing TiN is shown in Figure 3.62. In case of T15 HSS composites, the coercivity decreased with the increase in the TiN content, similar to the sintered hardness plot. However, the coercivity remained virtually unchanged in the triple tempered

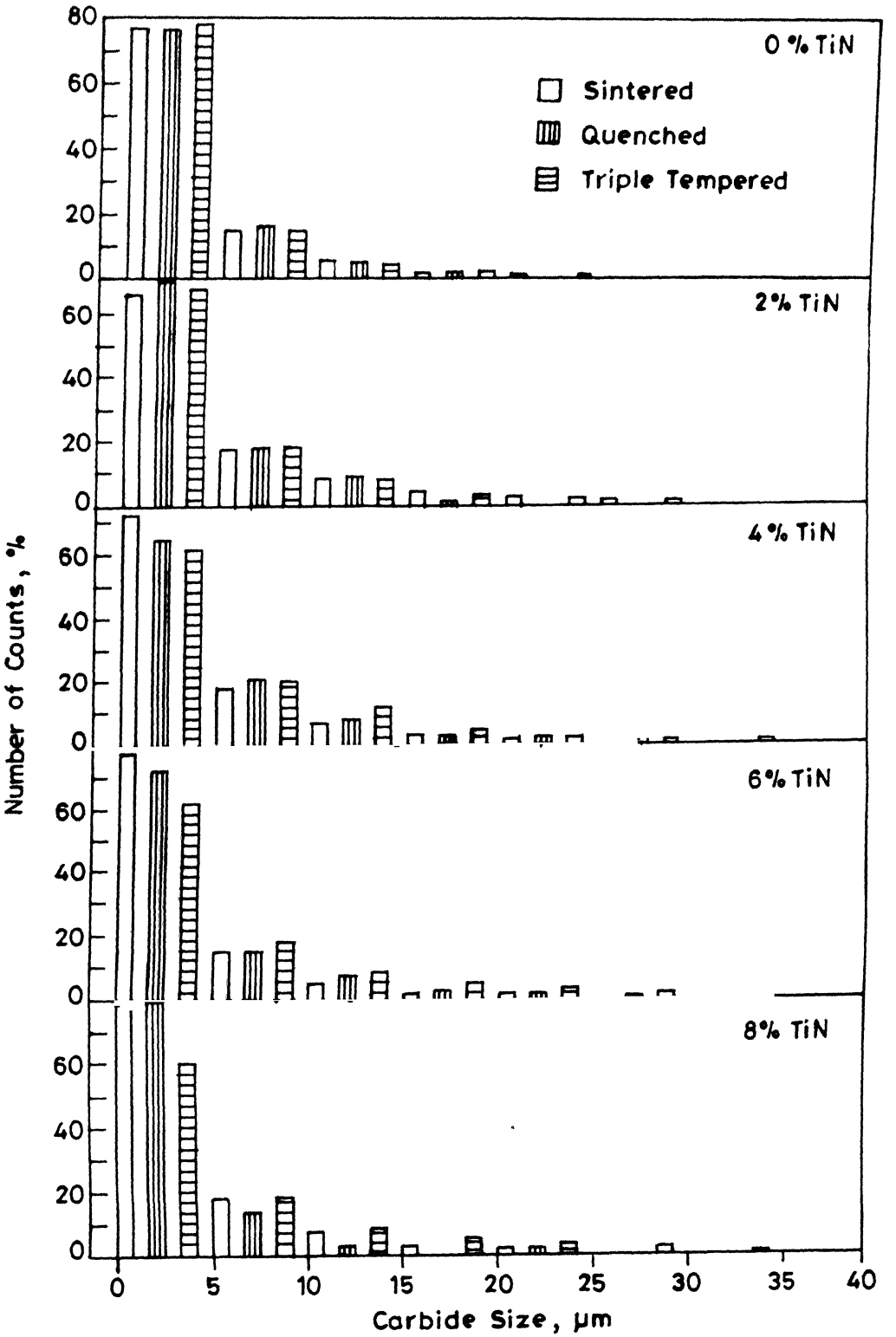

Fig.3.59 Size distribution of primary carbides in T15 HSS and its TiN containing composites.

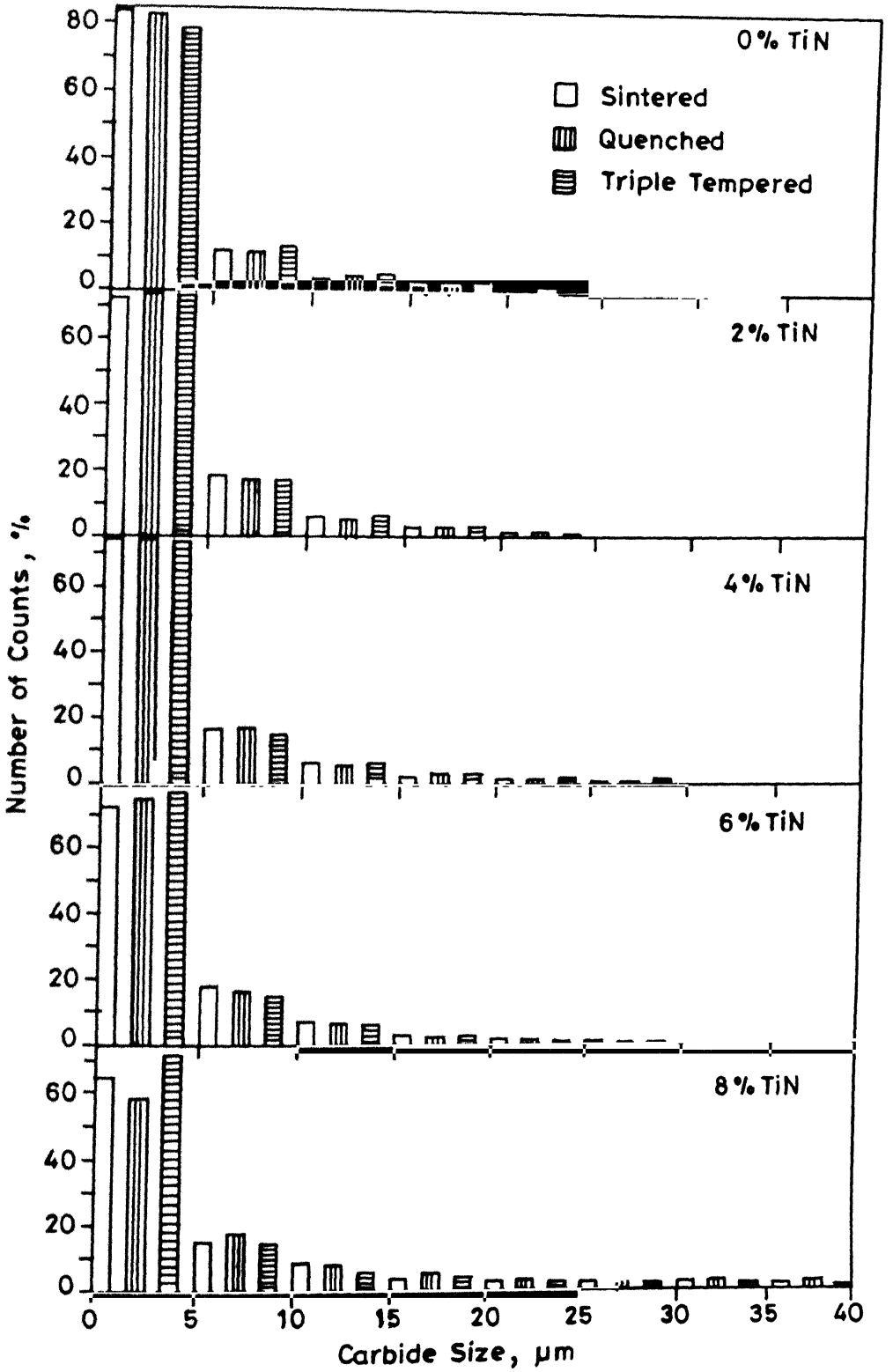

Fig. 3.60 Size distribution of primary carbides in T42 HSS and its TiN containing composites.

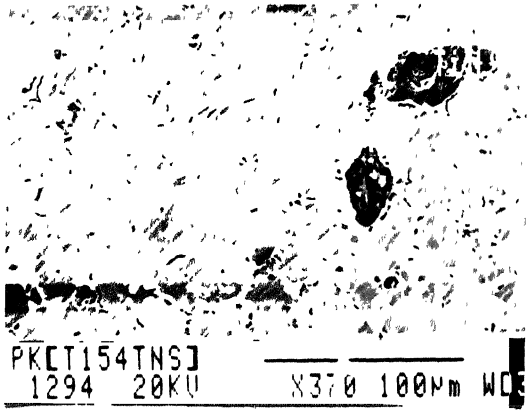

(a) Sintered

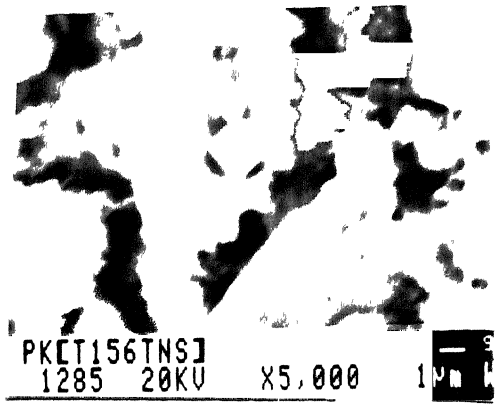

(b) Sintered

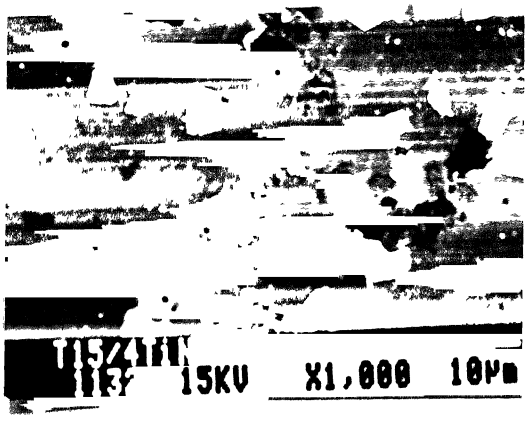

(c) Triple tempered

4% TiN

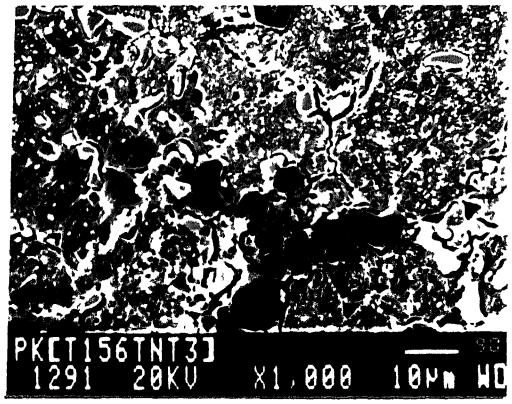

(d) Triple tempered

6% TiN

Figure 3.61. SEM photomicrographs of T15 HSS and its TiN containing composites in sintered and triple tempered conditions.

Table III.6: EDX analysis of various phases in T15 and T42 HSS containing TiN.

HSS composite	Description of phase	Mass % chemical analysis							Assigned phase
		Fe	Cr	Co	Mo	V	W	Ti	
T15 - 4% TiN Sintered	White, angular	11.43	2.55	0.95	15.92	5.16	63.50	0.43	M_6C type carbide
T15 - 6% TiN Sintered	White, cubic	1.03	0.23	0.08	0.24	0.05	3.34	95.02	TiN particle
T15 - 4% TiN triple tempered	Dark phase	1.51	3.50	0.15	8.81	28.73	57.27	-	MC type carbide
T15 - 6% TiN triple tempered	Dark phase	19.18	-	-	-	48.80	32.02	-	MC type carbide
T42 - 4% TiN Sintered	Black phase	6.58	0.62	0.85	0.66	0.68	1.94	88.67	TiN particle
T42 - 4% TiN Sintered	Grey particle adjacent to black phase	6.28	3.25	0.47	15.56	37.29	25.51	11.63	MC carbide
T42 - 4% TiN Sintered	White, angular	31.55	3.53	4.36	16.27	5.41	38.85	-	M_6C carbide

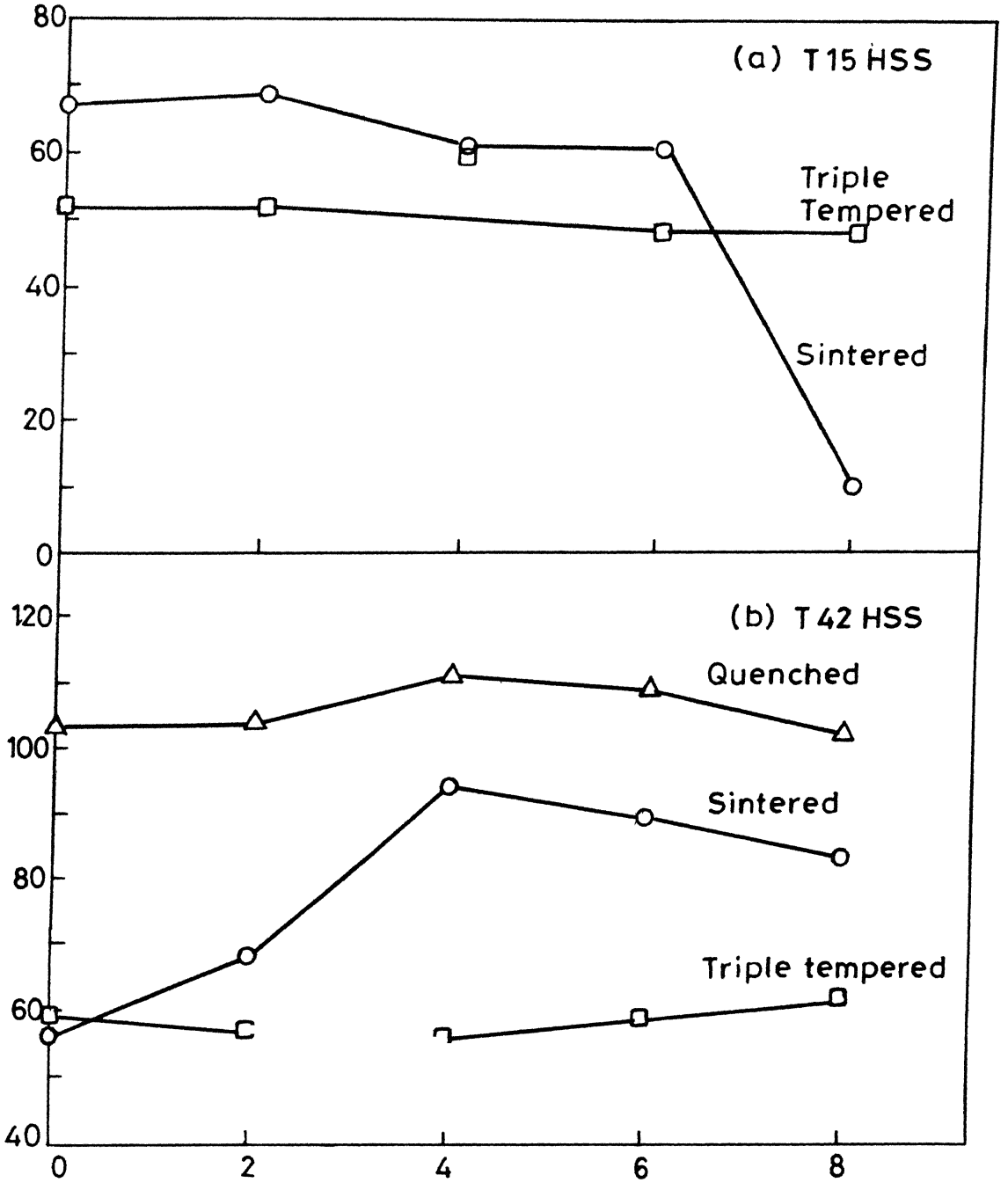

Fig. 3.62 Variation of coercivity with respect to TiN addition in (a) T15 HSS (b) T42HSS.

condition for all the composite compositions. The values obtained for any composites based on T42 HSS in either sintered or triple tempered condition were higher than those observed for T15 HSS based composites. 4 mass % TiN containing T42 HSS showed a peak coercivity value in the sintered condition. The trend was similar to the hardness variation. The coercivity of T42 HSS based composites after triple tempering remained practically unchanged similar to T15 grade.

III.4.7. Tool Life:

Figure 3.63 shows the tool life variation of T15 and T42 HSS based composites containing 2 and 4 mass % TiN. It is evident that the cutting tool life increased with the increase in the TiN content in either T15 or T42 HSS. In case of composites based on T15 HSS, increase in tool life of 8 and 35% above the base composition is noticed for composites containing 2 and 4 mass % TiN respectively, whereas for the corresponding composite based on T42 HSS, the respective increases noticed are 2 and 15% above the straight composition.

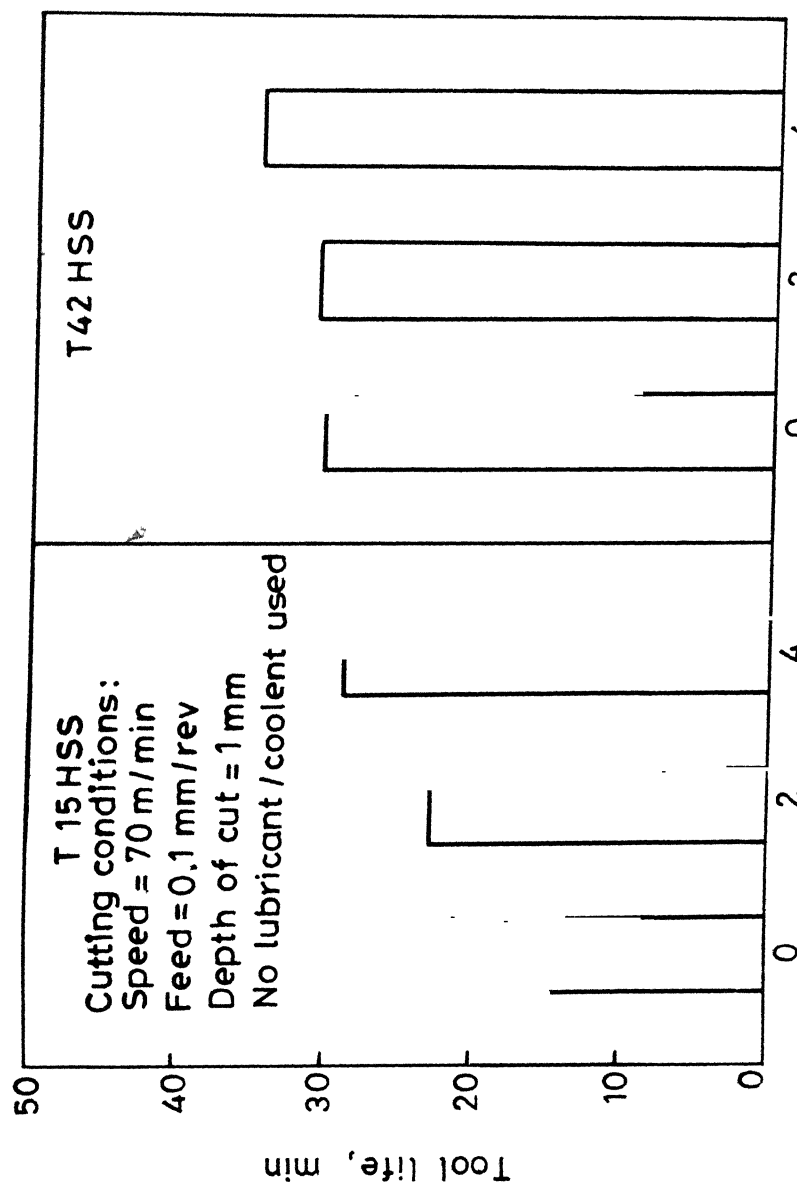

Fig.3.63 Tool life variation with TiN content in the composites of T15 and T42 HSS.

CHAPTER IV

DISCUSSIONS

IV.1. INTRODUCTION:

The role of various alloying elements in high speed steel has already been discussed in the first chapter. In HSS, the collective atomic percent of W and Mo (or tungsten equivalent) varies only slightly from specification to specification and these two elements perform similar functions and more or less interchange on an atomic basis. 1% Mo addition is considered equivalent to 1.6% W. Virtually all the conventionally produced high speed steels lie within the range of 2.6-2.9 atomic % carbon and 9.3-15 atomic % carbide formers [1]. The P/M route enables the range to be extended to higher C and V contents. The major differences in various grades of high speed steel emerge due to changes in carbon, vanadium and cobalt present. The normal restrictions on composition of conventional I/M HSS is relaxed in the case of P/M grades where higher atomic % of carbon as well as carbide formers can be used. A much higher vanadium and cobalt content can be promoted in P/M high speed steels as the undesirable effects of these elements on the forging behaviour of ingot material are eliminated [1, 78].

The basis of alloy design is that optimum secondary hardening characteristics are developed in a balanced high speed steel i.e. one in which the carbon content is the

stoichiometric value to accommodate all the carbide formers in the steel and to ensure that sufficient carbon is there to give maximum hardenability during heat treatment. Balance carbon, 'Cb', as suggested by Steven [109] and balance carbon difference, ΔC [93], calculated on the basis of 'Cb' is an important indicator for any HSS. These are calculated from the following formula:

Balance carbon, Cb = 0.033 W + 0.063 Mo + 0.06 Cr + 0.2 V

Balance carbon difference, ΔC = Cb - Ca

where Ca = actual carbon in composition.

A positive ΔC value indicates that sufficient carbon is not present to satisfy all the carbide formers as well as martensitic transformation. A negative ΔC value would on the other hand ensure that the carbon requirement of all the carbide formers is satisfied and sufficient carbon is available for the martensitic transformation of the matrix. In such a case, the requisite hardness value is achieved on the sacrifice of the toughness value.

As far as the role of carbon on the solidus temperature is concerned, an increase in 1% added carbon in high speed steel, lowers the latter by a factor of 111^{o}C [1]. This means that higher the carbon content, the closer the solidus temperature will approach the upper limit of the heat treatment range and greater the risk of incipient melting in hardening.

As far as vanadium is concerned, its main effect is to produce very hard vanadium carbide (MC) which is

important in promoting abrasion resistance. To avoid carbon depletion in the matrix, it is important to ensure that there is sufficient carbon available to satisfy the vanadium plus the requirement for hardening. It is generally considered that each 1% vanadium addition requires an additional carbon of 0.25%.

Cobalt addition in HSS gives improved hot-hardness and enables higher cutting speeds to be used. Its overall effect can be summarised as follows [78, 97-103]:

(a) Cobalt does not form carbides, but remains in solution in the matrix. The resultant solution hardening is less affected by an increase in temperature.

(b) Cobalt slows down the $\alpha \rightarrow \gamma$ transformation and increases the transformation temperature.

(c) It accelerates the decomposition of austenite and increases the critical cooling rate.

(d) Cobalt delays the precipitation of carbides from martensite during tempering and retards carbide coarsening, which contribute in high hot hardness. Moreover, by slowing down the diffusion of carbide-forming elements, it encourages the formation of a fine, well-dispersed carbide precipitate which increases wear resistance.

(e) Cobalt slows down grain growth. Thus the solutionising temperature can be raised and also the content of elements dissolved in austenite thereby increased.

(f) Cobalt improves the thermal conductivity and this entails the use of higher cutting speed as the heat generated at the tool-tip is conducted away more effectively.

In summary, the two grades of HSS viz. T15 and T42 studied in the present investigation have similar W-equivalents and differs as regards to the cobalt and vanadium content. T42 has higher cobalt content (10%) as compared to T15 (5%), whereas T15 has higher vanadium content (5%) as compared to T42 (3%). To match with vanadium contents, carbon content in T15 is comparatively higher (1.5%) as compared to that for T42 (1.3%).

IV.2. T15 AND T42 GRADE HSS:

IV.2.1. Densification:

The liquid phase sintering of high speed steels pertains to the supersolidus category, where solid and liquid phases have similar compositions and the volume fraction of phases remain constant as the sintering progresses. While heating to the sintering temperature, there is some amount of solid state sintering of the powder particles, which form a skeleton. After the formation of the liquid phase at the sintering temperature, this skeleton disintegrates into almost individual solid grains by the penetrating action of the liquid. The liquid phase is formed originally on the free surfaces of the powder particles and probably on the

grain boundaries within the powder itself. As the particles themselves are the sources of the liquid in such type of sintering viz. supersolidus, wettability is not a problem. The force provided by the surface tension of the liquid acts to rearrange the solid particles and interparticle voids are eliminated. The effective viscosity of the liquid is drastically reduced when the temperature is increased and rapid densification occurs. An increase in sintering temperature produces more amount of liquid phase causing rapid densification through particle rearrangement, apart from contribution by matrix particle deformation due to lowering in strength [36-41].

Sintering temperature is the most important process variable in supersolidus sintering of HSS. The optimum temperature for sintering a specific powder depends on its actual chemistry and process variables like powder particle size, green density and carbon addition. In the present investigation, for any given grade of HSS, the green compacts were pressed to different extents so as to give a constant porosity level of 24-26%. The densification process therefore, can be singularly related to the sintering temperature. The sintered density in case of either T15 or T42 HSS studied presently (Figure 3.2a and Figure 3.3a respectively) increased with the increase in the sintering temperature till the optimum full density (>98% Th.) was achieved. At temperatures lower than the optimum, densification was not achieved and larger pores could be seen in the sintered

microstructures (Figures 3.10a and 3.11a). The pore size and its volume fraction decreased as the optimum temperature was approached. The microstructure corresponding to the optimum sintering temperature consisted of fine and uniformly distributed carbides and matrix grains (Figures 3.10c and 3.11b respectively for T15 and T42 HSS). At higher sintering temperatures, the liquid volume fraction was higher, which enhanced densification. However, this was at the same time associated with grain coarsening (Figures 3.10d and 3.11d), which is an undesirable feature in HSS. The slight decrease in sintered density for samples sintered beyond the optimum sintering temperature is attributed to the emergence of solidification pores [30, 39, 50].

The optimum sintering temperature to achieve full density for T15 was 1270^{o}C as compared to 1230^{o}C for T42 HSS. T15, even having higher carbon content than that of T42, required a relatively higher sintering temperature mainly because of its relatively high W, V and less Mo contents. It is well known that Mo reduces the solidus temperature of the steel more than W [1, 6]. The effect of vanadium in HSS is to shift the phase boundaries more towards the right i.e., equivalent to a decrease in the carbon content [1, 6, 92]. From the above, it is concluded that the solidus temperature for T15 is higher thanthat for T42 HSS. Similar conclusion can be arrived from the 'balance carbon difference' [93] between the two grades as discussed in the previous section.

From the balance carbon difference, ΔC, calculated from the powder compositions given in Section II.1, it is seen that T15 has a balance carbon difference, ΔC equal to 0.061 as compared to ΔC of -0.091 for T42 grade HSS. This indicates that the matrix carbon content (assuming that all the carbide forming elements are tied up) is higher for T42 HSS as compared to the T15 grade. Consequently, the solidus temperature of T42 is lower than T15. This explains the higher optimum sintering temperature for T15 as compared to T42 HSS in order to produce a full density product.

IV.2.2. Heat Treatment and Microstructural Aspects:

High speed steels are always used after a suitable heat treatment which include transformation annealing/ stress relieving, austenitizing and hardening followed by multiple tempering. The heat treatment parameters dictate the end property and are selected in consonance with the intended steel application.

From the present DTA test result (Figure 3.4) it can be seen that the AC_m temperature for T42 HSS is $10^{o}C$ higher as compared to that of T15 HSS. This may be attributed to the relative higher cobalt content of T42 as compared to T15. In the annealed condition, the total cobalt content in the steel practically remains in the ferrite and most carbide forming elements are tied up in the form of carbides which remain undissolved [5]. Cobalt is known to increase the $\alpha \rightarrow \gamma$ transformation temperature [78] which

results in higher AC_m temperature for T42 HSS. The selection of the transformation annealing hold temperatures of 900°C and 760°C for both the grades of T15 and T42 HSS is thus justified in view of a rather little difference between the transformation temperatures.

The tempering temperature after oil quenching was determined on the basis of maximum hardness from the hardness vs. tempering temperature curve. Peak secondary hardness for T15 HSS was obtained at 560°C (Figure 3.7) as compared to 540°C for T42 HSS (Figure 3.8). This difference in the tempering temperature for peak hardness is mainly due to the increased cobalt content of T42 HSS as compared to T15 grade. Cobalt enhances the diffusivity of carbon by which greater precipitation of alloy carbides from the retained austenite occurs in cobalt containing HSS. As a result, the carbon content of the remaining austenite decreases thereby increasing the Ms temperature. It becomes possible for the remaining austenite to get transformed to martensite during cooling after subsequent tempering. Cobalt containing steels, thus have less amount of retained austenite as compared to the non-cobalt bearing grades.

During tempering, cobalt in HSS promotes greater precipitation of W and Mo from martensite as finely dispersed secondary carbides. This enhances precipitation hardening and increases the secondary hardness [1, 78, 94, 95]. The attainment of peak hardness at a rather lower tempering temperature (540°C) for T42 as compared to 560°C for T15 is

explained being due to higher cobalt content in the former.

The microstructural studies reveal that sintering at a lower temperature results in the presence of many large pores (Figure 3.10 and Figure 3.11a). As the temperature approaches the optimum, there is a decrease in the pore size as well as in its volume fraction. At the optimum sintering temperature, the microstructures are well developed (Figures 3.10c and 3.11b) with fine grain matrix, carbides and few isolated pores. Coarsening of the carbides as well as grains occurs when the sintering temperature was higher than the optimum (Figures 3.10d and 3.11d). During transformation annealing, the austenite grains get refined in addition to stress relieving [106]. Such a control during annealing helps in the achievement of uniform microstructure after hardening and triple tempering. During austenitizing, dissolution of various carbides in the matrix is brought about. Its sequence [1, 5] is such that the chromium rich carbides ($M_{23}C_6$) dissolve first followed by tungsten-molybdenum rich double carbide (M_6C). The refractory vanadium rich carbide (MC) is the last to dissolve. Correspondingly, the primary carbide content after quenching is lowered. During triple tempering, these dissolved carbides reprecipitate and the total carbide content again increases in addition to some coarsening associated with the increase in the carbide growth kinetics.

Coming to the quantitative metallography, the total volume fraction of primary carbides (MC + M_6C)

for either HSS (Figures 3.13 and 3.14) decreases in quenched condition mainly due to the dissolution of M_6C carbide. Because of the higher vanadium content in T15 HSS as compared to T42, the MC carbide precipitation in the former is favoured to a greater extent. This appears to be the reason why there is little change in the MC carbide content after triple tempering for T42 HSS and only the M_6C carbide volume fraction is changed. The increase in the total carbide volume fraction is related to the precipitation from the retained austenite during second and third temperings, and probably to some coarsening of the existing carbides as well.

The findings of the SEM study (Figures 3.15 and 3.16) corroborate the optical metallographic study results. The type of the primary carbides can be distinguished from the phase contrast. M_6C carbide appears white as compared to the MC carbide which is greyish in colour due to difference in their compositions. The EDX analysis results (Table III.3) also confirm this finding. The chromium rich carbides are of submicron size and could be resolved at a magnification above 5000X. The acicularity of the martensite was lowered from the first to the second tempering (Figures 3.16e and f) as martensite got decomposed with precipitation of alloy carbides resulting in the decrease of carbon content of the existing martensite. In the present investigation, the secondary carbides could not be resolved under the available SEM. The transformation of retained austenite to martensite during tempering due to

the associated increase in Ms temperature), could not be observed under SEM. However, the X-ray diffraction study results (Table III.2) confirmed the reduction in the retained austenite content during tempering.

IV.2.3. Mechanical Property:

The strengthening mechanisms in high speed steels are complex and these mechanisms operate in different proportions. The strength of HSS is highly structure sensitive and depends on the type of the heat treatment prior to service. The various mechanisms involved in strengthening HSS are [101-105]:

(i) Solid solution strengthening due to the presence of high contents of alloying elements like W, Mo, V, Cr, Co and carbon in the matrix. The presence of these elements induce lattice strains and raise the energy required to move dislocations.

(ii) Phase-transformation strengthening by the formation of martensite. The composition of martensite and the relative percentage in the structure determines the strength level. The martensitic transformation begins below the Ms temperature which itself is a function of the composition and prior thermal and mechanical history of the steel. In HSS, cobalt is known to increase the Ms temperature and so the Co containing HSS are known to have lower retained austenite which is a strength

reducing constituent in HSS. The size of the martensite grains and the Ms temperature are dependent on the prior austenite grain size which itself is a function of the time and temperature of the austenitization treatment: Smaller are the austenite grains, the smaller will be the martensitic phase.

(iii) Precipitation strengthening in HSS is imparted during tempering where the precipitation of fine, stable alloy carbides in the matrix result in secondary hardening and the strengthening associated with the resistance induced to dislocation movement. The precipitation process is dependent on the chemistry and thermal treatment of any steel. Higher level of alloying elements dissolved during the austenitization process result in greater amount of precipitation during cooling. Cobalt in HSS is known to enhance the precipitation process and result in greater secondary hardening and induce temper resistance to HSS by decreasing the growth and agglomeration of alloy carbides at higher temperatures.

There are also contributions to strengthening in HSS from the indirect strengthening mechanisms such as:

(i) grain size effect through Hall-Petch relationship. Cobalt steels are known to have finer grain sizes as compared to the non-cobalt bearing steels due to the restrictions for grain growth imposed by Co.

(ii) Coherency strains induced by the localised concentration variations of alloying elements due to the action of cobalt on the diffusivity of various alloying elements.

A. Sintered High Speed Steels:

The increase in the sintered hardness and TRS value with sintering temperature is associated with the decrease in porosity level (Figures 3.2 and 3.3). At temperatures higher than the optimum sintering temperature, both these properties remain either constant or decreased. This is attributed to the fact that the beneficial effect of decrease in porosity is nullified by the microstructural coarsening associated with higher sintering temperature, which is verified from the results of microstructural analysis (Figures 3.10d and 3.11d). Higher sintered hardness of T15 HSS in comparison to that of sintered T42 HSS may be attributed to higher dissolution of alloying elements during elevated temperature sintering in the matrix of the former causing solution hardening. A comparatively lower sintered TRS of T15 (1460 MPa) as compared to that of T42 (1800 MPa), in conjunction with relatively larger grain size of the former ($\sim$ 20 μm) undoubtedly establishes the fact that coarse matrix/carbide precipitates result in lowered TRS values.

The fracture of the sintered TRS test specimens (Figures 3.17a and b) is identified as a ductile one due to the presence of dimples on the fracture surface. These

dimples are probably due to the initiation and growth of microvoids between matrix and carbide particles which coalesce ahead of the crack tip. The fracture characteristics are more or less similar for both T15 and T42 grades of HSS.

B. Heat Treated High Speed Steels:

The higher triple tempered hardness of T42 HSS (960 HV_{10}) in comparison to that of T15 HSS (900 HV_{10}) is attributed to the higher cobalt content of T42 HSS. The combined effect of cobalt in strengthening the matrix and the dispersion strengthening due to the presence of very fine, stable, carbide precipitates which restrict the dislocation motion results in a relatively higher triple tempered hardness for T42 HSS. It is also known, that cobalt decreases the stability of retained austenite during tempering in addition to the solid solution strengthening of the matrix [78, 97-101]. It is obvious that the precipitated carbides in a concentrated solid solution hardened matrix would result in a stronger alloy as compared to similar precipitates in a lean solid solutions. Similarly, carbide precipitates in a fine grained matrix would impart further strengthening than that in coarse grained HSS with equivalent amount and type of precipitates. As is well known, cobalt increases the dislocation density and retards the recovery of the dislocation substructure, so that the number of nucleation sites for the subsequent precipitation of carbides is increased. It also increases the activity of carbon, which results in

a higher rate of nucleation with associated fall in growth rate of carbide precipitates [97]. As a consequence, the presence of cobalt in HSS results in an increase in Ms temperature, microstructural refinement and retention of dislocation substructure [101].

A relatively lower triple tempered TRS value of T42 HSS (1300 MPa) as compared to that of T15 steel (1950 MPa), may be attributed to the relatively larger cobalt content of T42 HSS [78, 96, 102]. Cobalt induces very fine dislocation nucleated precipitates of alloy carbides both in retained austenite and martensite leading to the retention of dislocation substructure as explained earlier. In addition to this, a high cobalt content strongly reduces the retained austenite values reducing the softer constituent content in the microstructure. Due to the above reasons, the TRS value of T42 HSS is relatively low.

The fracture surface of the triple tempered TRS test specimens (Figure 3.17c-e) is identified as a quasi-cleavage fracture which combines the features of both ductile and brittle natures. The origin of the main crack is not very clear from the fractographs. After the main crack has been initiated, the presence of divergent secondary cracks could be seen. Some of the carbide particles falling on the path of the propagating crack are seen to have fractured.

Elevated Temperature Compressive Yield Strength: A comparison between T15 and T42 HSS could reveal that at any testing temperature, the compressive yield strength of the latter is higher as compared to that of the former (Figure 3.9). This may be attributed to the relatively large cobalt content in T42 HSS, which increases the tempering resistance [78, 101-109]. As already described earlier, this is related to the increased nucleation rate of alloy carbides and their diminished growth rate thus leading to no increase in the interparticle spacings. This results in the continuation of the dispersion strengthening mechanism being operative even at higher temperatures. The increased quantity of stable, fine carbides in T42 HSS during tempering, resists matrix grain coarsening and increases the resistance to deformation. The increase in the $\alpha \rightarrow \gamma$ transformation temperature [78] combined with the reduced diffusivity of other alloying elements [98] with increase in cobalt content facilitates higher volume fraction of alloy carbide precipitates and retardation in the secondary carbide coarsening [97].

IV.2.4. Magnetic Coercivity:

Coercivity in a ferromagnetic metal is a measure of the demagnetizing force necessary to remove all the magnetic lines of force to valve of Bo in the B-H curve. It therefore represents the resistance to demagnetisation. High speed steels come under the category of hard magnetic materials, a typical example being the tungsten bearing permanent magnetic

steel. It is known that if iron supersaturated with carbon is isothermally aged to precipitate carbides, the coercivity of the specimen increases with aging time, passes through a maximum and then declines, in a manner analogous to the change in hardness during aging. The coercivity can be considered to vary with:

(a) Volume fraction of the precipitate,

(b) the size of the precipitated particles,

(c) precipitate morphology,

(d) precipitate habit, and

(e) magnetic property of the precipitate.

Electron microscopic studies [110] have contributed substantially in making the direct observations of the interaction of domain walls with precipitate particles. The coercivity variation in general falls parallel to the hardness variation. A higher coercivity of T42 steel in relation to T15 can be attributed to the enhanced lattice strain, because of higher cobalt content in the former.

IV.3. HSS BASED COMPOSITES:

IV.3.1. Role of HSS Compositions:

In any metal-ceramic particulate composites similar and dissimilar powder surfaces are in contact with the consequence that the atomic and defects migrations along and across the dissimilar contacts are greatly modified. As the second phase ceramic particles are harder than the metal matrix, the densification of the composite would be reduced

[111-114]. This effect is attributed to the constriction of the diffusion cross section for the lattice or grain boundary diffusion of matrix atoms [113], as well as the inhibition of dislocation motion by the dispersed particles [112, 115, 116]. As the particle size of dispersoids i.e. TiC or TiN(3.5 μm, 7 μm respectively) are much much smaller than that of the matrix phase (30-40 μm), the former can easily enter octahedral and tetrahedral positions in the matrix powder sites [117]. However, the assumption here is made that all the particles are spherical, a situation which is very much different from the real one. The difference in the powder morphology of either constituent can directly or indirectly change the formation and growth of necks during solid state sintering, which occurs in the present experimental condition for a significant period ($\sim$ 3.5 hrs.) in contrast to the liquid phase sintering (1.5 hrs.). It is worth noting that supersolidus sintering occurs at a fairly high temperature ($>0.89\ T_m$) in case of HSS and hence, the role of solid state sintering could not be ignored. As sintering progresses in such particulate composites, there would be all probability of diffusion barriers thus inhibiting the densification kinetics.

In the presently selected steels, major part of the densification during liquid phase sintering occurs by the rearrangement of the particles, where the amount of liquid phase at sintering temperature plays an important role. The liquid formation is associated with the melting of fine particles

preferentially along the surfaces of the large powder particles and also along the grain boundary within the particles in the optimum sintering temperature range. The presence of the stable TiC/TiN particles in the composites, restrictsthe particle rearrangement and grain growth stage required for densification during sintering. Such a feature becomes more prominent with increased content of the refractory compounds in the composite. It, therefore, becomes necessary to employ higher and higher sintering temperatures in order to make the melt less viscous and also to increase the liquid phase amount effectively. The densification behaviour with respect to sintering temperature observed for any of the composite systems studied presently supports the above conclusions (Figures 3.19, 3.20, 3.43 and 3.44). The optimum sintering temperature for achieving full density (>98% Th.) increases for the refractory compound rich composites (Figures 3.21, 3.22, 3.45 and 3.46).

The contact angle in case of liquid iron or cobalt is less than $90^{o}C$ with TiC solid, such that wettability is better for cobalt as compared to iron. Moreover, vacuum atmosphere exhibit better wettability than say H_2 [118]. As the cobalt content in T42 HSS is about two times than that of T15 grade, it would be expected that sinterability of T42 base composites would be better than that of T15 base. Coming to the other refractory compound i.e. TiN, literature data [118] reveal that unlike TiC neither cobalt or iron melt wets it. The contact angle by either melt is

more or less similar. This would naturally lead to relatively poor sinterability of composites containing TiN particles. As a matter of fact this is established by the present findings (Figures 3.20 and 3.44). Wetting data [118] also reveal that the presence of Mo in the melt improves wettability with either TiC or TiN which should mean a better densification of T42 grade HSS which contains ~3% Mo, as compared to T15 grade which is practically Mo free. The present results convincingly follow the above conclusions (Figures 3.19-3.22 and 3.43-3.46). The differences in the wettability of the two grades of HSS for the two refractory compounds are also evident from the EDX analysis of the TiC/TiN particles in the HSS matrix (Tables III.5 and III.6). The analysis of TiC/TiN particle in T42 HSS matrix is associated with higher Mo content than that observed in the corresponding T15 HSS matrix.

The strengthening mechanisms in metal-matrix particulate composites are complex. Various related mechanisms in strengthening are (i) coherency strain, (ii) strengthening where dislocation movements are easily blocked by the dispersoid particles (Orowan mechanism) and other modified models [119], (iii) indirect strengthening, where dispersed particles stabilize the grain size and the dislocation substructure, and (iv) direct strengthening by load sharing ability by strong ceramic particles. Apart from this, interfacial energy, stored energy, particles morphology are also responsible in contributing to strength. It is also

true that all the mechanisms do not necessarily operate for all particulate composites. In the present investigation, exclusive role of the Orowan strengthening mechanism is ruled out owing to the coarser size of the dispersoids (3.5 μm for TiC and 7 μm for TiN) and moreover apart from the tendency to agglomerate, their distribution may not perfectly uniform in the powder premixes. However, such a role does exist during secondary precipitated hardening, where the carbide particles are small in size. It is expected that TiC addition if properly bonded with the HSS matrix would behave similarly to the primary MC carbides. With the increase in the refractory compounds contents in the HSS matrix beyond 4 mass %, the need for higher sintering temperatures for achieving full density is justifiable. However, at the same time the use of higher sintering temperatures results in microstructural coarsening resulting in loss in the strength. Moreover, at higher temperature, the refractory compound particles tend to agglomerate, which is evident from the microstructure of particularly refractory compound rich composites (Figures 3.29-3.32, 3.53, 3.54, 3.61). On the other hand, a lower sintering temperature to circumvent the above adverse effect results in higher porosity, which contributs in the strength lowering.

For reducing the sintering temperature of refractory compound enriched HSS based composites, Bolton [55] and Martins et al [57] made use of a sintering aid (Cu-P alloy) which reduced the sintering temperature considerably. The

use of such a sintering aid has the inherent disadvantage of introducing a low melting eutectic phase which reduces the high temperature stable properties expected out of such HSS composites. Arai and Komatsu [65], Beltz et al [64], Uchida and Nakamura [66] reported the use of post-sintering Hipping/hot working for reducing the porosity of refractory compound enriched HSS composites. They combined the use of lower sintering temperatures and post-sintering operations to get a dense product. However, as the present investigation focuses on the development of a near-net shaped HSS based composites, the above two possibilities for reducing the sintering temperature were not contemplated.

The increase in the heat treated mechanical properties of the investigated HSS composites is purely due to the strengthening associated with the change in the microstructure of HSS and due to secondary hardening on account of precipitation of very fine, stable alloy carbides in the martensite matrix. This is evident from % increase in the TRS values (30% for straight T15 composition and 37% for T15 - 4% TiC composite) in triple tempered condition above that in the sintered condition. Similarly, the decrease in the TRS value of composites based on T42 HSS in the triple tempered condition is related to the effect of higher cobalt content in T42 HSS which has been discussed in Section IV.2.3.

IV.3.2. Role of Refractory Compounds:

All the investigated refractory compounds for the enrichment of HSS compositions can be classified into three groups. The first group of compounds, which dissolve completely in the matrix at the sintering temperature, do not serve in developing any worthwhile composite. Examples of such compounds are silicon carbide and chromium carbide in steels. The second group of compounds are refractory carbides such as WC, Mo_2C and VC etc. which are inherent in the microstructure of the steels. Their evolution can be brought about by a change in the chemistry and heat treatment of the steel. The presence of such compounds does not change the sintering conditions as wettability and bonding in the matrix do not pose any problem. The third group of refractory compounds are those which remain stable in the matrix at still high temperatures. Fourth group transition metal carbides and nitrides e.g. TiC and TiN fall in this group of the refractory compounds. The relative advantage of their addition depends on the wetting characteristics and so the bonding between the hard particles and the matrix. TiC has better wetting behaviour (contact angle $\angle 90^{\circ}$) as compared to TiN (contact angle $>90^{\circ}$) with iron. In addition, the wettability of these refractory compounds with cobalt melt is better than with iron. In case of TiN, both iron and cobalt have been found to have similar wetting characteristics. Also, the wetting characteristics in vacuum is better than

that in H_2 atmosphere [118]. This is the reason why liquid phase sintering of HSS is carried out preferably in vacuum.

Better densification behaviour in case of TiC containing composites based on either T15 or T42 HSS in comparison to those containing TiN is related to the higher wettability of TiC as compared to TiN. For either of the selected refractory compound, it is obvious that composites based on T42 HSS have better densification behaviour in comparison to the corresponding T15 HSS based composite. This difference in the densification behaviour is attributed to the molybdenum and relatively higher cobalt in T42 HSS than that in T15 HSS. The synergetic effect of cobalt and molybdenum in T42 HSS, thus results in a better densification response of T42 HSS based composites as compared to those based on T15 HSS.

The difference in the mechanical properties of TiC and TiN containing composites based on either HSS can be explained primarily on the basis of difference in their wetting characteristics. Such a difference results in different bond strengths between HSS and the particles of the different types of dispersoids. Selection of a relatively higher sintering temperature in case of TiN containing composites of either HSS because of poor wettability does result in the microstructural coarsening, as compared to those containing TiC dispersoids. The contributions of TiC in promoting strengthening in either HSS composite are mainly due to effects such as relatively smaller matrix

grain size associated to relatively lower sintering temperature, higher intrinsic hardness (2900 HV) of the compound, higher interfacial energy due to better bonding and relatively fine particle size (3.5 μm) of compound as compared to that of TiN. Corresponndingly, the TiC containing composites of either HSS show better overall properties e.g. higher hardness, TRS and elevated temperature compressive yield strengths as compared to TiN containing ones.

The distinctive densification response in either TiC or TiN composite can also be correlated on the basis of the differences in bondings, which these compounds posess.

In the presently selected refractory compounds, TiC/TiN, titanium pertains to early transition metals containing unfilled d shell, while both carbon and nitrogen correspond to sp electronic configuration for their valency electrons. Samsonov [88] discussed in detail the energetic stability of both types of elements and concluded that during formation of such refractory compounds the transition metals act as donors of electrons, so as to stabilize the sp^3 configuration of non metal atoms to different extents. Carbon whose isolated atoms possess s^2p^2 electronic configuration tend to acquire stable sp^3 configuration due to s → p transition during TiC formation. However, in case of nitrogen, whose isolated atoms have s^2p^3 configuration, owing to s → p transitions by the scheme $sp^4 \rightarrow sp^3 + p$, fully tend to acquire sp^3 configurations with one weakly bonded electron of p configuration. It is

this extra unbonded electron which is responsible for relatively lower hardness, lower melting point and higher plasticity in TiN as compared to strongly covalent bonded TiC. The poor wettability of this compound i.e. TiN with HSS melt is a direct manifestation of the above fact. Moreover, the enhanced matrix grain coarsening in case of TiN containing composites in a way is also related with the above findings, since to acquire full density a higher sintering temperature was necessary.

IV.4. TOOL LIFE:

Metal cutting process in general is a very complex phenomenon which involves the machine tool and type of operation, tool tip geometry, tool material, work material and above all the cutting conditions such as continuous/intermittent cutting operation, lubricant/coolant used, cutting speed, feed and depth of cut. In any standard situation, the cutting tool life of a HSS cutting tool depends on three major characteristics [2, 107, 108] which are:

(i) Wear resistance, necessary to retain the tool shape and cutting efficiency.

(ii) Toughness, enabling the tool to withstand the forces and shocks in interrupted cuts, and to avoid chipping of the cutting edge.

(iii) Hot hardness, enabling to retain hardness at the higher cutting temperature and thus cutting ability.

In addition to the above, the other properties of importance are coefficient of thermal expansion, and the thermal conductivity.

The presently investigated tool life test results (Table III.4) show that T42 grade HSS has a greater tool life (≈ 30 min) as compared to that of T15 grade (21 min). This may be attributed to the higher cobalt content in T42, which results in a combination of higher hardness and higher elevated temperature compressive yield strength. Moreover, cobalt increases thermal conductivity of HSS [78] resulting in a lower tip temperature under identical cutting conditions. Although the toughness of cobalt containing HSS is reported to be lower than [78, 96] non-cobalt containing ones, the beneficial effects of cobalt, such as increase in hardness, temper resistance and enhanced thermal conductivity, result in higher cutting tool life of former grade HSS under identical test conditions.

The wear resistance of the cutting tool can be directly related to the volume fraction of hard phase present in the microstructure. In HSS the wear resistance is directly proportional to the MC carbide (vanadium rich) content [1, 2, 107]. The enrichment of the presently studied two grades of HSS by TiC and TiN naturally increases the harder phase fraction in the resulting tool material. It is, therefore, expected that the wear resistance of such a tool would be better than the straight HSS provided that the related mechanical properties like TRS and elevated

temperature compressive yield strength are not adversely affected by such enrichments. The composites of either HSS viz. T15 and T42 grades containing TiC or TiN have shown better tool lives than the straight HSS. In addition, T15 HSS based composites showed relatively higher gain on the tool lives as compared to the T42 HSS based composites. This is due to the lower toughness of T42 HSS which probably further deteriorates with the increasing contents TiC.

Tool life of either grades of HSS viz. T15 or T42 enriched by TiC addition showed better cutting life as compared to the corresponding TiN containing composites. This may be attributed to the fact that the wetting behaviour of TiC with HSS matrix is better as compared to that of TiN [118]. Moreover, TiC possesses higher hardness (Table 1.1) [91] and bond strength [88] as compared to TiN. Due to the above reasons, TiC containing HSS cutting tools show better tool lives as compared to their TiN containing counterparts.

CHAPTER V

CONCLUSIONS

Based on the detailed studies on the sintering behaviour of the T15 and T42 HSS based composites and their properties, the following conclusions can be made:

1. Full density (>98% Theoretical density) in liquid phase sintered T15 and T42 HSS is achieved after vacuum sintering at 1270°C and 1230°C respectively.
2. In sintered condition, T15 HSS show relatively higher hardness and lower TRS value as compared to the corresponding in T42 HSS. This may be attributed to greater solution hardening effect associated with dissolution of higher amounts of alloy carbides at higher temperatures.
3. Peak hardness in T15 and T42 HSS is obtained after triple tempering for 1 hour during each tempering at 560°C and 540°C respectively.
4. The triple tempered hardness for T42 HSS is higher than that of T15 HSS whereas the trend is reverse in case of TRS, which is attributed to the effect of relatively higher cobalt content of T42 HSS.
5. The room and elevated temperature compressive yield strength of heat treated T42 HSS is higher than those for T15 HSS. This is attributed to the relatively higher cobalt content of T42 HSS indu-

6. The optimum sintering temperature (for achieving full density) increases for richer TiC/TiN containing composites based on T15 or T42 HSS. This is related to the presence of diffusion barriers between HSS powder particles and to the restrictions posed by these hard stable refractory particles for densification through particle rearrangement during supersolidus liquid phase sintering.

7. TiC containing composites based on either HSS, show better densification as compared to the corresponding composites containing TiN. This is attributed to the better wetting behaviour of TiC with HSS melt as compared to TiN.

8. TiC/TiN containing composites based on T42 HSS show better densification as compared to the corresponding T15 HSS composites. This is related to the enhanced wetting behaviour in T42 HSS melt containing ~3% molybdenum as compared to practically nil in T15 HSS.

9. Composites containing 4 mass % TiC give the best combination of mechanical properties like hardness, TRS and elevated temperature compressive yield strength in either HSS. The mechanical properties like hardness, TRS and compressive yield strength of T15 HSS composites remain unaltered and decrease for richer composites. In case of T42 HSS containing TiN, peak mechanical properties is observed for the composite containing 4% TiN.

10. The magnetic coercivity of T42 HSS is higher than T15 HSS in quenched and triple tempered conditions and marginally lower in sintered condition. In case of composites either in sintered and triple tempered conditions, the magnetic coercivity shows similar trend to that obtained for hardness. However, in case of T42 HSS based composites, the magnetic coercivity is higher as compared to the corresponding composite based on T15 HSS.

11. The grain size in sintered and triple tempered condition of either HSS based composites increases with increase in TiC/TiN content, mainly due to the use of higher sintering temperatures required for achieving full density.

12. The volume fraction of primary carbides (MC + M_6C) in either HSS increases during tempering. MC carbide in T42 HSS remains practically unchanged during heat treatment whereas in T15 HSS considerable increase is noticed. Amongst the two primary carbides, greater coarsening of less refractory M_6C carbide occurs in either HSS. The volume fraction primary carbides increases with the increase in TiC/TiN content in either HSS based composites. The MC carbide volume fraction linearly increases with the TiC content in either HSS whereas M_6C carbide undergoes marginal change. The MC carbide volume fraction virtually

remains unchanged for TiN containing composites based on either HSS.

13. The primary carbide size distribution shows more of coarser carbides for TiC/TiN rich composites which is attributed to the carbide coarsening resulting due to the use of higher sintering temperatures.

14. The tool life of T42 HSS is higher as compared to T15 HSS under the test conditions used in the present investigation. The tool life of TiC containing composites of either HSS base is superior to the corresponding TiN containing composite. T42 HSS containing 4% TiC gave maximum cutting tool life followed by similar composite of T15 HSS. For the composites containing either TiC/TiN, the percentage gain in the tool life is higher for T15 HSS as compared to T42 HSS.

REFERENCES

1. G. Hoyle, "High Speed Steels", Butterworths, London, 1988.

2. W.E. Henderer and B.F. von Turkovich, "New Developments in the Processing and Properties of HSS Tool Steels", Ed. M.G.H. Wells and L.W. Lherbier, The Metals Soc. of AIME, New York, 1980, p. 13.

3. "Metals Handbook", Vol. 6, 9th Ed., ASM, Metals Park, Ohio, 1988, pp. 51-59.

4. "Metals Handbook", Vol. 7, 9th Ed., ASM, Metals Park, Ohio, 1989, pp. 784-786.

5. P. Payson, "The Metallurgy of Tool Steels", John Wiley and Sons, New York, 1962.

6. J.P. Gill, "Tool Steels", ASM, Metals Park, Ohio, 1944, pp. 494-529.

7. F.A. Kirk, Metals Technology, May 1977, pp. 233-239.

8. T. Malkiewicz et al, Journal Iron Steel Inst., Vol. 193, 1959, pp. 25.

9. G.A. Roberts and R.A. Cary, "Tool Steels", 4th Ed., ASM, Metals Park, Ohio, 1980, pp. 647-664.

10. T. Mukherjee, "Materials for Metal Cutting", Proceedings of the Conference jointly sponsored by BISRA, Corporate Laboratories of BSC and ISI, held on 14-16 April, ISI, London, 1970, pp. 80-96.

11. P.K. Kar and G.S. Upadhyaya, Powder Metallurgy International, Vol. 22, No. 1, 1990, pp. 23-26.

12. R. Kieffer, P.E.H. Mayer, G. Jangg and G. Weissmann, "Modern Developments in Powder Metallurgy", Vol. 8, Ed. H. Hausner and W.E. Smith, Metal Powder Industries Federation (MPIF), Princeton, 1974, pp. 1-18.

13. E.A. Carlson, "Progress in Powder Metallurgy", Vol. 38, Ed. J.G. Bewley and S.W. McGee, MPIF, Princeton, 1983, pp. 271-284.

14. H.F. Fischmeister, Annual Review of Mat. Sc., Vol. 5, 1975, pp. 151-176.

15. R.J. Canston and J.J. Dunkley, Proceedings of Vth International Conference on Powder Metallurgy, Vol. 1, Czechoslovak Socialist Republic, 1978.

16. H. Takigawa, H. Manto, N. Kawai and K. Homma, Powder Metallurgy, No. 4, 1981, pp. 196-202.

17. W.T. Haswell, Jr., W. Stasko and F.R. Dax, "Processing Properties of High Speed Tool Steels", Ed. M.G.H. Wells and L.W. Lherbier, The Metallurgical Society of AIME, New York, 1980, pp. 147-158.

18. P. Hellman, "Processing and Properties of High Speed Tool Steels", Ed. M.G.H. Wells and L.W. Lherbier, The Metallurgical Society of AIME, New York, 1980, pp. 167-180.

19. "Metals Handbook", Vol. 16, 9th Ed., ASM, Metals Park, Ohio, 1988, pp. 60-67.

20. H. Sauer, J. Puber and R. Auer, Berg und Huttenm, Monatshefte, Vol. 120, No. 11, 1975, pp. 528-537 (H.B. Translation No. 9751).

21. R.P. Harvey, Preprint "Preformed P/M Tool Steel for Cutting Tools", Society of Manufacturing Engineers, Michigan, 1978.

22. A. Kasak and E.J. Dulis, "P/M Tool Steels", Preprint of the paper presented at Powder Metallurgy Conference, Coventry, U.K., Oct. 24-26, 1977.

23. J.J. Dunkley and R.J. Causton, Powder Metallurgy International, No. 3, 1976, pp. 115-117.

24. W.J. Huppmann, G.T. Brown, Preprint of the paper presented at P/M Conference, Coventry, Oct. 1977.

25. G. Bockstiegel, Powder Met. International, No. 3, 1974, pp. 116; No. 4, 1975, pp. 172; No. 1, 1972, pp. 7.

26. M.T. Podob and R.P. Harvey, "Processing and Properties of High Speed Tool Steels", Ed. M.G.H. Wells and L.W. Lherbier, The Metallurgical Society of AIME, New York, 1980, pp. 181-195.

27. E.J. Zickefoose, Preprint "Near Net Shapes", Society of Manufacturing Engineers, Michigan, 1982, pp. 305-320.

28. The Powdrex Process: A New Route to High Grade Tool Steels, Metals and Materials, Sept. 1977.

29. P.R. Brewin and J. Smart, Preprint of the paper presented at the Third International Conference on "New Frontiers in Tool Materials, Cutting Technique and Metal Forming", 15th-16th March, 1979 (Powdrex Ltd., Tonbridge, U.K.).

30. R. Wahling, P. Beiss and W.J. Huppmann, Powder Metallurgy, Vol. 29, No. 1, 1986, pp. 53-56.

31. Anon, Metal Powder Report, Vol. 32, No. 2, 1977, pp. 90-92.

32. E.A. Dickinson, Metal Powder Report, Vol. 32, No. 2, 1977, pp. 85-88.

33. M. Santos, I.M. Martins, M.M. Oliveira and H. Carvalhinhos, Paper presented at the conference "Tribology Trends in the 90's", Organised by Instituto Superior Tecnico, May 1988, Lisbon, Portugal.

34. C.S. Wright, J.D. Bolton, M.M. Rebbeck and A.S. Wronski, "Proceedings First International High Speed Steel Conference", Ed. G. Hackl and B. Hribernik, Montanuniversitat, Leoben, 1990, pp. 93-98.

35. W.B. Kent, "Proceesing and Properties of High Speed Tool Steels", Ed. M.G.H. Wells and L.W. Lherbier, The Metallurgical Society of AIME, New York, 1980, pp. 159-166.

36. L. Cambal and J.A. Lund, International Journal of Powder Metallurgy, Vol. 8, No. 3, 1972, pp. 131-140.

37. J.A. Lund and S.R. Bala, "Modern Developments in Powder Metallurgy", Vol. 6, Ed. H.H. Hausner and W.E. Smith, MPIF, Princeton, 1974, pp. 409-421.

38. R.M. German, "Liquid Phase Sintering", Plenum Press, New York, 1985.

39. R.M. German, International Journal of Powder Metallurgy, Vol. 26, No. 1, 1990, pp. 23-34.

40. S. Takajo and M. Nitta, In "Sintering-85", Ed. G.C. Kuszynski, D.P. Uskokovic, H. Palmer and M.M. Ristic, Plenum Press, New York, 1987, pp. 189-195.

41. K.M. Kulkarni, In "Sintering of Multi Phase Metal and Ceramic Systems", Ed. G.S. Upadhyaya, Sc. Tech. Publications, Vaduz, 1990, pp. 223-234.

42. K.M. Kulkarni, "Modern Developments in Powder Metallurgy", Vol. 19, Ed. P.U. Gummeson and D.A. Gustafson, MPIF, Princeton, 1988, pp. 329-344.

43. O. Grinder, L. Berglin and M. Sporrong, Paper presented at the 1984 Powder Metallurgy Conference, June 17-22, Toronto, MPIF, Princeton, 1984.

44. R.H. Palma, U. Martinez and J.J. Urcola, Powder Metallurgy, Vol. 32, No. 4, 1989, pp. 291-299.

45. I.H. Moon, J.S. Oh and I.S. Ahn, "Modern Developments in Powder Metallurgy", Vol. 17, Ed. E.N. Aqua and C.I. Whitman, MPIF, Princeton, 1985, pp. 441-450.

46. J. Smart, B.W. Reed and P.R. Brewin, Paper presented at the 1979 Powder Metallurgy group meeting, Inst.of Metals, London, 22-24 Oct., 1979.

47. J.V. Bee et al, Metal Powder Report, Vol. 43, 1988, pp. 177-184.

48. P.J. McGinn, P.Kumar, A.E. Miller and A.J. Hickl, Metallurgical Transactions, A, Vol. 15, 1989, pp. 1099.

49. M. Jeandin, J.L. Koutny and Y. Bienvenu, Powder Metallurgy, Vol. 26, 1983, pp. 17.

50. M.T. Podob and L.K. Woods, "Modern Developments in Powder Metallurgy", Vol. 13, Ed. H.H. Hansner, H.W. Antes and G.D. Smith, MPIF, Princeton, 1981, pp. 91-92.

51. A.N. Klein, R. Oberacker and F. Thurmmler, Metal Powder Report, Vol. 39, 1984, pp. 335.

52. K.M. Kulkarni, A. Ashurst and M. Svilar, "Modern Developments in Powder Metallurgy", Vol. 12-14, Ed. H.H. Hausner, H.W. Antes and G.D. Smith, MPIF, Princeton, 1981, pp. 93-120.

53. W.J.C. Price, M.M. Rebbeck, A.S. Wronski and S.A. Amen, Powder Metallurgy, Vol. 28, No. 1, 1985, pp. 1-6.

54. "Metals Handbook", Vol. 7, 9th Ed., ASM, Metals Park, Ohio, pp. 370-379.

55. J.D. Bolton, In Proceedings "Colloquium: Controlling the Properties of Powder Metallurgy Parts through Their Microstructure", Paris, 19-21 March, 1990, Organised by Societe Francaise De Metallurgie, Paris, Paper No. 15.

56. C. Johanny-Tresy, M. Jeandin, N. DeDave and J. Massol, ibid, Paper No. 14.

57. I.M. Martins, M.M. Oliveira and H. Carvalhinhos, ibid, Paper No. 16.

58. F. Thummler, R. Oberacker and R. Klausmann, "Modern Developments in Powder Metallurgy", Vol. 20, Ed. P.U. Gummeson and D.A. Gustafson, MPIF, Princeton, 1988, pp. 409-420.

59. P. Beiss, R. Wahling and D. Duda, "Modern Developments in Powder Metallurgy", Vol. 17, Ed. E.N. Aqua and C.I. Whitmann, MPIF, Princeton, 1985, pp. 331-357.

60. P. Hellmann, H. Wisell, Paper presented in SEMPS, P/M-78, June 1978, Vol. 1, Stockholm.

61. H. Brandis, E. Haberling and H.H. Weigand, "Processing and Properties of High Speed Tool Steels", Ed. M.G.H. Wells and L.W. Lherbier, The Metallurgical Society of AIME, New York, 1980, pp. 1-18.

62. G.A. Roberts and R.A. Cary, "Tool Steels", 4th Ed., ASM, Ohio, 1980, pp. 691-699.

63. R.A. Queeney, R.E. Masters, R.J. Beltz and J.D. Dankoff, "Modern Developments in Powder Metallurgy", Vol. 20, Ed. P.U. Gummeson and D.A. Gustafson, MPIF, Princeton, 1988, pp. 409-420.

64. R.J. Beltz, J.D. Dankoff and R.A. Queeney, "Progress in Powder Metallurgy", Vol. 41, 1985, MPIF, Princeton, pp. 235-250.

65. T. Arai and N. Komatsu, Tetsu-to-Hagane, Vol. 61, No. 2, 1975, pp. 241-250 (H.B. Translation No. 9406).

66. N. Uchida and H. Nakamura, Proceedings of 12th Int. Plansee Seminar, May 1989, Reutte, Austria, Vol. 2; Metallwerk Plansee, Reutte, 1989, p. 541.

67. S. Heiss and R. Kieffer, Austrian Patent No. 163611 (1946).

68. F.G. Wilson and P.W. Jackson, Powder Metallurgy, Vol. 16, No. 12, 1973, pp. 257-276.

69. N.S. Olenina, M.N. Goryushina, N.N. Gavrikov and T. Sh. Sergazin, Soviet P/M and Metal Ceramics, June 1981, pp. 416-418.

70. S.S. Kiparisov, G.A. Meerson, V.S. Panov, V.I. Tretyakov and M.M. Smirnova, Soviet P/M and Metal Ceramics, Sept. 1976, pp. 686-688.

71. S.S. Kiparisov, V.S. Panov, V.I. Tret'yakov and M.M. Smirnova, Soviet P/M and Metal Ceramics, July 1977, pp. 511-515.

72. S.S. Kiparisov, G.A. Meerson, V.S. Panov, M.M. Smirnova and A.F. Fokina, Soviet P/M and Metal Ceramics, Jan. 1977, pp. 31-36.

73. B. Edenhofer, J.W. Bouwman and F. Bless, in "Proceedings First International High Speed Steel Conference", Ed. G. Hackl and B. Hribernik, Montanuniversitat, Leoben, Austria, 1990, pp. 201-211.

74. H. Altena, ibid, pp. 212-223.

75. Private communications, British India Steels, Ahmedabad, India.

76. V.B. Akimenko, A.A. Gadkin et al, Physics of Sintering, Vol. 5, No. 1, 1973, pp. 49-56.

77. J. Arthur, J. Inst. of Metals, 84 (1956) pp. 327.

78. Yu. Geller, "Tool Steels", MIR Publishers, Moscow, 1978, pp. 440-455.

79. ASTM Standard: E 407-70 (Reapproved 1982), "Standard Methods for Microetching Metals and Alloys".

80. D.J. Blickwede, M. Cohen and G.A. Roberts, Trans. ASM, Vol. 42, 1950, pp. 1161-1196.

81. G. Petzow, "Metallographic Etching", ASM, Ohio, 1978, pp. 96-97.

82. ISO-3685.

83. R. Wahling, D. Duda and P. Beiss, In "Horizons in Powder Metallurgy", Part-I (Ed. W.A. Kaysser and W.J. Huppmann), Verlag Schmid Gmbh, Freiburg, 1986, p. 535.

84. C.S. Wright, A.S. Wronski and M.M. Rebbock, Metals Technology, Vol. 11, May 1984, pp. 181-188.

85. I. Kvasnicka, Powder Metallurgy, Vol. 26, No. 3, 1983, pp. 145-148.

86. K. Yamada, H. Kohzuki and Y. Okuno, Journal of Japan Society of Powder and Powder Metallurgy, Vol. 38, No. 1, 1991, pp. 31-34.

87. L. Chandrasekharan and A.P. Miodowink, "PM into the 1990's", Vol. 1, The Institute of Metals, London, 1990, pp. 398-406.

88. G.V. Samsonov, I.F. Pryadko and L.F. Pryadko, "A Configurational Model of Matter", Consultant Bureau, N.Y., 1973.

89. M.M. Michailow et al, Technologiea Awtomobilestrojenija, Vol. 1, 1958, pp. 25-26.

90. F. Frehn, French Patent No. 1427442 (1965) and 1429212 (1966).

91. G.V. Samsonov, "High Temperature Materials", No. 2, Properties Index", Plenum Press, New York, 1964.

92. J.O. Lord, "Alloy Systems - An Introductory Text", Pitman, New York, 1949, pp. 253.

93. S. Ni and S. Wang, In "Proceedings of the Ist International HSS Conference", Ed. G. Hackl and B. Hribernick, Montanuniversitat, Leoben, 1990, pp. 438-446.

94. R.S. Irani, C.S. Wright and A.S. Wronski, J. Mat. Sc. Letters, Vol. 1, 1982, pp. 318-320.

95. C.S. Wright and R.S. Irani, J. Mat. Science, Vol. 19, 1984, pp. 3389-3398.

96. P. Leckie-Ewing, Iron Age, Dec. 1950, pp. 115-118.

97. V.K. Chandhok, J.P. Hirth and E.J. Dulis, Trans. ASM, Vol. 56, 1963, pp. 677-692.

98. V.K. Chandhok, J.P. Hirth and E.J. Dulis, Trans. AIME, Vol. 224, 1962, pp. 858-864.

99. M. Ubrain, Cobalt, No. 12, 1961, pp. 1-14.

100. L. Habraken and D. Coutsouradis, Cobalt, No. 12, 1965, pp. 1-15.

101. A. Magnee, J.M. Drapier, J. Dumont, D. Coutsouradis and L. Habraken, "Cobalt Containing High Strength Steels", Centre D'Information Ducobalt, Brussels, 1974.

102. J.H. Woodhead and A.G. Quarrell, "The Role of Carbides in Low Alloy and Creep Resisting Steels", Published by Climax Molybdenum Company Ltd., London.

103. R.W.K. Honeycombe, "Metallurgical Developments in High Alloy Steels", ISI Special Report No. 86, ISI, London, 1964.

104. H.J. Goldschmidt, J. ISI, Vol. 170, 1952, pp. 189-204.

105. J.T. Berry, "High Performance High Hardness High Speed Steels", Climax Molybdenum Company, Greenwitch, 1970.

106. A. Basu, B.K. Ghosh, S. Jana and S.C. Dasgupta, Metals Technology, Vol. 7, No. 4, 1980, pp. 151-158.

107. E.M. Trent, "Metal Cutting", Butterworths, London, 1984.

108. G. Kuppuswamy, In, Mechanical Engineering Monograph Series "Principles of Metal Cutting: An Introduction", I.I.T., Madras, 1987.

109. G. Steven et al, Trans. ASM, Vol. 57, 1964, pp. 925-948.

110. J.T. Michalak and R.C. Glem, J. App. Phys., Vol. 32, 1961, pp. 1261.

111. M.H. Tikkanen, B.O. Rossel and O. Wiberg, Powder Met., Vol. 10, 1962, pp. 49.

112. M.H. Tikkanen, Physics of Sintering, Vol. 1, J. 1, 1969.

113. B.N. Singh and D.H. Houseman, Powder Met. Int., Vol. 3, 1971, pp. 1.

114. F.V. Lanel, G.S. Ansell and D.P. Borron, Met. Trans., Vol. 1, 1970, pp. 1772.

115. F.V. Lanel, Physics of Sintering, Vol. 4, 1972, pp. 1.

116. J. Berly, F.V. Lanel and G.S. Ansell, Trans. Met. Soc., AIME, Vol. 230, 1964, pp. 1641.

117. B.N. Singh, Powder Metallurgy, Vol. 15, No. 30, 1972, pp. 216.

118. P.S. Kisly, Kermeti, Naukova Dumka, Kiev, 1985 (in Russian).

119. G.S. Ansell, In "Oxide Dispersion Strengthening", Ed. G.S. Ansell et al, Gordon and Breach Sc. Pub. Inc., New York, 1968, pp. 61.